COMPUTER SIMULATION FOR TRANSIENT ANALYSIS OF MITR LOOP COMPONENTS

by

HERNAN GERARDO TROSMAN

B.S. Nuclear Engineering
University of Florida, 1992

Submitted to the Department of Nuclear
Engineering in Partial Fulfillment
of the Requirements for the Degree of

Master of Science

at the

Massachusetts Institute of Technology

May 1994

Signature of Author_____
Department of Nuclear Engineering
May 4, 1994

Certified by_____
Professor John E. Meyer
Thesis Supervisor

Certified by_____
Professor David D. Lanning
Thesis Supervisor

Approved by_____
Professor Allan F. Henry
Chairman, Departmental Committee on Graduate Students

COMPUTER SIMULATION FOR TRANSIENT ANALYSIS OF MITR LOOP COMPONENTS

by

Hernan Gerardo Trosman

Submitted to the Department of Nuclear Engineering
on May 4, 1994 in partial fulfillment of the
requirements for the Degree of Master of Science in
Nuclear Engineering

ABSTRACT

A computer program (TAMLOC) has been developed to simulate several transients for the MIT Nuclear Research Reactor. The transients under consideration include slow to moderate reactivity insertions, loss of heat sink, pump coastdown with attendant natural circulation, and small loss of coolant accidents. In addition to these accidents, the computer program can be used to analyze operational transients such as power maneuvering, startup, and shutdown. The intent of this research is to aid in the studies of an upgraded design of the present reactor MITR-II.

The modeling of the MIT Research Reactor is obtained by dividing the system into a few control volumes in which energy, mass, and momentum conservation laws are applied. The control volumes have been chosen to preserve the essential physical features of the system.

This computer code has been validated by comparing simulated results to available data from a reactor startup, a shutdown, and a pump coastdown. The simulated and measured temperatures are in good agreement. In addition, the results of simulation for several postulated accidents are presented for the present design (MITR-II) and for an upgraded design (MITR-III). The simulations and results from the TAMLOC code have been used as part of the basis for establishing proposed limiting safety system settings and operational limits for a proposed MITR-III design.

Thesis Supervisor: Dr. John E. Meyer
Title: Professor of Nuclear Engineering

Thesis Supervisor: Dr. David D. Lanning
Title: Professor of Nuclear Engineering

ACKNOWLEDGMENTS

I would like to express my greatest appreciation to Professor John Meyer for the supervision of this work. Without his guidance and encouragement, the completion of this thesis would not have been possible.

I would also like to extend special thanks to Professor David Lanning for his support, valuable advice, and assistance throughout my learning experience at MIT. He has been a great inspiration for me.

I am indebted to Daniel Doney for helping me give the computer code a "face" and to make it "user-friendly." The many sleepless nights he spent working with me on the data user interface are greatly appreciated.

Thanks are also due to Rachel Morton for helping me get along with my compilers and above all for exorcising the computers of any "demons" that would posses them.

I wish to express my gratitude to my office mates and MITR-III design group who contributed much to my learning experience at MIT:

Dr. Alan Henry,
Dr. Otto Harling,
Dr. John Bernard,
Mike McGuire,
Everett Redmond,
Lin-Wen Hu,
Sylvain Sardy, and
Ed Lau

I dedicate this thesis to my wife, Gracia Trosman, for without her moral support and love, this would have been an impossible task.

TABLE OF CONTENTS

LIST OF FIGURES

MITR-II SIMULATIONS

MITR-III SIMULATIONS (no scram)

MITR-III SIMULATIONS (with scram)

LIST OF TABLES

CHAPTER 1: INTRODUCTION

1.1 FOREWORD

Work has been initiated to prepare for the expiration of the operating license of the existing Massachusetts Institute of Technology Research Reactor (MITR-II). Several options, ranging from building an entirely new reactor to just extending the life of the present design, were considered during the first year of studies. Preliminary recommendations based on economic and reactor performance studies indicate that the existing reactor design should be retained. However, in order to support future research and industry needs, an upgrade to 10 MW is being proposed. This upgrade of the MITR-II could be done by using highly enriched uranium silicide dispersion (U_3Si_2-Al) fuel as shown by S. A. Parra[1].

To relicense an upgraded MITR-II (MITR-III), transient analyses must be performed to determine if the design meets all of the safety requirements. Several scenarios must be studied in detail such as reactivity insertion, total loss-of-flow, flow blockage, and loss-of-coolant transients.

1.2 OBJECTIVE

The objective of this research is to develop a computer program capable of simulating a wide range of the transient behavior applicable to the MITR-II system and to some similar systems. The range of application should include both normal operations such as power level maneuvering, reactor startup and shutdown, as well as faulted

---

[1] Parra, S. A, "The Physics and Engineering Upgrade of the Massachusetts Institute of Technology," Ph.D. Thesis, MIT Department of Nuclear Engineering, 1993.

operations such as complete loss-of-flow accident with attendant natural circulation cooling, reactivity insertion accidents, and partial loss-of-coolant accidents. The computer program development is based mostly on the adaptation of the computer code SPK (written by S. P. Kao[2]) to the MITR system.

For large reactivity insertions, a computer program that integrates the entire loop behavior is not necessary since most large reactivity insertion transients are completed before the entire loop can have an influence. Large reactivity insertions can be analyzed using other computer codes such as PARET[3] in which the inlet temperature to the reactor core is assumed constant. However, for slow reactivity transients, temperature and flow changes in the primary system become important, and therefore reactivity insertion capabilities are incorporated in this code.

1.3 MITR-II DESCRIPTION

The MITR-II reactor consists of a highly enriched compact core cooled and moderated by light water and reflected by heavy water. The core is located inside a core housing contained within two concentric tanks. The outermost tank is a 1.2 meter diameter tank filled with heavy water while the inner tank is a 0.51 meter diameter tank containing the core. Above the core, there is approximately 3 meters of water and the top of this water pool is maintained near atmospheric pressure. Figure 1.3-1 shows a vertical cross sectional layout of the MITR-II.

---

[2] Kao, S. P., "A Multiple-Loop Primary System Model for Pressurized Water Reactor Plant Sensor Validation," Ph.D. Thesis, MIT Department of Nuclear Engineering, 1984.

[3] Obenchain, C.F., "PARET- A Program for the Analysis of Reactor Transients," IDO-17282, AEC Research and Development Report, January 1969.

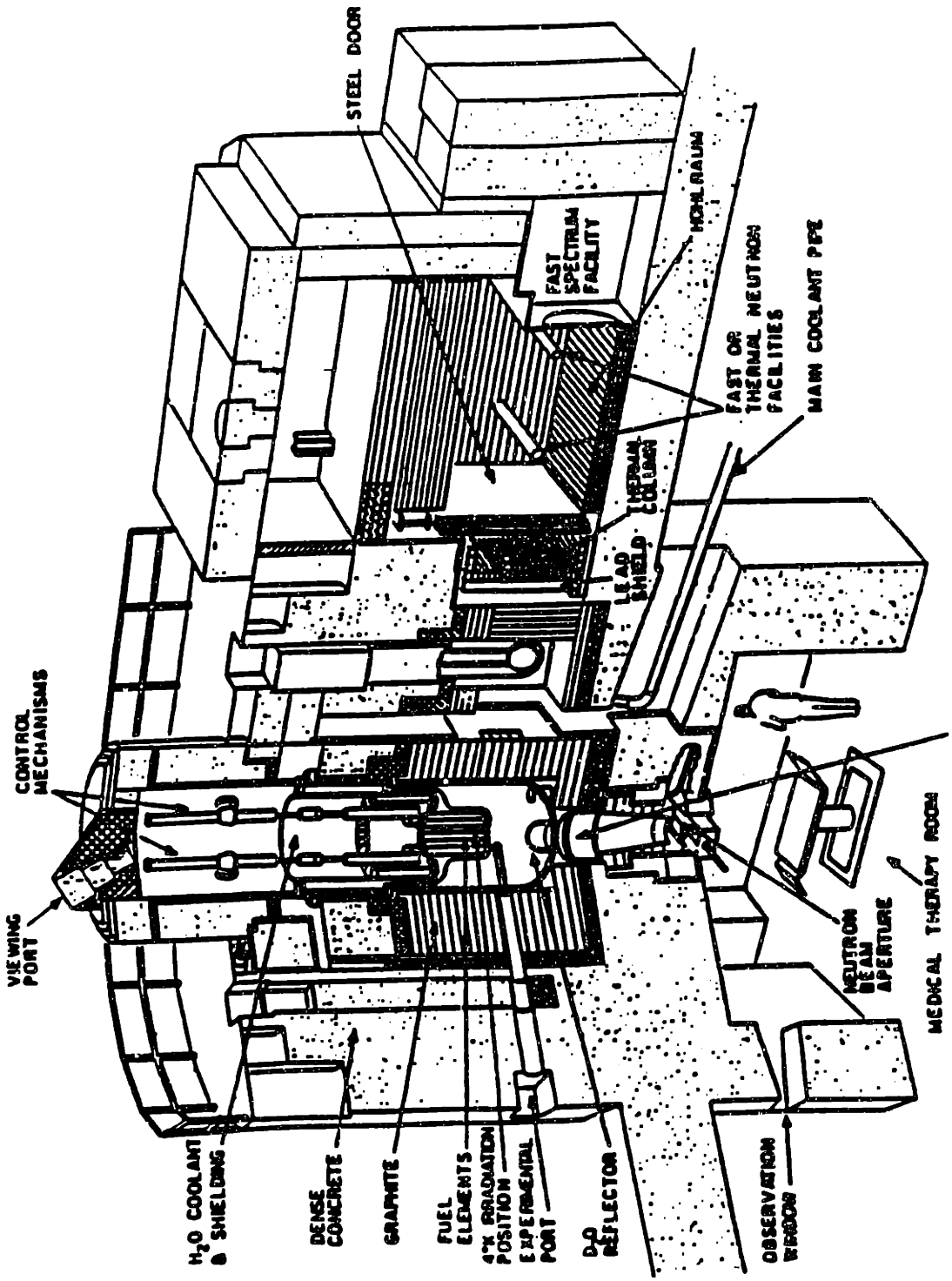

Figure 1.3-1. Vertical Cross-Sectional Layout of the MITR[4]

---

[4] Parra, S. A., ibid., page 16.

The heat generated in the core is removed by forced convection. Light water coolant enters the core tank via a piping system (commonly referred to as the cold leg) at about 1.8 meters above the core. It then flows downward through the annular region between the core tank and the heavy water tank until it reaches the bottom of the core housing where it is redirected upward through the fuel elements. Then, the flow moves slowly through a flow shroud and into the pool of water above the core (referred here as the mixing area). The flow exits the core tank near the top of the light water pool through another piping system (commonly referred to as the hot leg) where it is pumped by two parallel primary coolant pumps into two of three parallel heat exchangers. The heat exchangers, as the name implies, transfer the heat from the primary coolant to the secondary coolant (light water) where it is ultimately deposited into the atmosphere via two cooling towers.

The core consists of up to twenty-seven fuel assemblies arranged hexagonally in a tightly packed manner. Figure 1.3-2 shows a cross-sectional view of the MITR-II. There are three groups of fuel assemblies within the core housing: the A-ring -- a central group of three assemblies, the B-ring -- nine assemblies arranged hexagonally around the A-ring, and the C-ring -- a hexagonal arrangement of fifteen assemblies surrounding the B-ring. Normally, two of the A-ring assemblies and/or one of the B-ring assemblies can be replaced with in-core irradiation facilities[5].

The reactivity is controlled by six boron/stainless-steel shim blades and a single cadmium fine-control regulating rod. As seen in Figure 1.3-2, the shim blades are

---

[5] "MIT Research Reactor Systems Manual," Report No. MITNRL-004, Massachusetts Institute of Technology, page 1.4, 1980.

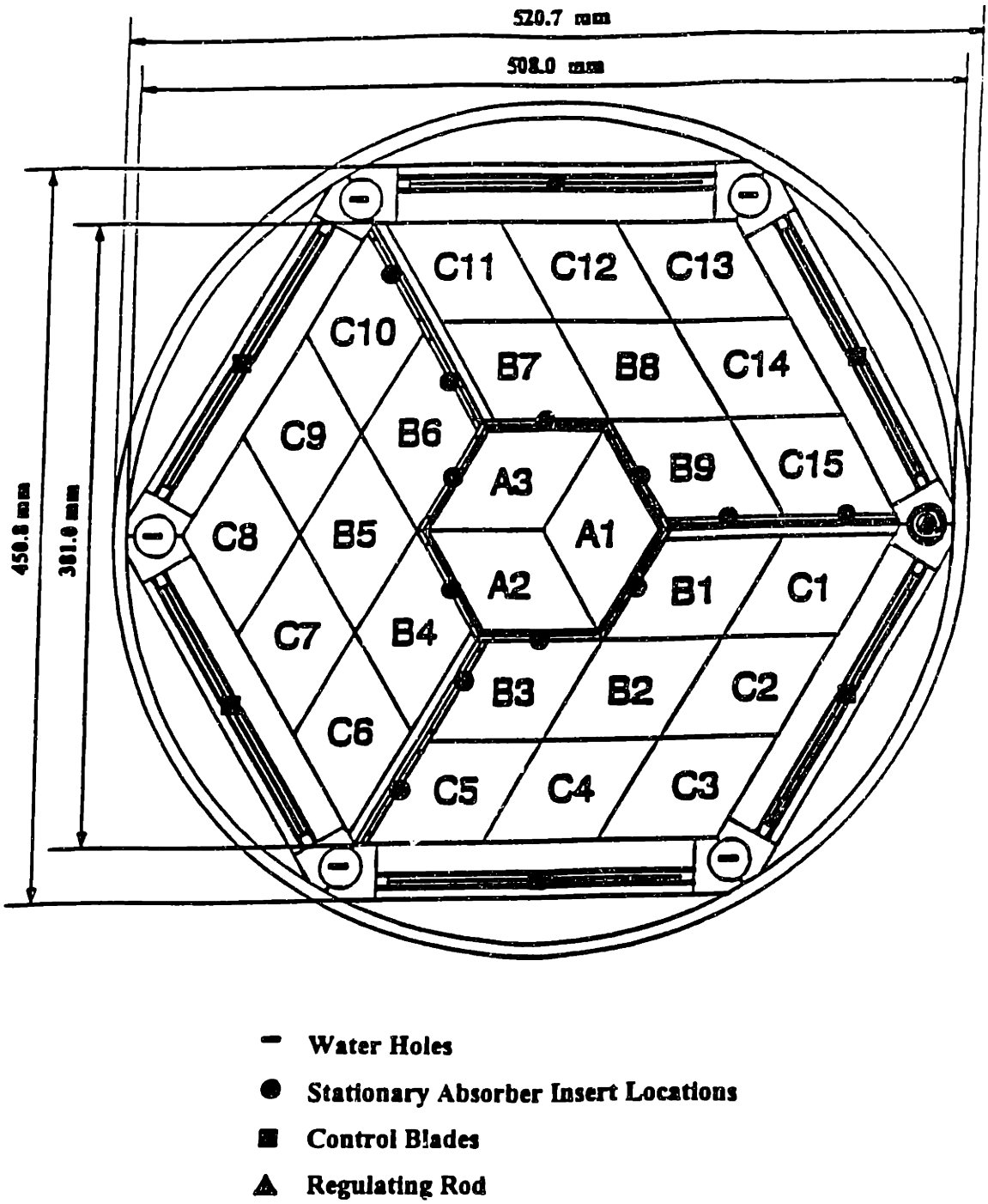

Figure 1.3-2. MITR-II Core Cross-Sectional View[6]

---

[6] Parra, S. A., ibid., page 19.

arranged symmetrically around the core. When the shim blades are inserted, they form a barrier preventing thermal neutrons from reentering the core from the D_2O reflector. The regulating rod function is to compensate for minor changes in reactivity due to xenon, temperature changes, etc. to maintain a specified power level.

A fuel assembly is shown in Figure 1.3-3; it consists of fifteen parallel fuel plates arranged in a rhombic shape. The fuel plate consists of a highly enriched uranium aluminide fuel meat clad with aluminum. To increase the heat transfer area of the fuel plates, the clad was designed with rectangular longitudinal fins.

The heat removal system consists of piping, valves, storage and expansion tanks, heat exchangers, filters, ion columns, instrumentation, and other miscellaneous equipment. Figure 1.3-4 shows a schematic of the MITR system. The system is designed such that, with flow of at least 1800 gpm and an outlet temperature (mixed-mean) of less than 60 $^{\circ}C$, it can transfer 6 MW of heat from the primary to the secondary water system and maintain the primary coolant temperature below boiling under all conditions. Light-water is drawn from the upper core tank, through a single eight-inch line which splits into two six-inch lines to two parallel primary coolant pumps. The pumps discharge through the primary side of the heat exchangers where the heat is transferred to the secondary cooling system. The outlets of the heat exchangers combine into a single eight-inch line returning the primary coolant to the inlet plenum. The inlet plenum contains two anti-siphon valves which, in the event of an inlet pipe rupture, will prevent the core from becoming uncovered by a siphoning action[7].

---

[7] "MIT Research Reactor Systems Manual," ibid., pages 3.1-3.2.

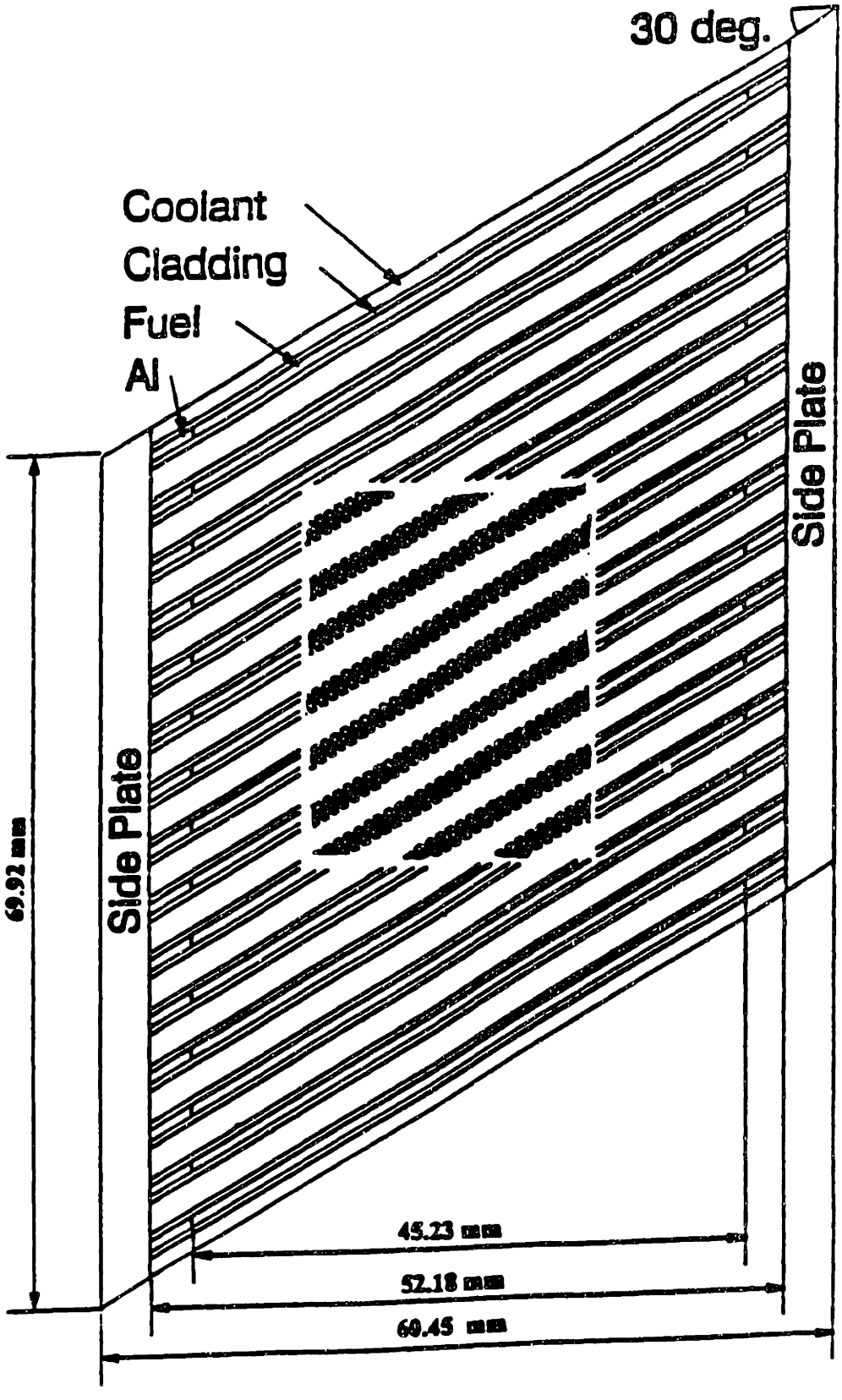

Figure 1.3-3. Cross-Sectional View of a Fuel Assembly[8]

[8] Parra, S. A., ibid., page 20.

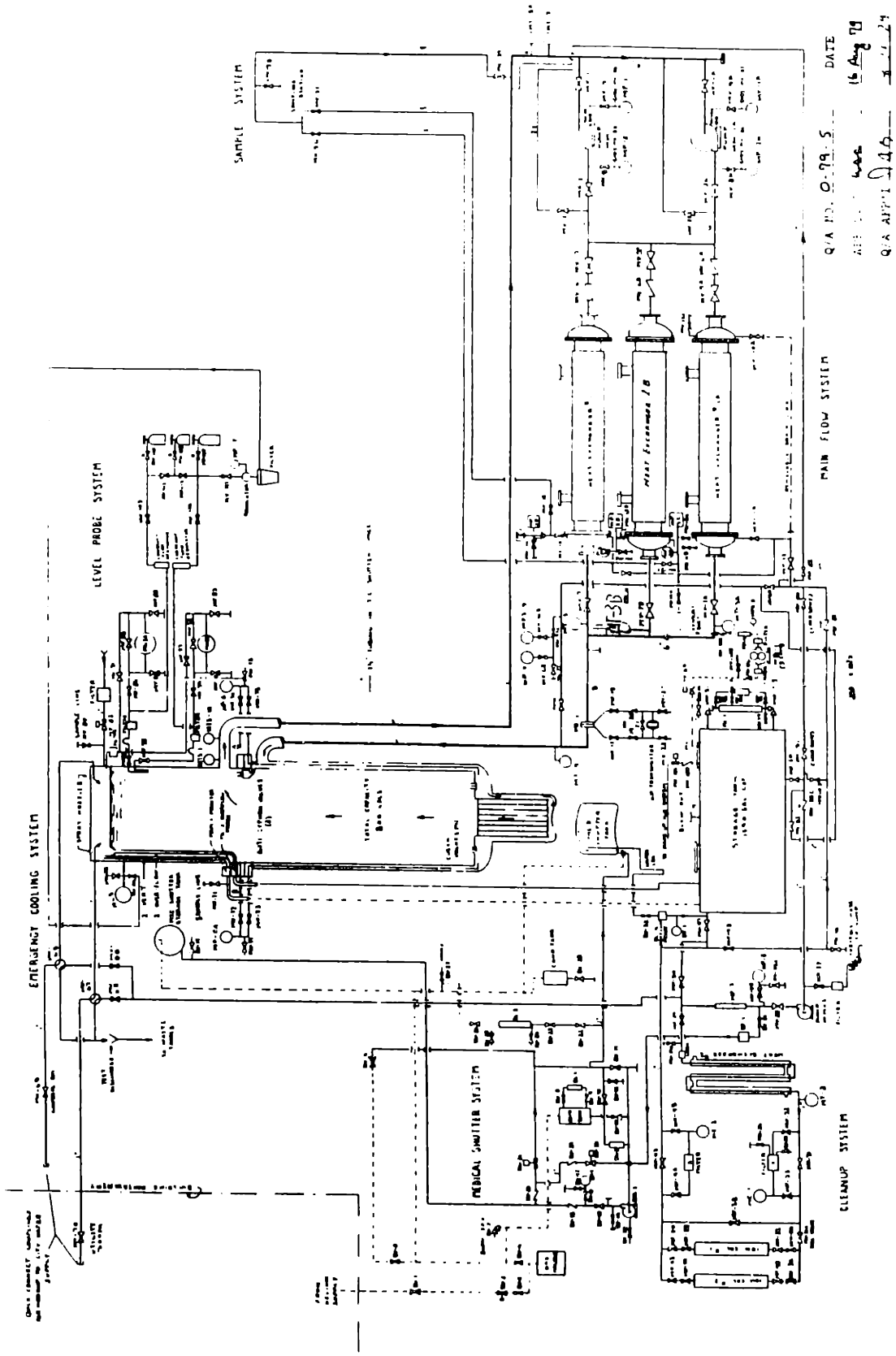

Figure 1.3-4. MITR-II Primary Coolant System[9]

[9] "MIT Research Reactor Systems Manual," ibid., page 3.18, Figure 3.2-1.

In the case of primary pump failure, a natural convective cooling loop is available to remove the decay heat from the core. This loop is shown in Figure 1.3-5. Under normal operation, this loop is maintained closed by the pressure difference generated by the primary coolant flow. When the flow decreases, the natural circulation valves open automatically and a natural convection loop driven by the density difference between the core and the downcomer is established. The flow shroud shown in Figure 1.3-5 was installed after the initial low-power testing of the MITR-II revealed significant power fluctuations whenever two primary pumps were operating[10]. The power fluctuations were attributed to control blade flutter caused by the water turbulence. In addition to preventing significant control blade oscillations, the flow shroud provides a chimney to enhance the driving force (buoyancy head) in the natural convection loop.

1.4 ORGANIZATION OF THESIS

The thermal models of the MITR loop components are presented in Chapter 2. The models include the primary system as well as the secondary side of the heat exchangers. Chapter 3 describes the momentum model of the MITR loop. This chapter is primarily concerned with the determination of the primary coolant flow rate. The point-kinetics and decay power models are presented in Chapter 4 along with a single-node fuel heat transfer model developed by J. E. Meyer[11]. Chapter 5 compares results obtained by running the code for some scenarios with available data. The results

---

[10] "MIT Research Reactor Systems Manual," ibid., page 1.8.

[11] Meyer, J. E., "Some Physical and Numerical Considerations for the SSC-S Code," BNL-NUREG-50913, 1978.

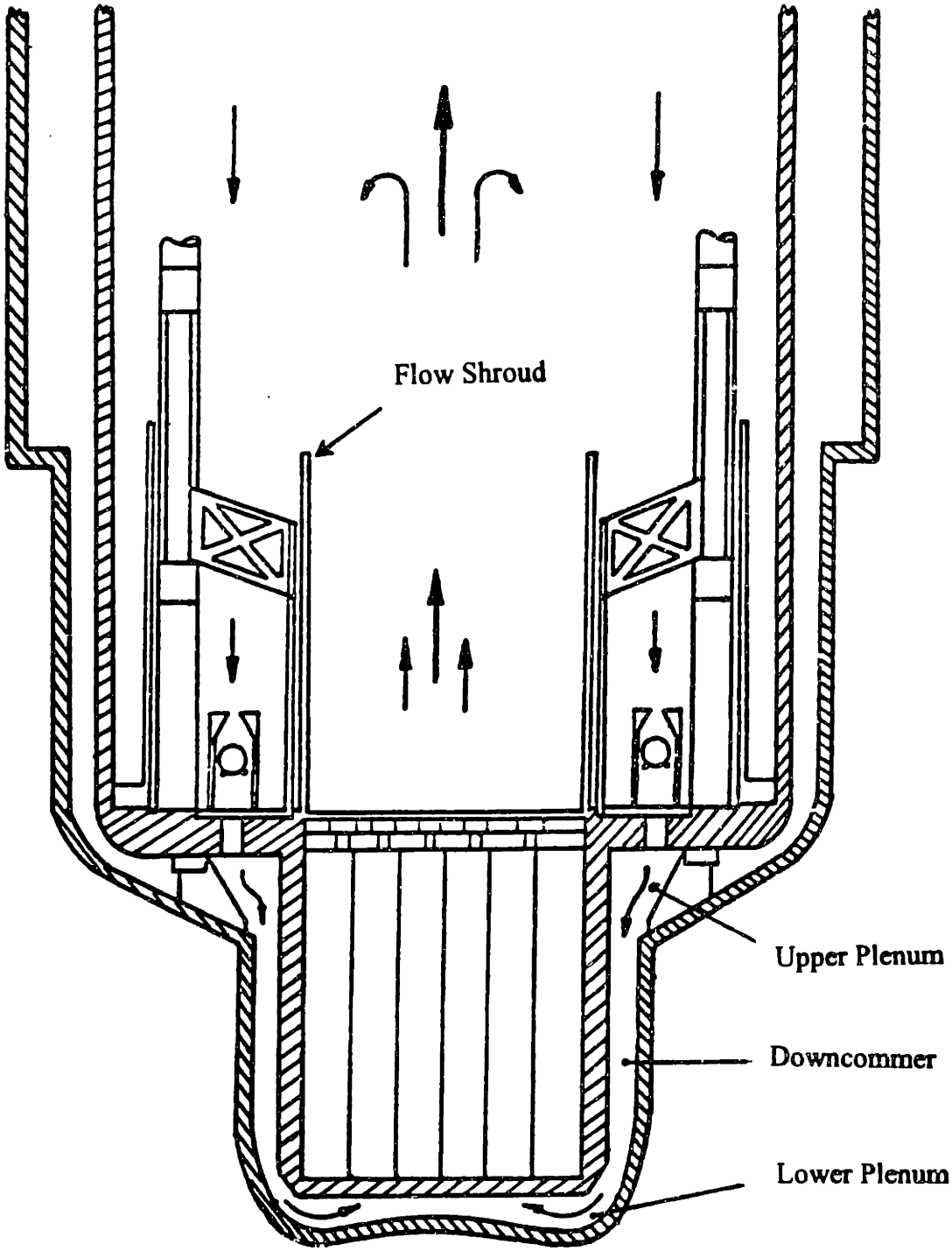

Figure 1.3-5. Natural Convection Loop[12]

[12] Bamdad-Haghighi, F., "Natural Convection analysis of the MITR-II During Loss of Flow Accident," Nucl. E. and S.M. Thesis, MIT Department of Nuclear Engineering, page 26, 1977.

of several transient simulations for MITR-II and MITR-III are also presented there. Finally, Chapter 6 contains a summary and suggested future work. Appendix A contains the nomenclature used throughout this thesis. The empirical correlations used are presented in Appendix B. In Appendix C, the user will find the necessary information to run the code effectively. Appendix D contains the code input data used in modeling the MITR transients presented in Chapter 5. Appendix E explains the method used in determining the initial conditions (steady-state calculations).

CHAPTER 2: MITR COMPONENTS THERMAL MODEL

2.1 INTRODUCTION

The control volume noding scheme used in modeling the MITR is shown in Figure 2.1. The primary coolant system is divided into the following components: reactor core, inside flow shroud, mixing area, underhead, hot leg, heat exchangers (2), and cold leg. The hot leg consists of the hot leg piping, the pump suction leg, pump impeller, and pump discharge leg. The cold leg consists of the cold leg piping and the downcomer. The inside flow shroud control volume is the region above the core surrounded by the flow shroud.

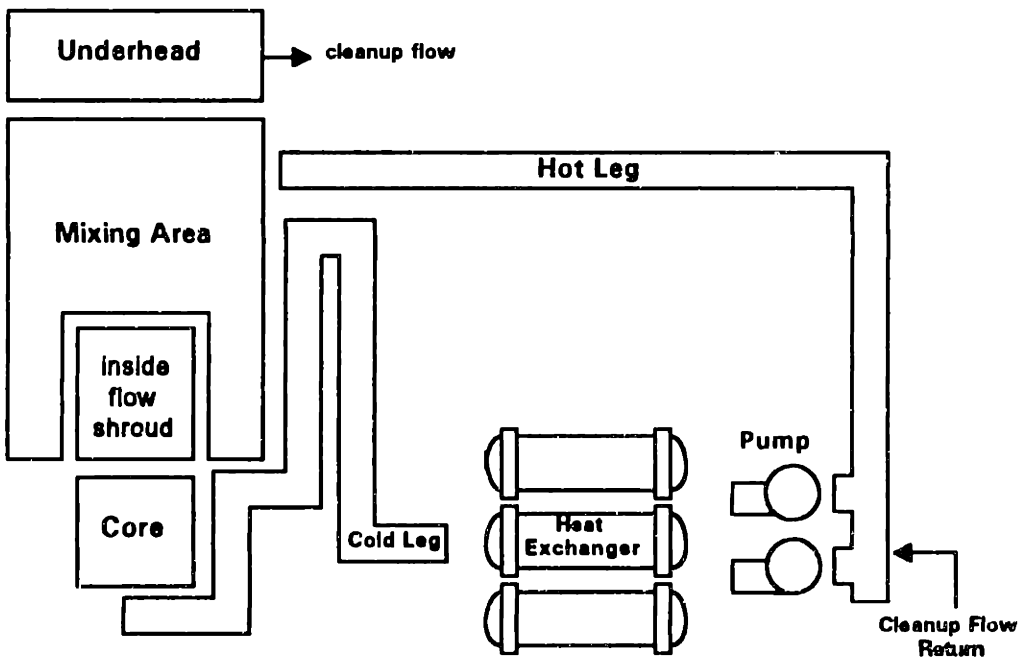

Figure 2.1. Control Volumes for MITR Thermal Model

The intent of this model is to reduce the number of control volumes (state variables) while maintaining the essential physical features. The mixing area control

volume has been chosen such that under steady-state conditions, a net mass flow rate equal to the cleanup flow rate exists between the mixing area and the underhead region.

2.2 ENERGY AND MASS CONSERVATION

A typical control volume is shown in Figure 2.2. The state variable for each control volume is chosen to be the mixture enthalpy, h, since the total mass and energy contents are functions of the mixture enthalpy and the pressure only. In evaluating the fluid properties, the pressure of the entire loop is assumed uniform and the reference value is taken at the top of the core. The mixture enthalpy is evaluated by adopting the Homogenous Equilibrium Model (HEM). The mass and energy conservation equations for a constant volume are as follows:

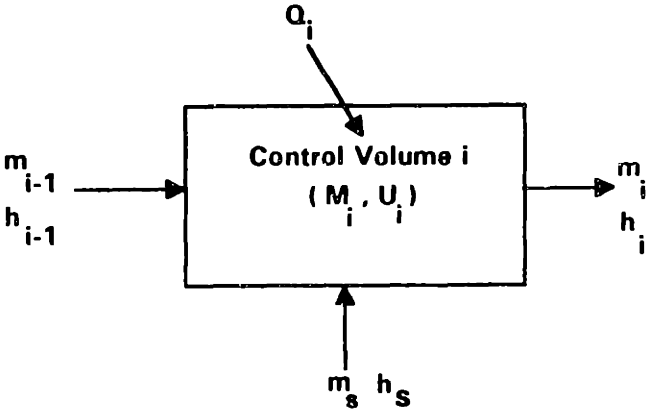

Figure 2.2. Typical Control Volume

$$\frac{dM_i}{dt} = m_{i-1} - m_i + m_s \tag{2.1}$$

and

$$\frac{dU_i}{dt} = (mh)_{i-1} - (mh)_i + (mh)_s + Q_i \tag{2.2}$$

where M_i and U_i are the total mass and internal energy content of control volume i. They can be defined as follows:

$$M_i \equiv \int_{V_i} \rho(h, p^*)\, dV \tag{2.3}$$

and

$$U_i \equiv \int_{V_i} \rho(h, p^*)\, h\, dV - p^* V_i \tag{2.4}$$

where $\rho(h, p^*)$ is the mixture density and p^* is a reference pressure for property evaluations (here taken to be the pressure at the top of the core).

The energy and mass conservation equations can be combined, resulting in an equation that is independent of enthalpy reference point[13]. This form is appropriate for use with approximate mass flow rates. The form is obtained by multiplying Equation 2.1 by an average mixture enthalpy of control volume i, $\langle h \rangle_i$, and subtracting the result from Equation 2.2 to obtain the following:

$$\frac{dU_i}{dt} - \langle h \rangle_i \frac{dM_i}{dt} = m_{i-1}(h_{i-1} - \langle h \rangle_i) - m_i(h_i - \langle h \rangle_i) + m_s(h_s - \langle h \rangle_i) + Q_i \tag{2.5}$$

where

$$\langle h \rangle_i = \frac{1}{2}(h_i + h_{i-1})$$

If the mass rate of change is small, we can assume that $m_i \approx m_{i-1} + m_s$. Then, Equation 2.5 becomes:

$$\frac{dU_i}{dt} - \langle h \rangle_i \frac{dM_i}{dt} = m_{i-1}(h_{i-1} - h_i) + m_s(h_s - h_i) + Q_i \tag{2.6}$$

---

[13] Kao, S. P, ibid., page 39.

The functional relationship for M_i and U_i in terms of h must be found in order to express Equation 2.6 in terms of the state variable. M_i and U_i can be defined in terms of the volume-averaged mixture density, $\langle\rho\rangle_i$, and the "volumetric" mixture enthalpy, $\langle e\rangle_i$, respectively as follows[14]:

$$M_i = \langle\rho\rangle_i V_i \tag{2.7}$$

and

$$U_i = \langle e\rangle_i V_i - p^* V_i \tag{2.8}$$

where $\langle\rho\rangle_i$ and $\langle e\rangle_i$ are defined in the following manner:

$$\langle\rho\rangle_i \equiv \frac{1}{V_i}\int_{V_i} \rho(h, p^*)\, dV \tag{2.9}$$

and

$$\langle e\rangle_i \equiv \frac{1}{V_i}\int_{V_i} \rho(h, p^*)\, h\, dV \tag{2.10}$$

Using a linear enthalpy profile assumption, and a linear transformation, $\langle\rho\rangle_i$ and $\langle e\rangle_i$ can be written as follows[15]:

$$\langle\rho\rangle_i \equiv \frac{1}{h_i - h_{i-1}}\int_{h_{i-1}}^{h_i} \rho(h, p^*)\, dh \tag{2.11}$$

and

$$\langle e\rangle_i \equiv \frac{1}{h_i - h_{i-1}}\int_{h_{i-1}}^{h_i} \rho(h, p^*)\, h\, dh \tag{2.12}$$

---

[14] Meyer, J. E. and Reinhard, E. A., "Numerical Techniques for Boiling Flow Stability Analyses," Trans. ASME Series C, 87, 311-312, 1965.

[15] Kao, S. P., ibid., pages 40-41.

By assuming that density varies linearly with enthalpy for subcooled liquid, and the specific volume varies linearly with enthalpy for a two-phase mixture, expressions for $\langle\rho\rangle_i$ and $\langle e\rangle_i$ can be obtained and are given in Tables 2.2-1 and 2.2-2[16].

Table 2.2-1

Volume-Averaged Density

Condition	$\langle\rho\rangle_i$
$h_{i-1} < h_i < h_f$	$\frac{1}{2}(\rho_i + \rho_{i-1})$
$h_{i-1} < h_f < h_i$	$\frac{1}{2}\beta(\rho_{i-1} + \rho_f) + \frac{(1-\beta)\ln\left(\frac{v_i}{v_f}\right)}{v_i - v_f}$ where $\beta = \left(\frac{h_f - h_{i-1}}{h_i - h_{i-1}}\right)$
$h_f < h_{i-1} < h_i$	$\frac{\ln\left(\frac{v_i}{v_f}\right)}{v_i - v_{i-1}}$

Table 2.2-2

Volume-Averaged "Enthalpy"

condition	$\langle e\rangle_i$
$h_{i-1} < h_i < h_f$	$\frac{1}{6}[(2h_i + h_{i-1})\rho_i + (2h_{i-1} + h_i)\rho_{i-1}]$
$h_{i-1} < h_f < h_i$	$\frac{\beta}{6}[(2h_{i-1} + h_f)\rho_{i-1} + (2h_{i-1} + h_f)\rho_{i-1}] +$ $(1-\beta)\left[\frac{h_i - h_f}{v_i - v_f} + \frac{(h_f v_i - h_i v_f)\ln\left(\frac{v_i}{v_f}\right)}{(v_i - v_f)^2}\right]$
$h_f < h_{i-1} < h_i$	$\frac{h_i - h_{i-1}}{v_i - v_{i-1}} + \frac{h_{i-1}v_i - h_i v_{i-1}}{(v_i - v_{i-1})^2}\ln\left(\frac{v_i}{v_{i-1}}\right)$

16 Kao, S. P., ibid., page 43.

Since M_i and U_i are functions of the inlet and exit enthalpy, Equation 2.6 can be written as follows:

$$\left(\frac{\partial u}{\partial h}\right)_i\left(\frac{dh}{dt}\right)_i+\left(\frac{\partial u_i}{\partial h}\right)_{i-1}\left(\frac{dh}{dt}\right)_{i-1}=m_{i-1}(h_{i-1}-h_i)+m_s(h_s-h_i)+Q_i \qquad (2.13)$$

where

$$\left(\frac{\partial u}{\partial h}\right)_i \equiv V_i\left[\left(\frac{\partial\langle e\rangle}{\partial h}\right)_i-\langle h\rangle_i\left(\frac{\partial\langle\rho\rangle}{\partial h}\right)_i\right]$$

and

$$\left(\frac{\partial u_i}{\partial h}\right)_{i-1} \equiv V_i\left[\left(\frac{\partial\langle e\rangle_i}{\partial h}\right)_{i-1}-\langle h\rangle_i\left(\frac{\partial\langle\rho\rangle_i}{\partial h}\right)_{i-1}\right]$$

The mass conservation equation can also be rewritten in the following manner:

$$\left(\frac{\partial M}{\partial h}\right)_i\left(\frac{dh}{dt}\right)_i+\left(\frac{\partial M_i}{\partial h}\right)_{i-1}\left(\frac{dh}{dt}\right)_{i-1}=m_{i-1}-m_i+m_s \qquad (2.14)$$

where

$$\left(\frac{\partial M}{\partial h}\right)_i=V_i\left(\frac{\partial\langle\rho\rangle}{\partial h}\right)_i \quad \text{and} \quad \left(\frac{\partial M_i}{\partial h}\right)_{i-1}=V_i\left(\frac{\partial\langle\rho\rangle_i}{\partial h}\right)_{i-1}$$

The partial derivatives in Equations 2.13 and 2.14 are given in Table 2.2-3[17].

Table 2.2-3

Partial Derivatives of Equations 2.13 and 2.14

Partial	Approximation
$\left(\frac{\partial\langle\rho\rangle}{\partial h}\right)_i$	$\frac{\rho_i-\langle\rho\rangle_i}{h_i-h_{i-1}}$
$\left(\frac{\partial\langle\rho\rangle_i}{\partial h}\right)_{i-1}$	$\frac{\langle\rho\rangle_i-\rho_{i-1}}{h_i-h_{i-1}}$
$\left(\frac{\partial\langle e\rangle}{\partial h}\right)_i$	$\frac{(\rho h)_i-\langle e\rangle_i}{h_i-h_{i-1}}$
$\left(\frac{\partial\langle e\rangle_i}{\partial h}\right)_{i-1}$	$\frac{\langle e\rangle_i-(\rho h)_{i-1}}{h_i-h_{i-1}}$

[17] Kao, S. P., ibid., page 46.

Equations 2.13 and 2.14 have an undesirable numerical behavior in that any rapid changes at the control volume inlet are immediately propagated to the outlet. To avoid this numerical behavior, a donor-cell differencing technique is adopted and is described in Section 2.4.

2.3 SPECIAL CONTROL VOLUMES

Until this point all of the equations obtained were for the typical control volume of Figure 2.2 using a linear enthalpy profile assumption. However, for the inside flow shroud, mixing area and the underhead regions a complete enthalpy mixing assumption has been adopted instead. Therefore, following is the conservation of mass and energy for the control volume shown in Figure 2.2 with an uniform enthalpy profile assumption.

$$\frac{d\langle M\rangle_i}{dt} = m_{i-1} - m_i + m_s \tag{2.15}$$

$$\frac{d\langle U\rangle_i}{dt} = (mh)_{i-1} - (mh)_i + (mh)_s - p^* \frac{dV_i}{dt} \tag{2.16}$$

where

$$\langle M\rangle_i = V_i \rho_i$$

and

$$\langle U\rangle_i = \langle M\rangle_i h_i - p^* V_i$$

Notice that in defining the mass and energy contents of control volume i, no distinction is made between the outlet and the average mixture density due to the uniform enthalpy profile. The same applies to the mixture enthalpy.

By multiplying Equation 2.15 by h_i, subtracting the result from Equation 2.16, and assuming that p* changes slowly so that $V_i\frac{dp^*}{dt}$ can be set equal to zero, the following equation is obtained.

$$\langle M\rangle_i\left(\frac{dh}{dt}\right)_i = m_{i-1}(h_{i-1}-h_i)+m_s(h_s-h_i) \tag{2.17}$$

The time rate of change of the mass in the control volume can be written as follows:

$$\frac{d\langle M\rangle_i}{dt} = V_i\left(\frac{\partial\langle\rho\rangle}{\partial\langle h\rangle}\right)_i\left(\frac{dh}{dt}\right)_i+\rho_i\left(\frac{dV}{dt}\right)_i = m_{i-1}-m_i+m_s \tag{2.18}$$

In the case of a control volume which has a level and a constant cross-sectional area, an equation for the fluid level can be written as follows:

$$(LA)_i\left(\frac{\partial\langle\rho\rangle}{\partial\langle h\rangle}\right)_i\left(\frac{d\langle h\rangle}{dt}\right)_i+(\rho A)_i\left(\frac{dL}{dt}\right)_i = m_{i-1}-m_i+m_s \tag{2.19}$$

where A is the cross-sectional area of control volume i, and L is the liquid level in control volume i. Equation 2.19 can be written numerically in a semi-implicit form:

$$(\rho A)_i^n\Delta L_i^{n+1}+(AL)_i^n\left(\frac{\partial\langle\rho\rangle}{\partial\langle h\rangle}\right)^n_i\Delta h_i^{n+1} = \Delta t\,(m_{i-1}-m_i+m_s)^{n+1} \tag{2.20}$$

Equation 2.20 can be applied to the underhead region to determine the water level at each time step. If the water level drops below the bottom of the underhead region, equation

2.20 is then applied to the mixing area control volume. However, the water level is not allowed to drop below the anti-siphon valve height.

2.4 DONOR-CELL DIFFERENCING SCHEME

As previously mentioned, Equations 2.13 and 2.14 have an undesirable numerical behavior. To avoid this behavior, a donor-cell differencing scheme is utilized by replacing the left-hand side of Equation 2.13 by the following[18]:

$$\left(\frac{\partial u}{\partial h}\right)_i\left(\frac{dh}{dt}\right)_i+\left(\frac{\partial u_i}{\partial h}\right)_{i-1}\left(\frac{dh}{dt}\right)_{i-1}=\left[\left(\frac{\partial u}{\partial h}\right)_i+\left(\frac{\partial u_i}{\partial h}\right)_{i-1}\right]\left(\frac{dh}{dt}\right)_i\equiv\left(\frac{\partial u}{\partial h}\right)_{i,i-1}\left(\frac{dh}{dt}\right)_i \qquad (2.21)$$

where

$$\left(\frac{\partial u}{\partial h}\right)_{i,i-1}\equiv V_i\left\{\left(\frac{\partial\langle e\rangle}{\partial h}\right)_i+\left(\frac{\partial\langle e\rangle_i}{\partial h}\right)_{i-1}-\langle h\rangle_i\left[\left(\frac{\partial\langle\rho\rangle}{\partial h}\right)_i+\left(\frac{\partial\langle\rho\rangle_i}{\partial h}\right)_{i-1}\right]\right\}$$

Applying the donor-cell differencing scheme to the energy conservation equation, the resulting equation is as follows:

$$\left(\frac{\partial u}{\partial h}\right)_{i,i-1}\left(\frac{dh}{dt}\right)_i=m_{i-1}(h_{i-1}-h_i)+m_s(h_s-h_i)+Q_i \qquad (2.22)$$

To solve Equation 2.22 numerically, an implicit finite-difference equation is obtained:

$$\left(\frac{\partial u}{\partial h}\right)_{i,i-1}^{n}\Delta h_i^{n+1}=\Delta t\, m_{i-1}^{n+1}(h_{i-1}-h_i)^{n+1}+\Delta t\, m_s^{n+1}(h_s-h_i)^{n+1}+\Delta t\, Q_i^{n+1} \qquad (2.23)$$

where

$$\Delta h_i^{n+1}=h_i^{n+1}-h_i^n$$

---

[18] Kao, S. P., ibid., page 47.

The superscripts n and n+1 represent the present and advanced time indices, respectively. The new enthalpy, that is the enthalpy at time n+1, can be written as $h^{n+1} = h^n + \Delta h^{n+1}$. Inserting this expression into Equation 2.23 yields the following:

$$\left[\left(\frac{\partial u}{\partial h}\right)^n_{i,i-1} + \Delta t\, m^{n+1}_{i-1} + \Delta t\, m^{n+1}_{s}\right]\Delta h^{n+1}_i - \Delta t\, m^{n+1}_{i-1}\Delta h^{n+1}_{i-1} = \Delta t\, m^{n+1}_{i-1}(h_{i-1} - h_i)^n +$$

$$\Delta t\, m^{n+1}_{s}(h^{n+1}_{s} - h^n_i) + \Delta t\, Q^{n+1}_i \qquad (2.24)$$

In the following sections, Equations 2.24 and 2.17 are applied to the relevant control volumes of the MITR.

2.4.1 CORE

The following figure illustrates the core control volume and its boundary conditions. The core consists of the fuel elements and structural material. The heat source, Q_{th}, is the thermal power deposited within the core, produced from fission reactions and decay heat from fission products and activated elements. A small portion of this heat is deposited directly into the coolant while most of the heat is transferred to the coolant convectively.

As shown in Figure 2.4.1, some of the primary flow bypasses the core. This bypass flow goes directly to the mixing area. It is assumed that the multiple enthalpies at the inlet of the mixing area mix instantaneously.

Since the downcomer surrounds the core, there is a possible transfer of heat from the core to the downcomer through the core housing. This rate of heat transfer depends

on the average temperature difference between the core and the downcomer. However, the magnitude of this heat transfer is negligible (less than 1 % of core power) and thus ignored.

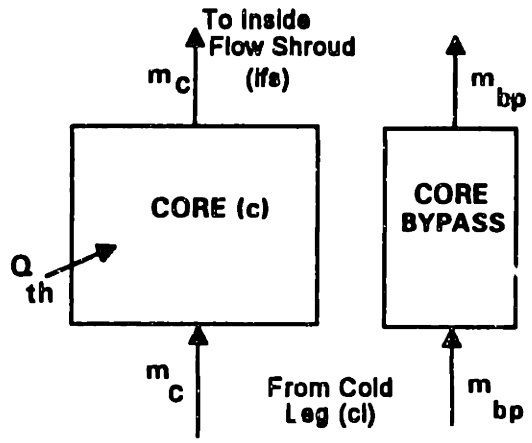

Figure 2.4.1. Core Control Volume

Applying Equation 2.24 to the core control volume with no external mass flow rate source, m_s, the following equation is obtained:

$$\left[\left(\frac{\partial u}{\partial h}\right)^{n}_{c,cl} + \Delta t\, m_c^{n+1}\right]\Delta h_c^{n+1} - \Delta t\, m_c^{n+1}\Delta h_{cl}^{n+1} = \Delta t\, m_c^{n+1}(h_{cl} - h_c)^n + \Delta t\, Q_{th}^{n+1} \qquad (2.25)$$

The core hot channel has been modeled here also. The flow through the hot channel is assumed to be the nominal channel flow times a user specified flow disparity. In addition, the heat deposited into the hot-channel is calculated as the nominal heat per channel times the radial nuclear peaking factor and the enthalpy-rise engineering hot-channel factor. The radial peaking factor and the enthalpy-rise engineering hot-channel factor are specified by the user.

2.4.2 INSIDE FLOW SHROUD

After the reactor startup tests, control blade oscillations were observed and attributed to the primary coolant flowing along the control blades. As a consequence, a hexagonal flow shroud was installed above the core preventing significant control blade vibration. In addition to preventing control blade oscillations, the shroud acts as a chimney enhancing the buoyancy pressure head during natural circulation.

The inside flow shroud, mixing area, and underhead control volumes differ from the other control volumes in that a complete enthalpy mixing assumption is made. That is, the enthalpy profile across its entire volume is assumed uniform. The following figure illustrates the inside flow shroud control volume.

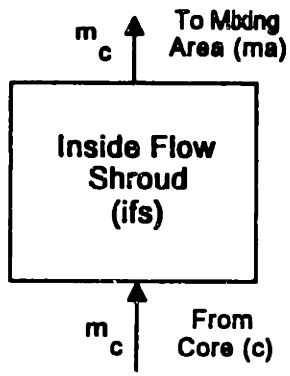

Figure 2.4.2. Inside Flow Shroud Control Volume

Applying Equation 2.17 to the inside flow shroud control volume, one obtains the following equation:

$$\langle M\rangle^{n}_{ifs}\Delta h^{n+1}_{ifs} + \Delta t\, m^{n+1}_{c}\Delta h^{n+1}_{ifs} - \Delta t\, m^{n+1}_{c}\Delta h^{n+1}_{c} = \Delta t\, m^{n+1}_{c}(h_{c} - h_{ifs})^{n} \qquad (2.26)$$

2.4.3 MIXING AREA

The mixing area is connected to the underhead region by a mixing and a surge flow. The mixing flow occurs even in the absence of a transient and tends to thermally equilibrate these control volumes. This flow was modeled as an exchange of equal mass flows between the mixing area and underhead region. Although this phenomenon does not lead to net flow between the control volumes, energy is exchanged.

In a transient scenario where the fluid expands or contracts thermally, a surge flow, m_{su}, occurs between the mixing area and the underhead region. The mixing area is connected to the downcomer through four natural circulation valves since, in the case of a loss-of-flow transient, the fission product decay heat must be removed by natural convective cooling. Also, the reactor core tank was designed to avoid full drainage in the case of a loss-of-coolant accident by providing two anti-siphon valves near the top of the mixing area region. However, the anti-siphon valves are not modeled here except as to prohibit the water level from dropping below their height. The following figure illustrates the mixing area control volume with its boundary conditions.

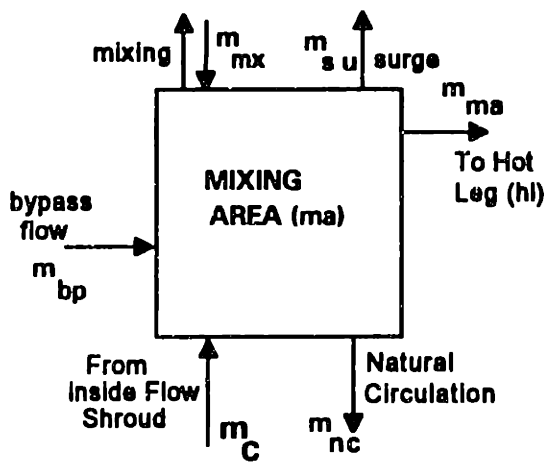

Figure 2.4.3. Mixing Area Control Volume

Although there is a possible heat transfer between the mixing area and the downcomer through the core housing, it has been neglected since its magnitude is small compared to the convective heat transfer. Applying Equation 2.17 to the mixing area control volume, one obtains the following equation:

$$\langle M\rangle^{n}_{ma}\Delta h^{n+1}_{ma} - \Delta t\, m^{n+1}_{c}\Delta h^{n+1}_{ifs} + \Delta t\, m^{n+1}_{c}\Delta h^{n+1}_{ma} - \Delta t\, m^{n}_{su}\Delta h^{n+1}_{ma} + \Delta t m^{n}_{su}\Delta h^{n+1}_{su} -$$

$$\Delta t\, m^{n+1}_{mx}\Delta h^{n+1}_{uh} + \Delta t\, m^{n+1}_{mx}\Delta h^{n+1}_{ma} - \Delta t\, m^{n+1}_{nc}\Delta h^{n+1}_{ma} + \Delta t\, m^{n+1}_{nc}\Delta h^{n+1}_{nc} - \Delta t\, m^{n+1}_{bp}\Delta h^{n+1}_{cl} +$$

$$\Delta t\, m^{n+1}_{bp}\Delta h^{n+1}_{ma} = \Delta t\, m^{n+1}_{c}(h_{ifs} - h_{ma})^{n} + \Delta t\, m^{n+1}_{mx}(h_{uh} - h_{ma})^{n} + \Delta t\, m^{n+1}_{bp}(h_{cl} - h_{ma})^{n} -$$

$$\Delta t\, m^{n}_{su}(h_{su} - h_{ma})^{n} - \Delta t\, m^{n+1}_{nc}(h_{nc} - h_{ma})^{n} \qquad (2.27)$$

Note: $h_{su} = \left\{ \begin{array}{l} h_{ma}\text{ , when } m_{su} > 0 \\ h_{uh}\text{ , when } m_{su} < 0 \end{array} \right\}$ and $h_{nc} = \left\{ \begin{array}{l} h_{ma}\text{ , when } m_{nc} > 0 \\ h_{cl}\text{ , when } m_{nc} < 0 \end{array} \right\}$

2.4.4 UNDERHEAD

The underhead region provides a surge volume to compensate for coolant volume changes due to thermal expansion and contraction. Like the mixing area, the underhead enthalpy is assumed to be completely mixed.

It is from this control volume that the cleanup flow is extracted. This flow, as the name implies, is extracted from the primary flow path to clean and maintain the purity of the primary system coolant. In addition, it acts to maintain the water level in the core tank constant by means of continuous overflow. An off gas system is provided to remove radioactive gas from the top of the underhead region. This system also maintains the pressure at the top of the liquid slightly below atmospheric pressure.

An emergency core cooling system (ECCS) is located close to the top of the core tank. The ECCS consists of two spray nozzles and their associated piping. However, the emergency core cooling system is not modeled here since it is beyond the scope of this thesis. The following figure illustrates the underhead control volume model (ECCS not included).

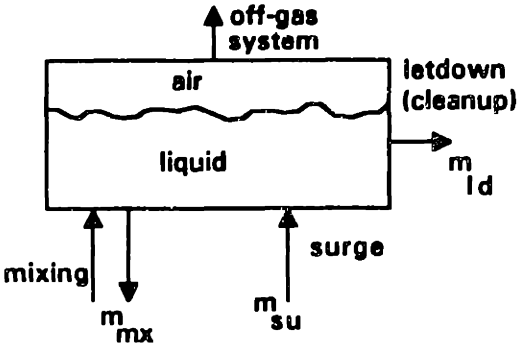

Figure 2.4.4. Underhead Control Volume

Applying Equation 2.17 to the underhead control volume, one obtains the following equation:

$$\langle M\rangle_{uh}^{n}\Delta h_{uh}^{n+1} - \Delta t\, m_{mx}^{n+1}\Delta h_{mx}^{n+1} + \Delta t\, m_{mx}^{n+1}\Delta h_{uh}^{n+1} + \Delta t\, m_{su}^{n}\Delta h_{uh}^{n+1} - \Delta t\, m_{su}^{n}\Delta h_{su}^{n+1} =$$

$$\Delta t\, m_{su}^{n}(h_{su} - h_{uh})^{n} + \Delta t\, m_{mx}^{n+1}(h_{mx} - h_{uh})^{n} \qquad (2.28)$$

2.4.5 HOT LEG

The hot leg control volume consists of the hot leg piping, the pumps' suction legs, the pumps' impellers, and the pumps' discharge legs.

The cleanup system discharges flow into the primary coolant pumps' suction and is, therefore, the external mass flow rate source, m_{ch} , of this control volume. However, when the reactor is operated in a shutdown cooling mode, the cleanup flow discharges directly to the reactor's inlet line. The hot leg control volume is illustrated in the following figure.

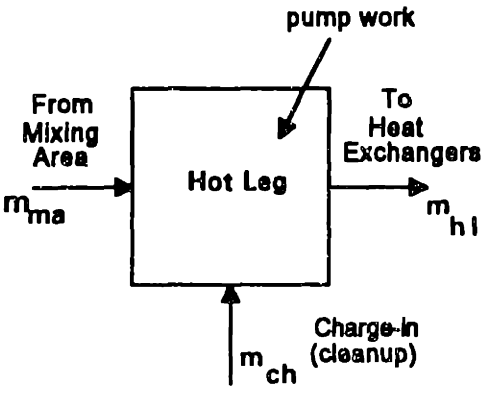

Figure 2.4.5. Hot Leg Control Volume

Applying Equation 2.24 to the hot leg control volume, one obtains the following equation:

$$\left(\frac{\partial u}{\partial h}\right)^{n}_{hl,\,ma} \Delta h_{hl}^{n+1} - \Delta t\, m_{ma}^{n+1} \Delta h_{ma}^{n+1} + \Delta t\, m_{ma}^{n+1} \Delta h_{hl}^{n+1} + \Delta t\, m_{ch}^{n+1} \Delta h_{hl}^{n+1} =$$

$$\Delta t\, m_{ch}^{n+1} (h_{ch}^{n+1} - h_{hl}^{n}) + \Delta t\, m_{ma}^{n+1} (h_{ma} - h_{hl})^{n} + \Delta t \sum_{j} m(j)^{n+1} \frac{\Delta p(j)_{pump}^{n+1}}{\rho_{hl}^{n}} \qquad (2.29)$$

where j is the pump index and $\Delta p(j)_{pump}^{n+1}$ represents the pressure rise across pump j at the advanced time.

2.4.6 HEAT EXCHANGERS (Primary Side)

The MITR has three heat exchangers: two Ram'en-type lamella heat exchangers and one shell-and-tube heat exchanger. Under normal operations, only two of the heat exchangers are used. The heat exchanger transfers the heat from the primary coolant to the secondary coolant where it is ultimately transferred to the atmosphere via cooling towers. In addition to the heat removed by the secondary coolant, Q_{hx} , some of the primary coolant heat is stored in the heat exchanger metal. Since the inlet piping is common to both heat exchangers, it is assumed that the inlet enthalpy to each heat exchanger is the same. The following figure represents the heat exchanger control volume.

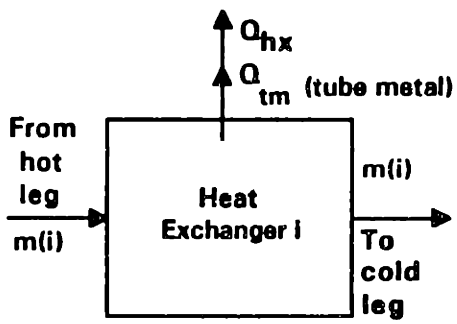

Figure 2.4.6. Heat Exchanger Control Volume

Applying Equation 2.22 to the heat exchanger control volume, one obtains the following equation:

$$\left(\frac{\partial u}{\partial h}\right)^{n}_{hx(i),hl} \Delta h^{n+1}_{hx(i)} - \Delta t\, m(i)^{n+1} \Delta h^{n+1}_{hl} + \Delta t\, m(i)^{n+1} \Delta h^{n+1}_{hx(i)} + \frac{1}{2}\left(\frac{[V\rho C_p]_{tm(i)}}{(C_p)_{hx(i)}}\right)\Delta h^{n+1}_{hx(i)} =$$

$$\Delta t\, m(i)^{n+1}(h_{hl} - h_{hx(i)})^{n} - \Delta t\, Q^{n+1}_{hx(i)} \qquad (2.30)$$

2.4.7 COLD LEG

The cold leg control volume consists of the cold leg piping and the reactor downcomer. There are multiple enthalpies at the cold leg inlet due to more than one heat exchanger discharging flow to the cold leg. Therefore, for Equations 2.11 and 2.12 to be well-defined, an instantaneous enthalpy mixing approximation at the cold leg inlet is adopted.

To incorporate loss-of-coolant capacity into the model, a leakage flow, m_b, is extracted from the cold leg at the average cold leg temperature. The following figure illustrates the cold leg control volume model.

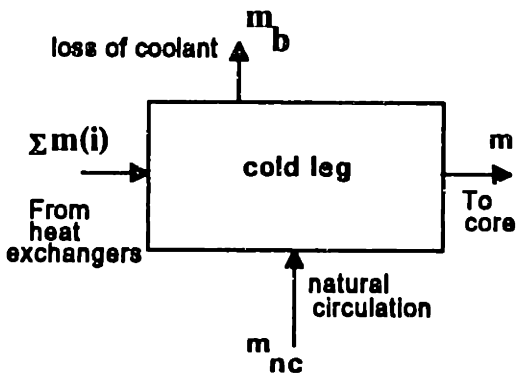

Figure 2.4.7. Cold Leg Control Volume

Applying Equation 2.24 to the cold leg control volume, one obtains the following equation:

$$\left(\frac{\partial u}{\partial h}\right)^{n}_{cl,hx}\Delta h_{cl}^{n+1} - \Delta t\sum_{i} m(i)^{n+1}\Delta h_{hx(i)}^{n+1} - \Delta t\, m_{nc}^{n+1}\Delta h_{nc}^{n+1} + \Delta t\sum_{i} m(i)^{n+1}\Delta h_{cl}^{n+1} +$$

$$\Delta t\, m_{nc}^{n+1}\Delta h_{cl}^{n+1} - \Delta t\, m_{b}^{n+1}\Delta h_{cl}^{n+1} = \Delta t\, m_{nc}^{n+1}(h_{nc} - h_{cl})^{n} +$$

$$\Delta t\, m_{b}^{n+1}(h_{cl} - \langle h\rangle_{cl})^{n} + \Delta t\sum_{i} m(i)^{n+1}(h_{hx(i)} - h_{cl})^{n} \qquad (2.31)$$

Note that heat transfer to the heavy water tank is neglected.

2.4.8 OVERALL MASS CONSERVATION

In solving the mass conservation equation of each control volume, a slow mass rate of change approximation was adopted (i.e., $m_i \approx m_{i-1} + m_s$). As a consequence, no meaningful information can be obtained from each individual control volume conservation equation. A mass conservation equation for the entire MITR primary system must be used. However, since the underhead region water level is variable, a separate equation will be written to determine the underhead region liquid level (Equation 2.20). The following equation represents the mass conservation for the entire loop excluding the underhead region, and it is used until the underhead region empties completely.

$$\left(\frac{\partial M}{\partial h}\right)_{cl}^{n} \Delta h_{cl}^{n+1} + \left(\frac{\partial M_{cl}}{\partial h}\right)_{hx1}^{n} \Delta h_{hx1}^{n+1} + \left(\frac{\partial M_{cl}}{\partial h}\right)_{hx2}^{n} \Delta h_{hx2}^{n+1} + \left(\frac{\partial M}{\partial h}\right)_{c}^{n} \Delta h_{c}^{n+1} + \left(\frac{\partial M_{c}}{\partial h}\right)_{cl}^{n} \Delta h_{ci}^{n+1} +$$

$$V_{ifs}\left(\frac{\partial \langle \rho \rangle}{\partial \langle h \rangle}\right)_{ifs} + V_{ma}\left(\frac{\partial \langle \rho \rangle}{\partial \langle h \rangle}\right)_{ma}^{n} \Delta h_{ma}^{n+1} + \left(\frac{\partial M}{\partial h}\right)_{hl}^{n} \Delta h_{hl}^{n+1} + \left(\frac{\partial M_{hl}}{\partial h}\right)_{ma}^{n} \Delta h_{ma}^{n+1} +$$

$$\left(\frac{\partial M}{\partial h}\right)_{hx1}^{n} \Delta h_{hx1}^{n+1} + \left(\frac{\partial M_{hx1}}{\partial h}\right)_{hl}^{n} \Delta h_{hl}^{n+1} + \left(\frac{\partial M}{\partial h}\right)_{hx2}^{n} \Delta h_{hx2}^{n+1} + \left(\frac{\partial M_{hx2}}{\partial h}\right)_{hl}^{n} \Delta h_{hl}^{n+1} =$$

$$\Delta t \, (m_{ch}^{n+1} - m_{b}^{n+1} - m_{su}^{n}) \qquad (2.32)$$

If the water level drops below the top of the mixing area the surge flow is set equal to zero and Equation 2.32 is rewritten to allow for a variable mixing area water level. Therefore, the following equation along with a water level equation for the mixing area (Equation 2.20) is used instead.

$$\left(\frac{\partial M}{\partial h}\right)_{cl}^{n}\Delta h_{cl}^{n+1}+\left(\frac{\partial M_{cl}}{\partial h}\right)_{hx1}^{n}\Delta h_{hx1}^{n+1}+\left(\frac{\partial M_{cl}}{\partial h}\right)_{hx2}^{n}\Delta h_{hx2}^{n+1}+\left(\frac{\partial M}{\partial h}\right)_{c}^{n}\Delta h_{c}^{n+1}+\left(\frac{\partial M_{c}}{\partial h}\right)_{cl}^{n}\Delta h_{cl}^{n+1}+$$

$$V_{lfs}\left(\frac{\partial\langle\rho\rangle}{\partial\langle h\rangle}\right)_{lfs}+\left(\frac{\partial M}{\partial h}\right)_{hl}^{n}\Delta h_{hl}^{n+1}+\left(\frac{\partial M_{hl}}{\partial h}\right)_{ma}^{n}\Delta h_{ma}^{n+1}+\left(\frac{\partial M}{\partial h}\right)_{hx1}^{n}\Delta h_{hx1}^{n+1}+\left(\frac{\partial M_{hx1}}{\partial h}\right)_{hl}^{n}\Delta h_{hl}^{n+1}+$$

$$\left(\frac{\partial M}{\partial h}\right)_{hx2}^{n}\Delta h_{hx2}^{n+1}+\left(\frac{\partial M_{hx2}}{\partial h}\right)_{hl}^{n}\Delta h_{hl}^{n+1}=\Delta t\,(m_{ch}-m_{b}-m+m_{ma}+m_{nc})^{n+1} \qquad (2.33)$$

2.5 HEAT EXCHANGER HEAT TRANSFER MODEL

The heat exchanger energy transfer rate is calculated using the log-mean temperature difference between the primary and secondary system and the overall heat transfer coefficient[19]. The heat transfer rate can be written as follows:

$$Q_{hx}=U_o\,A_o\,\Delta T_{lm} \qquad (2.34)$$

where

ΔT_{lm} = log-mean temperature difference;

A_o = total outside surface area of heat exchanger; and

U_o = overall heat transfer coefficient based on the outside surface area

The overall heat transfer coefficient for a shell-and-tube heat exchanger is given by:

$$\frac{1}{U_o}=\frac{A_o}{h_i A_i}+\frac{r_o \ln\left(\frac{r_o}{r_i}\right)}{k_t}+\frac{1}{h_o}+r_{ff} \qquad (2.35)$$

---

[19] Strohmayer, W. H., "Dynamic Modeling of a vertical U-Tube Steam Generators for Operational Safety Systems," Ph.D. Thesis, MIT Department of Nuclear Engineering, page 4-19, 1982.

where

h_i = heat transfer coefficient on the secondary side

h_o = heat transfer coefficient on the primary side

A_i = Total surface area of heat exchanger primary side

k_t = tubes thermal conductivity

r_{ff} = fouling factor

The lamella heat exchangers are modeled as flat plates; thus, the overall heat transfer coefficient is given by:

$$\frac{1}{U_o A_o} = \frac{1}{h_i A_i} + \frac{d}{k_t A_o} + \frac{1}{h_o A_o} + r'_{ff} \tag{2.36}$$

where d is the lamella plate thickness. The log-mean temperature difference is as follows:

$$\Delta T_{lm} = \frac{(T_{pi} - T_{so}) - (T_{po} - T_{si})}{\ln\left(\frac{T_{pi} - T_{so}}{T_{po} - T_{si}}\right)} \tag{2.37}$$

where the subscripts *pi* and *po* represent the primary inlet and outlet to the heat exchanger respectively and *si* and *so* represent the secondary inlet and outlet respectively. If in a transient the secondary inlet temperature becomes larger than the primary outlet temperature or the primary inlet temperature drops below the secondary outlet temperature, Equation 2.37 becomes undefined. A method developed by Strohmayer

overcomes this difficulty[20]. If the difference between the primary outlet and secondary inlet temperature drops below a small specified number ε (e.g., ε = 1 °C), the log-mean temperature difference is replaced by the following average temperature difference:

$$\Delta\langle T\rangle_{hx} = \eta(T_{pi} - T_{so}) + (1-\eta)(T_{po} - T_{si}) \tag{2.38}$$

where the weighting factor, η, is defined as follows:

$$\eta(T_{pi} - T_{so}) + (1-\eta)\varepsilon = \Delta T^{*}_{lm} \tag{2.39}$$

and the reference log-mean temperature difference, ΔT^{*}_{lm}, is based on the temperature difference ε and is defined in the following manner:

$$\Delta T^{*}_{lm} = \frac{(T_{pi} - T_{so}) - \varepsilon}{\ln\left(\frac{T_{pi}-T_{so}}{\varepsilon}\right)} \tag{2.40}$$

Similarly, if the difference between the primary outlet and secondary inlet temperatures drops below ε, the log-mean temperature difference is replaced by the average temperature difference defined in Equation 2.38. However, the weighting factor becomes:

$$(1-\eta)(T_{po} - T_{si}) + \eta\varepsilon = \Delta T^{*}_{lm} \tag{2.41}$$

and the reference log-mean temperature difference is

$$\Delta T^{*}_{lm} = \frac{\varepsilon - (T_{po} - T_{si})}{\ln\left(\frac{\varepsilon}{T_{po}-T_{si}}\right)} \tag{2.42}$$

---

[20] Strohmayer, W. H., ibid., Chapter 4, pages 20-25.

The energy conservation on the secondary side of the heat exchanger can be formulated by using a control volume similar to the one used for the primary side. A figure of the heat exchanger secondary side control volume follows.

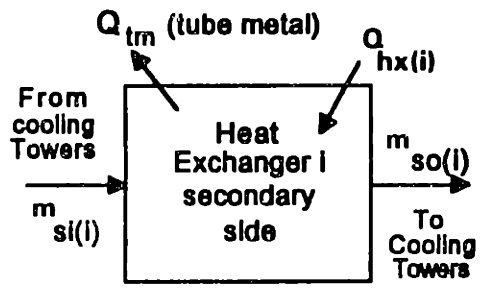

Figure 2.5. Heat exchanger Secondary Side

Applying Equation 2.24 to the heat exchanger secondary side control volume, one obtains the following equation:

$$\left(\frac{\partial u}{\partial h}\right)^{n}_{sk(i),so(i)} \Delta h^{n+1}_{so(i)} + \Delta t\, m^{n+1}_{sk(i)} \Delta h^{n+1}_{so(i)} = \Delta t\, m^{n+1}_{sk(i)} (h^{n+1}_{sk(i)} - h^{n}_{so(i)}) + \Delta t\, Q^{n+1}_{hx(i)} \qquad (2.43)$$

The heat transfer rate at the advanced time can be approximated as follows:

$$Q^{n+1}_{hx(i)} = Q^{n}_{hx(i)} + \left(\frac{\partial Q_{hx(i)}}{\partial h_{sk(i)}}\right)^{n} \Delta h^{n+1}_{sk(i)} + \left(\frac{\partial Q_{hx(i)}}{\partial h_{so(i)}}\right)^{n} \Delta h^{n+1}_{so(i)} + \left(\frac{\partial Q_{hx(i)}}{\partial h_{hl}}\right)^{n} \Delta h^{n+1}_{hl} +$$

$$\left(\frac{\partial Q_{hx(i)}}{\partial h_{hx(i)}}\right)^{n} \Delta h^{n+1}_{hx(i)} \qquad (2.44)$$

2.6 THERMAL STATE-SPACE MODEL

The state-space model for the MITR loop consists of eleven conservation equations : the energy/mass equations and the underhead or mixing area level equation. There are a total of ten energy equations in which the state variable is the mixture

enthalpy. The conservation equations can be written in the following matrix form[21]:

$$\underline{\underline{T}}^n \Delta \underline{u}^{n+1} = \underline{\underline{V}}^n \underline{o}^{n+1} + \underline{s}^n \tag{2.45}$$

where $\underline{u}$ is the state vector:

$$\underline{u} = [h_c, h_{ifs}, h_{ma}, h_{uh}, h_{hl}, h_{hx1}, h_{hx2}, h_{cl}, h_{so1}, h_{so2}, Lev]^T$$

and $\underline{o}$ is the boundary-condition vector:

$$\underline{o} = [m_{fd}, m_{ch}, m_b, m^n_{su}, m_c, m_{nc}, m_{ma}, m_{bp}, Q_{th}, Q^n_{hx1}, Q^n_{hx2}]^T$$

The equations are placed in rows in the following order: (1) core, (2) inside flow shroud, (3) mixing area, (4) underhead, (5) hot leg, (6 and 7) heat exchangers primary side, (8) cold leg, (9 and 10) heat exchangers secondary side, (11) underhead region or mixing area water level. The ordering of the equations changes if the user chooses to investigate transients with one heat exchanger only. This would reduce the system of equations to a total of nine equations: eight energy equations and the water level equation. For the partially filled underhead region case with two heat exchangers (normal conditions), matrices $\underline{\underline{T}}$ and $\underline{\underline{V}}$ have the following structure, respectively:

---

[21] Kao, S. P., ibid., page 61.

T_{11}	0	0	0	0	0	0	T_{18}	0	0	0
T_{21}	T_{22}	0	0	0	0	0	0	0	0	0
0	T_{32}	T_{33}	T_{34}	0	0	0	T_{38}	0	0	0
0	0	T_{43}	T_{44}	0	0	0	0	0	0	0
0	0	T_{53}	0	T_{55}	0	0	0	0	0	0
0	0	0	0	T_{65}	T_{66}	0	0	T_{69}	0	0
0	0	0	0	T_{75}	0	T_{77}	0	0	T_{10}	0
0	0	0	0	0	T_{86}	T_{87}	T_{88}	0	0	0
0	0	0	0	T_{95}	T_{96}	0	0	T_{99}	0	0
0	0	0	0	T_{105}	0	T_{107}	0	0	T_{1010}	0
0	0	0	T_{114}	0	0	0	0	0	0	T_{1111}

0	0	0	0	V_{15}	0	0	0	V_{19}	0	0
0	0	0	0	V_{25}	0	0	0	0	0	0
0	0	0	V_{34}	V_{35}	V_{36}	0	V_{38}	0	0	0
0	0	0	V_{44}	0	0	0	0	0	0	0
0	V_{52}	0	0	0	0	V_{57}	0	0	0	0
0	0	0	0	0	0	0	0	0	V_{610}	0
0	0	0	0	0	0	0	0	0	0	V_{711}
0	0	V_{83}	0	0	V_{86}	0	0	0	0	0
0	0	0	0	0	0	0	0	0	V_{910}	0
0	0	0	0	0	0	0	0	0	0	V_{1011}
V_{111}	0	0	V_{114}	0	0	0	0	0	0	0

The elements of matrices $\underline{\underline{T}}$ and $\underline{\underline{V}}$ are given in Tables 2.6-1 and 2.6-2, respectively. The elements of the residual vector, $\underline{s}$, are given in Table 2.6-3. Once the boundary condition vector is determined, the state-space equation 2.45 can be solved for the state vector, $\underline{u}$.

Then, Equation 2.32 is used to solve for the surge mass flow rate, m_{su}^{n+1}. The charging, letdown, and break flows are assumed to be given as well as the charging enthalpy.

Since the momentum conservation equations (Chapter 3) are solved first, the mass flow rates are evaluated at the advanced time. The surge flow rate between the mixing area and the underhead region is dependent on the overall fluid inventory which in turn depends on the enthalpies around the entire loop. Therefore, the surge flow at the present time, n, is used in solving the state-space model.

If the underhead region drains completely some elements of matrices $\underline{\underline{T}}$ and $\underline{\underline{V}}$ will change since the underhead level equation will be replaced by the mixing area level equation. The elements that change when the underhead region drains completely are given in Table 2.6-4.

Table 2.6-1
Elements of Matrix $\underline{\underline{T}}$

T_{11}	$\left(\frac{\partial u}{\partial h}\right)_{c,cl} + \Delta t\, m_c^{n+1}$
T_{18}	$-\Delta t\, m_c^{n+1}$
T_{21}	$-\Delta t\, m_c^{n+1}$
T_{22}	$\langle M \rangle_{fs} + \Delta t\, m_c^{n+1}$
T_{32}	$-\Delta t\, m_c^{n+1}$
T_{33}	$\langle M \rangle_{ma} + \Delta t\, m_c^{n+1} + \Delta t\, m_{mx}^{n+1} - \Delta t\, m_{su}^{n} - \Delta t\, m_{nc}^{n+1} + \Delta t\, m_{bp}^{n+1}$
T_{34}	$-\Delta t\, m_{mx}^{n+1}$
T_{38}	$-\Delta t\, m_{bp}^{n+1}$
T_{43}	$-\Delta t\, m_{mx}^{n+1}$
T_{44}	$\langle M \rangle_{uh} + \Delta t\, m_{su}^{n} + \Delta t\, m_{mx}^{n+1}$
T_{53}	$-\Delta t\, m_{ma}^{n+1}$

T_{55}	$\left(\frac{\partial u}{\partial h}\right)_{hl,ma} + \Delta t\, m_{ma}^{n+1} + \Delta t\, m_{ch}^{n+1}$
T_{65}	$-\Delta t\, m(1)^{n+1} + \Delta t \left(\frac{\partial Q_{hx1}}{\partial h_{hl}}\right)$
T_{66}	$\left(\frac{\partial u}{\partial h}\right)_{hx1,hl} + \Delta t\, m(1)^{n+1} + \frac{1}{2}\left[\frac{(V\rho C_p)_{tm1}}{(C_p)_{hx1}}\right] + \Delta t \left(\frac{\partial Q}{\partial h}\right)_{hx1}$
T_{69}	$\Delta t \left(\frac{\partial Q_{hx1}}{\partial h_{so1}}\right)$
T_{75}	$-\Delta t\, m(2)^{n+1} + \Delta t \left(\frac{\partial Q_{hx2}}{\partial h_{hl}}\right)$
T_{77}	$\left(\frac{\partial u}{\partial h}\right)_{hx2,hl} + \Delta t\, m(2)^{n+1} + \frac{1}{2}\left[\frac{(V\rho C_p)_{tm2}}{(C_p)_{hx2}}\right] + \Delta t \left(\frac{\partial Q}{\partial h}\right)_{hx2}$
T_{710}	$\Delta t \left(\frac{\partial Q_{hx2}}{\partial h_{so2}}\right)$
T_{86}	$-\Delta t\, m(1)^{n+1}$
T_{87}	$-\Delta t\, m(2)^{n+1}$
T_{88}	$\left(\frac{\partial u}{\partial h}\right)_{cl,hx} + \Delta t\, m_{nc}^{n+1} - \Delta t\, m_{b}^{n+1} + \Delta t \sum_{i} m(i)^{n+1}$
T_{95}	$-\Delta t \left(\frac{\partial Q_{hx1}}{\partial h_{hl}}\right)$
T_{96}	$-\Delta t \left(\frac{\partial Q}{\partial h}\right)_{hx1}$
T_{99}	$\left(\frac{\partial u}{\partial h}\right)_{sl1,so1} + \Delta t\, m_{sl1}^{n+1} - \Delta t \left(\frac{\partial Q_{hx1}}{\partial h_{so1}}\right)$
T_{105}	$-\Delta t \left(\frac{\partial Q_{hx2}}{\partial h_{hl}}\right)$
T_{107}	$-\Delta t \left(\frac{\partial Q}{\partial h}\right)_{hx2}$
T_{1010}	$\left(\frac{\partial u}{\partial h}\right)_{sl2,so2} + \Delta t\, m_{sl2}^{n+1} - \Delta t \left(\frac{\partial Q_{hx2}}{\partial h_{so2}}\right)$
T_{114}	$A_{uh}(Lev - L_{lfs} - L_{ma})\left(\frac{\partial \langle \rho \rangle}{\partial \langle h \rangle}\right)_{uh}$
T_{1111}	$(\rho A)_{uh}$

Table 2.6-2
Elements of Matrix $\underline{\underline{V}}$

V_{15}	$\Delta t\,(h_{cl} - h_c)$
V_{19}	Δt
V_{25}	$\Delta t\,(h_c - h_{ifs})$
V_{34}	$-\Delta t\,(h_{su} - h_{ma}) - \Delta t\,\Delta h_{su}^{n+1}$
V_{35}	$\Delta t\,(h_{ifs} - h_{ma})$
V_{36}	$-\Delta t\,(h_{nc} - h_{ma}) - \Delta t\,\Delta h_{nc}^{n+1}$
V_{38}	$\Delta t\,(h_{cl} - h_{ma})$
V_{44}	$\Delta t\,(h_{su} - h_{uh}) + \Delta t\,\Delta h_{su}^{n+1}$
V_{52}	$\Delta t\,(h_{ch}^{n+1} - h_{hl})$
V_{57}	$\Delta t\,(h_{ma} - h_{hl})$
V_{610}	$-\Delta t$
V_{711}	$-\Delta t$
V_{83}	$\Delta t\,(h_{cl} - \langle h \rangle_{cl})$
V_{86}	$\Delta t\,(h_{nc} - h_{cl}) + \Delta t\,\Delta h_{nc}^{n+1}$
V_{910}	Δt
V_{1011}	Δt
V_{111}	$-\Delta t$
V_{114}	Δt

Table 2.6-3
Elements of Vector $\underline{s}$

s_3	$\Delta t\, m_{mx}^{n+1}(h_{uh} - h_{ma})$
s_4	$\Delta t\, m_{mx}^{n+1}(h_{ma} - h_{uh})$
s_5	$\Delta t \sum_j m(j)^{n+1} \frac{\Delta p(j)_{pump}^{n+1}}{\rho_{hl}}$
s_6	$\Delta t\, m(1)^{n+1}(h_{hl} - h_{hx1}) - \Delta t \left(\frac{\partial Q_{hx1}}{\partial h_{sl1}}\right) \Delta h_{sl1}^{n+1}$
s_7	$\Delta t\, m(2)^{n+1}(h_{hl} - h_{hx2}) - \Delta t \left(\frac{\partial Q_{hx2}}{\partial h_{sl2}}\right) \Delta h_{sl2}^{n+1}$
s_8	$\Delta t \sum_j m(i)^{n+1}(h_{hx(i)} - h_{cl})$

S_9	$\Delta t\, m_{sl1}^{n+1}(h_{sl1}^{n+1} - h_{so1}^{n}) + \Delta t\left(\frac{\partial Q_{hx1}}{\partial h_{sl1}}\right)\Delta h_{sl1}^{n+1}$
S_{10}	$\Delta t\, m_{sl2}^{n+1}(h_{sl2}^{n+1} - h_{so2}^{n}) + \Delta t\left(\frac{\partial Q_{hx2}}{\partial h_{sl2}}\right)\Delta h_{sl2}^{n+1}$

Table 2.6-4
New Elements for a Complete Underhead Drainage Case

T_{113}	$[V_{ma'} + A_{ma}(Lev - L_{ifs})]\left(\frac{\partial\langle\rho\rangle}{\partial\langle h\rangle}\right)_{ma}$
T_{114}	0
T_{1111}	$(\rho A)_{ma}$

where $V_{ma'}$ represents the volume of the mixing area adjacent to the inside flow shroud control volume.

2.6 SUMMARY

The MITR loop was divided into eight control volumes: core, inside flow shroud, mixing area, underhead region, hot leg, two heat exchangers, and cold leg. The energy and mass conservation equations for the core, hot leg, heat exchangers, and cold leg were written assuming a linear enthalpy profile in each component. For the inside flow shroud, mixing area and underhead region, a uniform enthalpy profile was adopted. A small mass rate of change approximation was used in formulating the conservation equation of all control volumes. The conservation equations were written numerically using an implicit finite-difference approximation and a donor-cell differencing scheme was used to avoid undesirable numerical behavior.

The state variable of each control volume was chosen to be the mixture enthalpy. The mixture enthalpy was calculated using the HEM model. In evaluating fluid

properties, the loop pressure was assumed uniform with the reference value at the top of the core.

A state-space model was constructed by combining the energy equations and the water level equation in a matrix form. The solution of the state-space equation are obtained by a Gauss elimination process (forward elimination-backward substitution). The time step size for the numerical solution is limited by the transport time through the reactor core since it is the shortest flow path. The time step size is allowed to vary with flow rate thereby saving computing time for the slow flow rate cases (e.g., natural circulation).

CHAPTER 3: MOMENTUM MODEL

3.1 INTRODUCTION

In this chapter a momentum model for the MITR loop is developed. As in the thermal model (Chapter 2), the MITR loop is divided into several control volumes. The control volumes are chosen to preserve the essential physical features of the system. For the momentum model formulation, the control volumes are the same as in the thermal model except for the following three modifications: (1) the underhead region is omitted since it is not part of the main flow path, (2) the cold leg control volume now consists of the cold leg piping only, and (3) the downcomer region is subdivided into four regions. The downcomer subdivisions are shown in Figure 3.1.

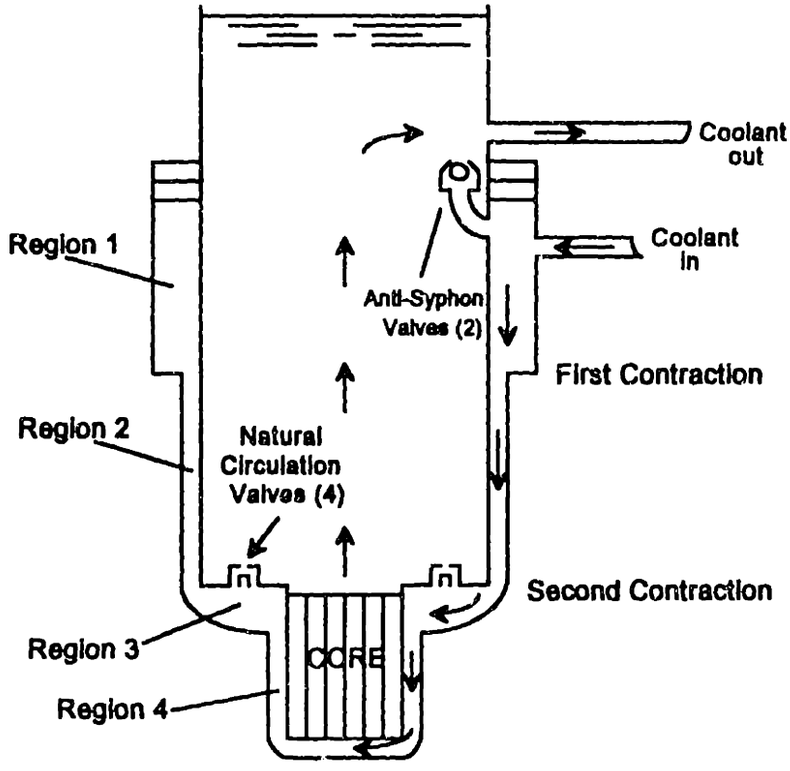

Figure 3.1. Core Tank Downcomer

3.2 MOMENTUM GOVERNING EQUATIONS

In formulating the governing equations for the momentum model, several simplifications are made: (1) the dynamic head changes in going from one control volume to the next as well as the single-phase (liquid) acceleration head terms are neglected since they are small compared to losses (e.g., friction and form); (2) the natural circulation valve dynamic behavior is not represented in this model. The valves are assumed to be either fully-open or fully-closed depending on the pressure difference across the valves; (3) the anti-siphon flow path is not modeled except as to prohibit the water level from dropping below the anti-siphon valve height; and (4) small mass flow rates (e.g., cleanup flow, surge, etc.) are ignored. The following figure illustrates the control volumes and the flow paths available in the MITR loop.

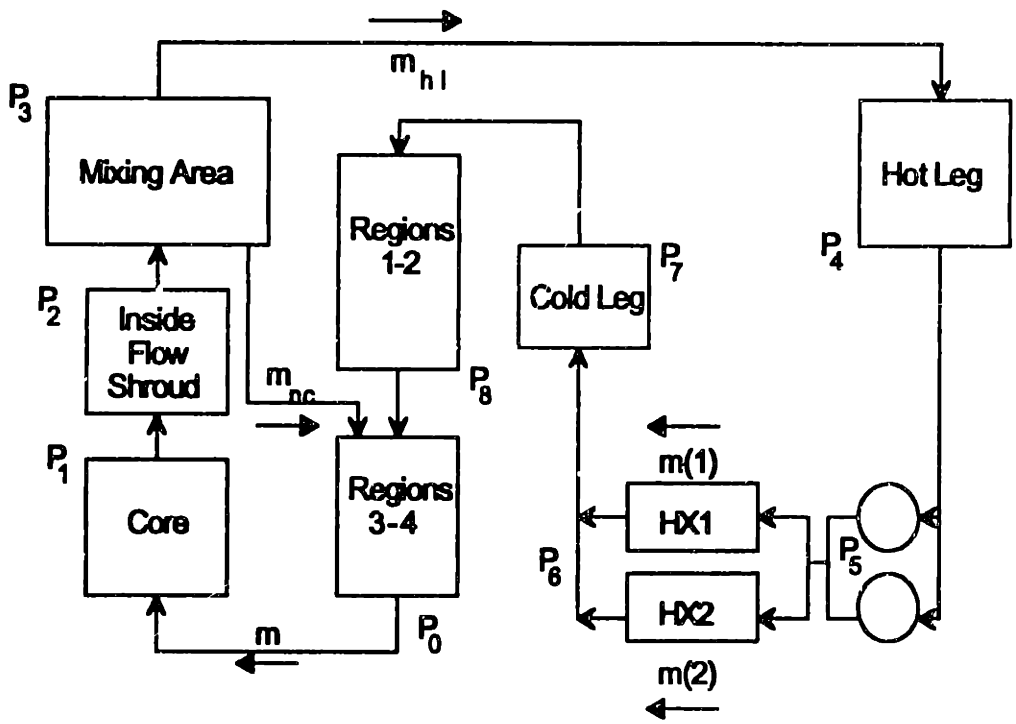

Figure 3.2. MITR Flow Paths and Pressure Locations

As shown in Figure 3.2, there are two possible MITR flow paths: (1) the "normal" loop in which flow goes through the heat exchangers, and (2) the natural circulation loop. Some of the MITR-II primary system parameters such as form-loss coefficients, equivalent diameters, flow areas, etc., were gathered by Chi Kao[22] and are given in Table 3.2.1.

Table 3.2.1

MITR-II Primary System Parameters

	Flow Area per Channel (m^2)	Total Coolant Volume (m^3)	D_e (m)	Inlet Elevation (m)	Outlet Elevation (m)	K	Number of Channels
Core	1.31E-4	3.75E-2	2.24E-3*	7.13	7.79	2.05	330**
Inside Flow Shroud	0.130	0.099	0.387	7.79	8.55	0.00	1
Mixing Area	0.923	1.920	1.084	7.79	9.87	0.00	1
Hot Leg	0.032	0.427	0.203	9.77	2.69	4.58	1
Heat Exchanger 1	not available	not available	not available	2.69	2.69	not avail-able	not available
Heat Exchanger 1a	3.89E-5	1.68E-4	7.04E-3	2.69	2.69	7.30	885
Cold Leg	0.032	0.468	0.203	2.69	9.66	2.17	1
Region 1	0.339	0.413	0.180	9.66	8.44	0.00	1
Region 2	0.111	0.076	0.063	8.44	7.75	0.30	1
Region 3	0.004	0.016	0.220	7.75	7.74	0.18	1
Region 4	0.029	0.018	0.040	7.74	7.13	0.00	1

* The core equivalent diameter accounts for the fins.

** The value associated with 22 fuel assemblies.

[22] Kao, C., "Simulation of MITR-II Primary System in Steady State," MIT Department of Nuclear Engineering Internal Report, 1992.

The following paragraphs contain the momentum conservation equations for each of the loops mentioned above.

3.2.1 MITR LOOP

Since the entire loop does not have a single mass flow rate, the loop is divided into sections in which a single mass flow rate exists. The sections are the following: (1) from region 3 inlet to inside flow shroud outlet, (2) from mixing area inlet to hot leg outlet, (3) from pump suction leg inlet to pump outlet, (4a and 4b) from heat exchanger inlet to outlet, and (5) from cold leg inlet to region 2 outlet. The momentum conservation equations of each section follows:

- *Section 1 (from region 3 inlet to inside flow shroud outlet)*

$$\sum_i \left(\frac{L}{A}\right)_i \frac{dm}{dt} + \sum_i \Delta\left(\frac{m^2}{2\rho A^2}\right)_i + \Delta p_1 = -\sum_i \left(\frac{fL}{2D_e\langle\rho\rangle A^2}\right)_i m^2 - \sum_i \left(\frac{K}{2\langle\rho\rangle A^2}\right)_i m^2 - \sum_i \langle\rho\rangle_i g \Delta z_i \qquad (3.1)$$

where i represents region 3, region 4, the core, and the inside flow shroud control volumes. The first two terms of the left-hand side are the inertial and acceleration head losses for section 1. Δp_1 is the difference in outlet and inlet pressure for section 1 (p_2 - p_8). The terms on the right-hand side are the friction, form, and buoyancy head losses for section 1 where Δz_i is the difference in height between the outlet and inlet of component i. K and f are the form-loss coefficient and the friction factor, respectively.

- *Section 2 (from mixing area inlet to hot leg outlet)*

$$\sum_j \left(\frac{L}{A}\right)_j \frac{dm_{hl}}{dt} + \sum_j \Delta\left(\frac{m_{hl}^2}{2\rho A^2}\right)_j + \Delta p_2 = -\sum_j \left(\frac{fL}{2D_e\langle\rho\rangle A^2}\right)_j m_{hl}^2 - \sum_j \left(\frac{K}{2\langle\rho\rangle A^2}\right)_j m_{hl}^2 -$$

$$\sum_j \langle\rho\rangle_j g \Delta z_j \qquad (3.2)$$

where j represents the mixing area and the hot leg control volumes. Note that there is no acceleration term within the mixing area since the density, flow area, and mass flow rate are assumed uniform. Δp_2 is the difference in pressure between the hot leg outlet and mixing area inlet (p_4 - p_2).

- *Section 3 (pump)*

$$\Delta p_3 = \rho_{hl} * g * H(m_p, \omega) \qquad (3.3)$$

where Δp_3 is the difference in pressure between the pump outlet and inlet (p_5 - p_4). The pump head, H, delivered to the fluid is dependent on the flow through the pump, m_p, and the pump angular speed, ω. ρ_{hl} is the fluid density at the pump suction leg and g is the acceleration due to gravity.

- *Sections 4a and 4b (heat exchangers)*

$$\left(\frac{L}{A}\right)_{hx1} \frac{dm(1)}{dt} + \Delta\left(\frac{m(1)^2}{2\rho A^2}\right)_{hx1} + \Delta p_4 = -\left(\frac{fL}{2D_e\langle\rho\rangle A^2}\right)_{hx1} m(1)^2 - \left(\frac{K}{2\langle\rho\rangle A^2}\right)_{hx1} m(1)^2 \qquad (3.4)$$

and

$$\left(\frac{L}{A}\right)_{hx2} \frac{dm(2)}{dt} + \Delta\left(\frac{m(2)^2}{2\rho A^2}\right)_{hx2} + \Delta p_4 = -\left(\frac{fL}{2D_e\langle\rho\rangle A^2}\right)_{hx2} m(2)^2 - \left(\frac{K}{2\langle\rho\rangle A^2}\right)_{hx2} m(2)^2 \qquad (3.5)$$

The difference in pressure between the heat exchangers outlet and inlet is represented by Δp_4 (p_6 - p_5).

- *Section 5 (from cold leg inlet to region 2 outlet)*

$$\sum_k \left(\frac{L}{A}\right)_k \frac{dm_{hl}}{dt} + \sum_k \Delta\left(\frac{m_{hl}^2}{2\rho A^2}\right)_k + \Delta p_5 = -\sum_k \left(\frac{fL}{2D_e\langle\rho\rangle A^2}\right)_k m_{hl}^2 - \sum_k \left(\frac{K}{2\langle\rho\rangle A^2}\right)_k m_{hl}^2 -$$

$$\sum_k \langle\rho\rangle_k g\Delta z_k - \left(\frac{K_{throttle}}{2\langle\rho\rangle_{cl} A_{throttle}^2}\right) m_{hl}^2 \qquad (3.6)$$

Subscript k represents the cold leg, region 1, and region 2 control volume. Δp_5 is the pressure difference between region 2 outlet and cold leg inlet (p_8 - p_6). The K-loss from a throttle valve is included to allow the loop to have different initial mass flow rate conditions while maintaining a momentum balance of the system.

Since $\Delta p_1 + \Delta p_2 + \Delta p_3 + \Delta p_4 + \Delta p_5 = 0$, the momentum conservation equations can be combined to obtain two equations having the following form:

$$\sum_l \left(\frac{L}{A}\right)_l \frac{dm}{dt} + \sum_m \left(\frac{L}{A}\right)_m \frac{dm_{hl}}{dt} + \left(\frac{L}{A}\right)_{hx1} \frac{dm(1)}{dt} = F(m, m_{hl}, m(1), \omega) \qquad (3.7)$$

and

$$\sum_l \left(\frac{L}{A}\right)_l \frac{dm}{dt} + \sum_m \left(\frac{L}{A}\right)_m \frac{dm_{hl}}{dt} + \left(\frac{L}{A}\right)_{hx2} \frac{dm(2)}{dt} = N(m, m_{hl}, m(2), \omega) \qquad (3.8)$$

where subscript m represents the cold leg, hot leg, mixing area, and regions 1-2 control volumes. ω represent the angular velocity of pump 1 and pump 2. Functions F and N represent the pump head and the acceleration, friction, form, and gravity head losses around the MITR loop for the two possible paths (heat exchangers).

3.2.2 NATURAL CIRCULATION LOOP

There are four natural circulation valves close to the bottom of the mixing area which, under the right pressure conditions, discharge flow to the downcomer (region 3). The driving force of this loop is provided by the buoyancy head which arises from the difference in fluid density between the core and the downcomer. The natural circulation valves are collapsed into one equivalent valve for simplicity. The following condition is necessary for the natural circulation valve to open.

$$p_8 < p_2 - \rho_{ma} g \Delta z_{shroud} + \frac{(\rho_{ball} - \rho_{cl}) g V_{ball}}{A_{nc}} \tag{3.9}$$

where

Δz_{shroud} = height difference between the bottom and top of the flow shroud,
V_{ball} = natural circulation ball volume,
ρ_{ball} = natural circulation ball density, and
A_{nc} = flow area of the natural circulation valve

If the inequality shown above is true, then the natural circulation valve is assumed to open. Once the status of the valve is known, an equation for the pressure drop across the valve can be written as follows:

$$p_8 - p_2 \equiv -\Delta p_1 = -\left(\frac{K_{nc}}{2\rho_x A_{nc}^2}\right) m_{nc} |m_{nc}| - \rho_{ma} g \Delta z_{shroud} \tag{3.10}$$

where K_{nc} is the form-loss coefficient for the natural circulation valve.

By combining Equations 3.10 and 3.1, an equation having the following form is obtained:

$$\sum_i \left(\frac{L}{A}\right)_i \frac{dm}{dt} = Y(m, m_{nc}) \tag{3.11}$$

where the function Y represents the acceleration, friction, form and gravity head terms for the natural circulation loop.

The pressure drop across the valve is first determined from the momentum calculation around the loop assuming the natural circulation valve is closed. If the inequality 3.9 is false the natural circulation flow, m_{nc}, is set equal to zero. In the loss-of-flow case, the flow decrease will cause the pressure below the natural circulation valve, P_g, to decrease. However, as soon as the inequality 3.9 becomes true, the pressure below the valve still momentarily exceeds the pressure above the valve leading to an upward flow through the natural circulation valve. In this case the density, ρ_x, is given the value of the cold leg outlet (ρ_{cl}). Note that in this case the natural circulation flow will take on a negative value (bypass flow). Eventually, the buoyancy head will provide the forcing drive for the natural circulation loop and the normal downward flow will take place. Then the density, ρ_x, is given the value of the mixing area (ρ_{ma}). In this case the natural circulation flow will have a positive value indicating the normal direction of flow.

3.3 PUMP MOMENTUM EQUATIONS

The pumping head delivered by the coolant pumps is represented by the following characteristic head-capacity relation:

$$Y = c_1 + c_2 x + c_3 x^2 + c_4 x^3 \tag{3.12}$$

where $Y = \left(\frac{H}{H_r}\right)\left(\frac{\omega_r}{\omega}\right)^2$ and $x = \left(\frac{m}{m_r}\right)\left(\frac{\rho_r}{\rho}\right)\left(\frac{\omega_r}{\omega}\right)$

H = pump head,

ρ = fluid density at the hot leg exit,

ω = pump rotational speed.

The subscript r represents the rated conditions.

The coefficients of Equation 3.12 were obtained by Renee DuBord[23] from the head-capacity curve of the MITR-II primary coolant pumps experimentally determined by Chi Kao. The head-capacity curve for the pumps is shown in the following figure.

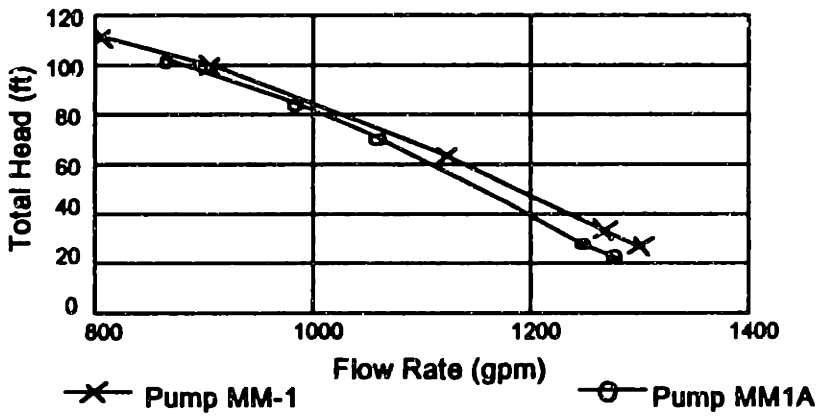

Figure 3.3. Pump Head-Capacity Curves

It is necessary to determine the pump rotor speed as a function of time since the pump head depends on it. By applying the conservation of angular momentum to the pump rotor and associated rotating components, the following relationship is obtained[24]:

$$I\frac{d\omega}{dt} = T_e - T_b - T_w \qquad (3.13)$$

where

---

[23] DuBord, R., "Pump Coast-Down Simulation for the MITR-II," MIT Department of Nuclear Engineering, 1992.

[24] Rust, J. H., Nuclear Power Plant Engineering, Haralson Publishing Co., Buchanon, GA, 1979.

ω is the pump rotor speed;

I is the pump moment of inertia;

T_e is the electric torque;

T_b is the brake-horse-power torque; and

T_w is the windage and bearing loss torque.

The electric torque is the torque provided by the electric motor. When the power is cut off, the electric torque is assumed to decay to zero instantaneously. The brake-horse-power torque is the torque imparted by the fluid to the pump impeller at a given flow and rotor speed. The brake-horsepower torque is calculated from the following ideal pump relationship:

$$T_b = \frac{m H}{\omega \rho} \tag{3.14}$$

The windage and bearing loss torque is due to friction losses and is determined as follows[25]:

$$\frac{T_w}{T_{wr}} = \left\{ \begin{array}{cc} \left(\frac{\omega}{\omega_r}\right)^2 & \omega > 0.19\omega_r \\ 0.035 & 0 < \omega < 0.19\omega_r \\ 0.1 & \omega = 0 \end{array} \right\} \tag{3.15}$$

This relation was obtained for a PWR pump and assumed to be applicable for an MITR pump as well.

3.4 MASS CONSERVATION EQUATIONS

In order to have a closed model, relationships among the mass flow rates are necessary. These relationships can be obtained from observation of Figure 3.2-1 and are as follows:

---

[25] Kao, S. P., ibid., page 128.

$$m(1)+m(2)=m_{hl} \tag{3.16}$$

$$m=m_{hl}+m_{nc} \tag{3.17}$$

3.5 MOMENTUM STATE-SPACE MODEL

It was shown in Section 3.2.1 that two state equations can represent the MITR loop momentum balance:

$$\sum_i \left(\frac{L}{A}\right)_i \frac{dm}{dt}+\sum_m \left(\frac{L}{A}\right)_m \frac{dm_{hl}}{dt}+\left(\frac{L}{A}\right)_{hx1} \frac{dm(1)}{dt}=F(m,m_{hl},m(1),\omega)$$

and

$$\sum_i \left(\frac{L}{A}\right)_i \frac{dm}{dt}+\sum_m \left(\frac{L}{A}\right)_m \frac{dm_{hl}}{dt}+\left(\frac{L}{A}\right)_{hx2} \frac{dm(2)}{dt}=N(m,m_{hl},m(2),\omega)$$

In addition, the pump rotor speed equation 3.16 can be written as follows:

$$\frac{d\omega}{dt}=G(m_p,\omega) \tag{3.18}$$

where m_p is the mass flow rate through the pump. Both pumps are assumed to behave identically. Thus, the pumps will have the same angular speed with each pump providing half of the total mass flow rate through the loop.

Combining the above equations with the mass conservation equations of Section 3.4 and the momentum conservation equations for the natural circulation loop (Equations 3.11 and 3.14), a momentum state space model is obtained as follows[26]:

$$\underline{\underline{B}}\,\dot{\underline{y}}=\underline{h}(\underline{y}) \tag{3.19}$$

where

$$\underline{y}=[m,\ m_{hl},\ m(1),\ m(2),\ m_{nc},\ \omega]^T$$

---

[26] Kao, S. P., ibid., page 129.

and

$$\underline{h} = [F, N, Y, G, 0, 0]^T$$

Equation 3.19 can be written numerically using a semi-implicit form as follows:

$$\left[\underline{\underline{B}} - \Delta t \underline{\underline{J}}\right]^n \Delta \underline{y}^{n+1} = \Delta t\, \underline{h}^n \tag{3.20}$$

or

$$\left(\underline{\underline{B}}^+\right)^n \Delta \underline{y}^{n+1} = \Delta t\, \underline{h}^n \tag{3.21}$$

where $\underline{\underline{J}}$ is the Jacobian of $\underline{h}$ given by $\left(\frac{\partial \underline{h}}{\partial \underline{y}}\right)$. Matrix $\underline{\underline{B}}^+$ has the following structure:

$b_1(1)$	$b_1(2)$	$b_1(3)$	0	0	0
$b_2(1)$	$b_2(2)$	0	$b_2(4)$	0	$b_2(6)$
$b_3(1)$	0	0	0	$b_3(5)$	0
0	$b_4(2)$	0	0	0	$b_4(6)$
-1	1	0	0	1	1
0	-1	1	1	0	0

The elements of matrix $\underline{\underline{B}}^+$ are given in Table 3.5-1.

Table 3.5-1

Elements of Matrix $\underline{\underline{B}}^+$

$b_1(1)$	$\sum_i \left(\frac{L}{A}\right)_i - \Delta t \left(\frac{\partial F}{\partial m}\right)$
$b_1(2)$	$\sum_m \left(\frac{L}{A}\right)_m - \Delta t \left(\frac{\partial F}{\partial m_{hl}}\right)$
$b_1(3)$	$\left(\frac{L}{A}\right)_{hx1} - \Delta t \left(\frac{\partial F}{\partial m(1)}\right)$
$b_1(6)$	$-\Delta t \left(\frac{\partial F}{\partial \omega}\right)$
$b_2(1)$	$\sum_i \left(\frac{L}{A}\right)_i - \Delta t \left(\frac{\partial N}{\partial m}\right)$
$b_2(2)$	$\sum_m \left(\frac{L}{A}\right)_m - \Delta t \left(\frac{\partial N}{\partial m_{hl}}\right)$
$b_2(4)$	$\left(\frac{L}{A}\right)_{hx2} - \Delta t \left(\frac{\partial N}{\partial m(2)}\right)$
$b_2(6)$	$-\Delta t \left(\frac{\partial N}{\partial \omega}\right)$

$b_3(1)$	$\sum_i \left(\frac{L}{A}\right)_i - \Delta t \left(\frac{\partial Y}{\partial m}\right)$
$b_3(5)$	$-\Delta t \left(\frac{\partial Y}{\partial m_{nc}}\right)$
$b_4(2)$	$-\Delta t \left(\frac{\partial G}{\partial m_{hl}}\right)$
$b_4(6)$	$1 - \Delta t \left(\frac{\partial G}{\partial \omega}\right)$

If the inequality 3.9 is false, then the natural circulation valve is closed. In this case, the state vector and driving function vector become:

$$\underline{y} = [m,\ m(1),\ m(2),\ \omega]^T$$

and

$$\underline{h} = [F,\ N,\ G,\ 0]^T$$

The elements of matrix $\underline{\underline{B}}^+$ for the case of a closed natural circulation valve are shown in Table 3.5-2.

Table 3.5-2

Elements of Matrix $\underline{\underline{B}}^+$ (closed natural circulation)

$b_1(1)$	$\sum_i \left(\frac{L}{A}\right)_i + \sum_m \left(\frac{L}{A}\right)_m - \Delta t \frac{\partial F}{\partial m}$
$b_1(2)$	$\left(\frac{L}{A}\right)_{hx1} - \Delta t \frac{\partial F}{\partial m(1)}$
$b_1(4)$	$-\Delta t \frac{\partial F}{\partial \omega}$
$b_2(1)$	$\sum_i \left(\frac{L}{A}\right)_i + \sum_m \left(\frac{L}{A}\right)_m - \Delta t \frac{\partial N}{\partial m}$
$b_2(3)$	$\left(\frac{L}{A}\right)_{hx2} - \Delta t \frac{\partial N}{\partial m(2)}$
$b_2(4)$	$-\Delta t \frac{\partial N}{\partial \omega}$
$b_3(1)$	$-\Delta t \frac{\partial G}{\partial m}$
$b_3(4)$	$1 - \Delta t \frac{\partial G}{\partial \omega}$
$b_4(1)$	-1.0
$b_4(2)$	1.0
$b_4(3)$	1.0

Once the initial conditions are determined from a steady-state calculation, the pressure condition across the natural circulation valve is calculated to determine if the valve is open or closed. Then, the mass flow rates at the advanced time are calculated by inverting matrix $\underline{\underline{B}}^{+}$. The pressure difference across the natural circulation valve is evaluated to determine the valves' status at each time step.

3.6 SUMMARY

The momentum model for the MITR was obtained by dividing the entire loop into sections for which a single mass flow rate approximation could be used. By combining all the resultant momentum conservation equations, two governing equations were obtained representing the two different flow paths available (two heat exchangers). In addition, a momentum conservation equation was written for the natural circulation flow path.

By conserving the angular momentum of the pump impeller and rotor, an equation for the rotational speed of the pumps is written in terms of electric, break-horse-power, and windage-and-bearing torques.

All of the equations are combined into a state-space model by writing them in a matrix form. The initial calculations are performed assuming the natural circulation valves are closed. Then, a force-balance on the natural circulation valve determines the status of the valve at each time step indicating the matrix to be inverted when solving for the loop mass flow rates and the pumps' angular speed.

CHAPTER 4: REACTOR KINETICS AND FUEL HEAT TRANSFER MODELS

4.1 INTRODUCTION

The nuclear power generated in the core is from two sources: fission and post-fission radioactive decay. A small percentage of this power gets deposited in the reflector. The power produced from fission is calculated using the point-kinetics model and the power produced from the decay of fission products is obtained by summing the powers of seven decay groups.

The fuel heat transfer model used is a single-node model developed by J. E. Meyer[27]. It is based on using the steady-state temperature distributions to determine the average plate temperature at the advanced time. In addition, uniform properties for each fuel region (fuel meat and clad) are evaluated at the average temperature of the fuel plate.

4.2 POINT-KINETICS

The point-kinetics equations are the governing equations for the time rate of change of the amplitude function, T, and the precursor concentration of group i, C_i.

$$\frac{dT}{dt} = \left(\frac{\rho - \beta}{\Lambda}\right)T + \sum_i \lambda_i C_i + S \tag{4.1}$$

and

$$\frac{dC_i}{dt} = \frac{\beta_i}{\Lambda}T - \lambda_i C_i \tag{4.2}$$

where

ρ = reactivity;
β_i = effective delayed-neutron fraction of precursor group i;
Λ = prompt-neutron lifetime;
λ_i = decay time constant for precursor group i;

---

[27] Meyer, J. E., "Some Physical and Numerical Considerations for the SSC-S Code," BNL-NUREG-50913, 1978.

S = neutron source; and

$$\beta = \sum_i \beta_i$$

The point-kinetic equations can be normalized to obtain the following:

$$\frac{d\chi_i}{dt} = \lambda_i \left(P - \chi_i \right) \tag{4.3}$$

$$\frac{dP}{dt} = \left(\frac{\rho - \beta}{\Lambda} \right) P + \sum_i \frac{\chi_i \beta_i}{\Lambda} + S' \tag{4.4}$$

where

χ_i= Normalized precursor concentration of group i, (e.g., at steady-state and 70 percent power, χ_i=0.70),

P= Normalized amplitude function (e.g., at steady-state and 70 percent power, P=0.70), and

S'= Normalized neutron source (The neutron source divided by the "rated" amplitude function).

Equation 4.3 can be solved analytically if the time dependence of the normalized amplitude function is known. In this model, the amplitude function is approximated as linear for each time interval. The calculations are performed as follows:

$$P(t) = P^n + \left(\frac{P^{n+1} - P^n}{\Delta t} \right) t \tag{4.5}$$

Inserting Equation 4.5 into Equation 4.3 yields the following:

$$\frac{d\chi_i}{dt} = \lambda_i \left[P^n + \left(\frac{P^{n+1} - P^n}{\Delta t} \right) t - \chi_i \right] \tag{4.6}$$

By solving this linear differential equation, the following expression for the precursor concentration is obtained.

$$\chi_l^{n+1} = \chi_l^n \exp(-\lambda_l \Delta t) + P^n[1 - \exp(-\lambda_l \Delta t)] + \frac{\Delta P^{n+1}}{\lambda_l \Delta t}[\exp(-\lambda_l \Delta t) - 1 + \lambda_l \Delta t] \tag{4.7}$$

For small time intervals, Δt, the exponential term can be approximated as:

$$\exp(-\lambda_l \Delta t) \approx 1 - \lambda_l \Delta t + \frac{(\lambda_l \Delta t)^2}{2} - \frac{(\lambda_l \Delta t)^3}{6}$$

Therefore, Equation 4.7 reduces to the following form:

$$\chi_l^{n+1} = \chi_l^n \left[1 - \lambda_l \Delta t + \frac{(\lambda_l \Delta t)^2}{2} - \frac{(\lambda_l \Delta t)^3}{6} \right] + P^n \left[\lambda_l \Delta t - \frac{(\lambda_l \Delta t)^2}{2} + \frac{(\lambda_l \Delta t)^3}{6} \right] +$$

$$\frac{\Delta P^{n+1}}{\lambda_l \Delta t} \left[\frac{(\lambda_l \Delta t)^2}{2} - \frac{(\lambda_l \Delta t)^3}{6} \right] \tag{4.8}$$

Since we have an expression for the normalized precursor concentration at the advanced time, the equation for the time rate of change of the normalized amplitude function can be solved implicitly. Equation 4.4 is written numerically as follows:

$$\Delta P^{n+1} = \Delta t \left(\frac{\rho^{n+1} - \beta}{\Lambda} \right) P^{n+1} + \Delta t \sum_l \frac{\chi_l^{n+1} \beta_l}{\Lambda} + \Delta t \, S'^{\,n+1} \tag{4.9}$$

After inserting Equation 4.8 into Equation 4.9 and rearranging, the change in the amplitude function during the time interval, Δt, can expressed as:

$$\Delta P^{n+1} = \frac{\Delta t\left(\frac{\rho^{n+1}-\beta}{\Lambda}\right)P^n + \Delta t\sum_i \frac{\beta_i}{\Lambda}[\chi_i(1-a)+P^n a] + \Delta t\, S'^{n+1}}{\left(1-\Delta t\left(\frac{\rho^{n+1}-\beta}{\Lambda}\right)-\sum_i\left[\frac{\beta_i}{\Lambda\lambda_i}\left(\frac{(\lambda_i\Delta t)^2}{2}-\frac{(\lambda_i\Delta t)^3}{6}\right)\right]\right)} \qquad (4.10)$$

where $a \equiv \lambda_i\Delta t - \frac{(\lambda_i\Delta t)^2}{2} + \frac{(\lambda_i\Delta t)^3}{6}$.

The initial precursor concentrations and amplitude function are obtained from a steady-state calculation. The change in the amplitude function and the precursor concentrations can be calculated from the initial conditions and the calculations proceed by using Equations 4.8 and 4.10 for each time interval.

The calculations are first performed with a time-step size equal to the "thermal" (Chapter 2) time-step size. Then, the time-step is halved and the calculations are repeated. If the results differ by more than a prescribed error (0.01), the time-step is halved again and continued until two consecutive results meet the convergence criteria.

A simplified version (one precursor group) of the point-kinetics subroutine has been benchmarked against well-known analytical results. Four step reactivity insertions were considered: (1) -6.67 dollars, (2) 20 cents , (3) 60 cents, and (4) 1.53 dollars. The "thermal" time-step used for the first three cases was 0.20 seconds, and 0.001 for case 4. A very small time-step was used for case 4 because it would not converge otherwise. The results are shown in Figures 4.2-1 through 4.2-4.

Reactivity can be inserted into the core by three mechanisms: a mechanical change (e.g., control blade withdrawn), fuel temperature changes, and fluid density changes. The reactivity worth of the control blades is provided by the user in tabular form. The

reactivity feedback coefficients are also user's input, allowing different core configurations to be modeled.

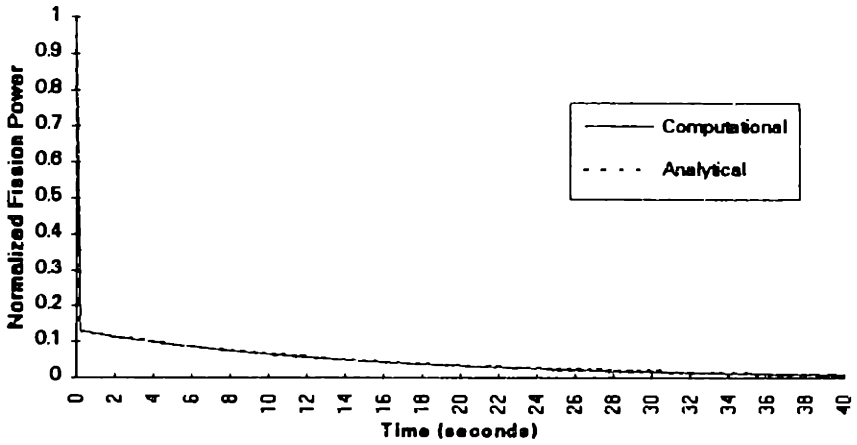

Figure 4.2-1. Normalized Fission Power for a -$6.67 Step Insertion

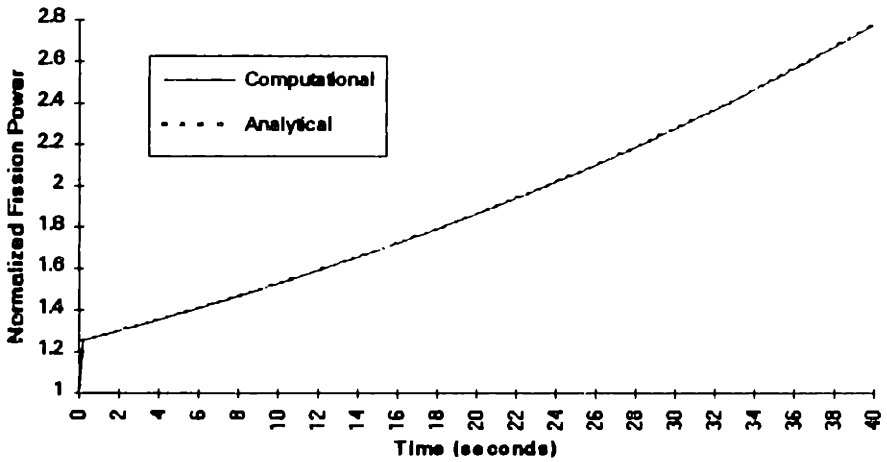

Figure 4.2-2. Normalized Fission Power for a 20 Cent Step Insertion

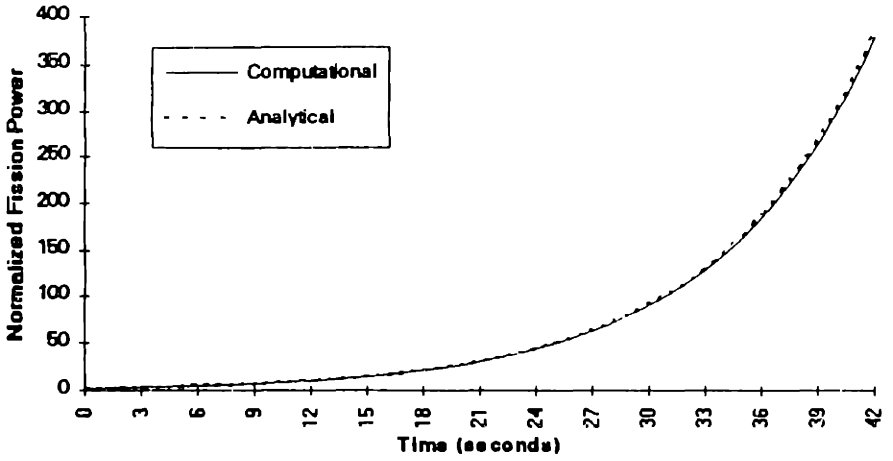

Figure 4.2-3. Normalized Fission Power for a 60 cent Step Insertion

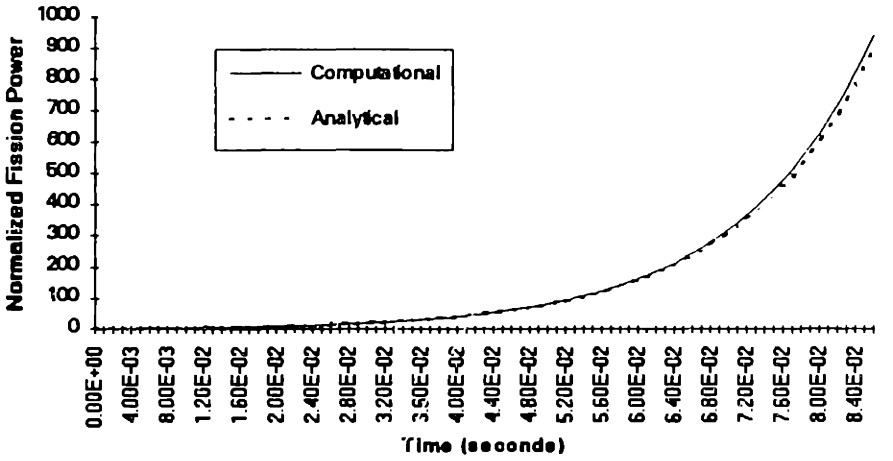

Figure 4.2-4. Normalized Fission Power for a $1.53 Step Insertion

4.3 DECAY POWER

Radioactive decay contributes to the overall power produced in the core. It is most important for post-scram scenarios since the decay heat persists long after the fission chain is terminated. The normalized decay power produced in the core can be obtained

by summing the powers of seven decay-product groups[28]:

$$Q_d = \sum_{i=1}^{7} (\beta_d C_d)_i \tag{4.11}$$

where

$(\beta_d)_i$ = fraction of decay power for group i $\left(\sum_{i=1}^{7} (\beta_d)_i = 1\right)$, and

$(C_d)_i$ = normalized decay power for group i; $(C_d)_i = 1$ at steady-state and full power.

The time rate of change of $(C_d)_i$ is given by the following equation:

$$\frac{d(C_d)_i}{dt} = (\lambda_d)_i[P - (C_d)_i] \tag{4.12}$$

where P is the normalized amplitude function and $(\lambda_d)_i$ is the decay constant for group i. The values for β_d's and λ_d's are given in Table 4.3. The decay power group constants are derived from the ENDB/B-IV calculations based on U^{235} and 10^{13} seconds of irradiation time[29].

Table 4.3

Decay Power Group Constants

Group	β_d	$\lambda_d(sec^{-1})$
1	0.097	1.280
2	0.220	0.152
3	0.237	1.93E-2
4	0.187	1.88E-3
5	0.132	1.43E-4
6	0.072	1.25E-5
7	0.055	2.20E-7

---

28 Kao, S. P., ibid., page 54.

29 Bjerke, M. A., et al., "A Review of Short-Term Fission-Product-Decay Power," Nuclear Safety, Vol. 18, No. 5, 1977.

The normalized nuclear power is given by:

$$N = (1 - f_d)P + f_d Q_d \tag{4.13}$$

where N is the normalized nuclear power and f_d is the fraction of decay power at steady-state equilibrium conditions. The pumps' work has been included in the hot leg energy conservation equation and, therefore, it is not included as part of the heat source described here.

4.4 FUEL HEAT TRANSFER MODEL

Figure 4.4 illustrates a cross sectional view of the MITR-II fuel plate. The fuel plate consists of two regions: a fuel meat, and a finned clad. In the single-node model, the fuel plate is lumped into one element. The heat conduction equation for the fuel plate is the following:

$$(mC_p)_p \frac{dT_p}{dt} = q''_N - U_p(T_p - T_b) \tag{4.14}$$

where

T_b = bulk coolant temperature

T_p = average plate temperature

U_p = plate overall heat transfer coefficient

q''_N = plate surface heat flux (flat plate approximation)

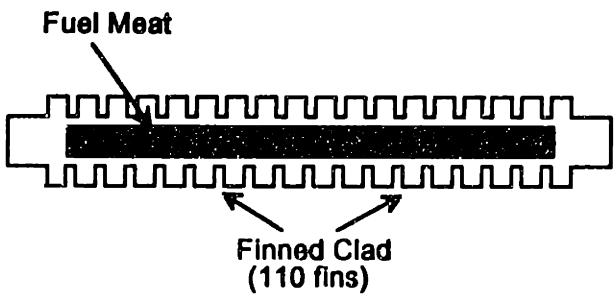

Figure 4.4. Fuel Plate Cross Sectional View

The plate mass per unit plate surface area, m_p, is the sum of the volume-averaged fuel and clad masses.

$$m_p = m_{fuel} + m_{clad} \tag{4.15}$$

The fuel volume-averaged mass can be written as follows:

$$m_{fuel} = \frac{A_{fuel}}{P_T}\rho_{fuel} \tag{4.16}$$

where

A_{fuel} = cross sectional area of the fuel meat

P_T = total outside perimeter of the fuel plate (flat plate approximation).

ρ_{fuel} = fuel density

A similar expression can be written for the clad volume-averaged mass:

$$m_{clad} = \frac{A_{clad}}{P_T}\rho_{clad} \tag{4.17}$$

The average heat capacity of the fuel plate is defined as follows:

$$(C_p)_p = \frac{(mC_p)_{fuel} + (mC_p)_{clad}}{m_p} \tag{4.18}$$

Assuming that the steady-state arithmetic average temperature can be used to represent the energy storage, and the thermal conductivities and capacities are uniform in the fuel plate, then the average fuel plate temperature is given by:

$$T_p = \frac{(mC_p)_{clad}(T_f + T_c) + (mC_p)_{fuel}(T_{cntr} + T_f)}{2(mC_p)_p} \tag{4.19}$$

where

T_f = fuel meat surface temperature

T_c = clad surface temperature

T_{cntr} = fuel meat centerline temperature

Define two temperature ratios f_p and f_1 as follows[30]:

$$f_p = \frac{T_p - T_c}{T_{cntr} - T_c} \tag{4.20}$$

and

$$f_1 = \frac{T_f - T_c}{T_{cntr} - T_c} \tag{4.21}$$

By substituting Equations 4.20 and 4.21 into Equation 4.19, the following result is obtained:

$$f_p = \frac{(mC_p)_p f_1 + (mC_p)_f}{2(mC_p)_p} \tag{4.22}$$

By the steady-state assumption, the fuel plate surface heat flux is given by the following relationships for the fuel, the clad, and the entire plate, respectively:

$$q'' = U_{fuel}(T_{cntr} - T_f) \quad \text{(fuel meat)} \tag{4.23}$$

where

$$U_{fuel} = \frac{k_{fuel}}{w/2}$$

and w is the fuel meat thickness.

$$q'' = U_{clad}(T_f - T_c) \quad \text{(clad)} \tag{4.24}$$

where

$$U_{clad} = \frac{K_{clad}}{t}$$

and t is the clad thickness. A similar equation can be written for the entire fuel plate as follows:

$$q'' = U_T(T_{cntr} - T_c) \tag{4.25}$$

---

30 Kao, S. P., ibid., page 209.

where

$$\frac{1}{U_T} = \frac{1}{U_{clad}} + \frac{1}{U_{fuel}}$$

From observation of Equations 4.22 trough 4.24, the following relationship between the temperature ratios (f_1 and f_p) and the overall heat transfer coefficients can be obtained:

$$f_1 = \frac{U_T}{U_{clad}} \tag{4.26}$$

and

$$\frac{1}{U_p} = \frac{1}{h_p} + \frac{f_p}{U_T} \tag{4.27}$$

where h_p is the heat transfer coefficient at the surface of the fuel plate. The heat transfer coefficient is calculated using the correlations given in Appendix B.

Once the heat transfer parameters are well-defined, the heat conduction equation can be solved. The heat conduction equation can be written in the following manner.

$$\frac{dT_p}{dt} = \frac{Q_N/A}{(mC_p)_p} - \frac{(T_p - T_b)}{\tau_p} \tag{4.28}$$

where Q_N is the fission and decay power deposited in the fuel, A is the total heat transfer surface area (flat plate approximation), and τ_p is the time constant of the fuel plate:

$$\tau_p = \frac{(mC_p)_p}{U_p} \tag{4.29}$$

Equation 4.28 can be solved numerically using a semi-implicit scheme resulting in the following:

$$\Delta T_p^{n+1} = \left(1 + \frac{\Delta t}{\tau_p^n}\right)^{-1}\left[\frac{\Delta t\, Q_N^n}{A(mC_p)_p^n} - \frac{\Delta t}{\tau_p^n}(T_p - T_b)^n\right] \tag{4.30}$$

The surface heat is determined by:

$$(q'')^{n+1} = U_p^n(T_p^{n+1} - T_b^n) \tag{4.31}$$

Therefore,

$$(T_{cntr} - T_c)^{n+1} = \frac{(q'')^{n+1}}{U_T^n} \tag{4.32}$$

Finally, by substituting Equation 4.32 into Equation 4.20, the plate surface temperature is obtained:

$$T_c^{n+1} = T_p^{n+1} - \left[(q'')^{n+1}\left(\frac{f_p^n}{U_T^n}\right)\right] \tag{4.33}$$

The hot-spot clad wall temperature is calculated using the same method except the heat flux, q", is multiplied by the radial and axial nuclear peaking factors specified by the user. In addition, the convective heat transfer coefficient, h_p, is divided by the heat-flux engineering hot-channel factor.

4.5 SUMMARY

The normalized fission power is found by solving the normalized point-kinetics equations. In solving these equations for a single time step, a linear temporal profile of the power was used to permit the precursor equation to be solved analytically. This assumption then allows for the normalized amplitude equation (normalized fission power) to be solved numerically using a fully-implicit method. However, from the nature of the assumption, the model is limited to slow and moderate transients for convergence.

The normalized decay power is obtained by summing the powers of seven decay product groups. The group decay constants and fractions were obtained from the ENDF/B-IV calculations based on U^{235} and 10^{13} seconds of irradiation time.

The fuel temperatures are calculated by lumping the fuel plate into one equivalent element. The heat conduction equation is solved for the average fuel plate temperature using a semi-implicit numerical scheme. The cladding temperature is solved by using the steady-state Newton's law of cooling.

CHAPTER 5: VALIDATION AND RESULTS

5.1 INTRODUCTION

To determine the code's ability to simulate the MITR transient behavior, simulated results are compared to available data for shutdown and startup transients as well as a pump coastdown transient. The shutdown and startup data were gathered by Lin Wen Hu for the calibration of a computer code written by Dr. John Bernard[31]. The pump coastdown data is available from in-core temperature measurements made as part of the reactor startup procedure to full licensed power.

Several transients are analyzed with the code for both the existing reactor (MITR-II) and a proposed upgraded design (MITR-III). The transients under study include a complete loss of heat sink, continuous control blade withdrawal at various speeds, and pump coastdown with attendant natural circulation. In addition, Limiting Safety System Settings (LSSS) and operating limits for the MITR-III are proposed from the results of the simulations.

5.2 VALIDATION

The data taken for both reactor startup and shutdown include power, heat exchangers primary and secondary outlet temperatures, cooling tower outlet temperature, and hot leg inlet temperature. The temperature readings were taken manually with a one and a half minute cycle from a Speedomax recorder within the control room.

---

[31] Hu, L. W., "MITR-II Simulator," 22.39 Term Project, MIT Nuclear Engineering Department, 1993.

5.2.1 REACTOR STARTUP

After reaching criticality at 500 kW, the power was raised in a stepwise manner shown in Figure 5.2.1-1. The entire transient from subcriticality lasted approximately 113 minutes, however, significant temperature differences were not observed until 55 minutes elapsed and the reactor was critical. Due to the increase in power, the cooling towers outlet temperature increased from 23°C to 27°C approximately in the first 96 minutes. Then, the cooling towers fan was turned on allowing for further power increase. Thereafter, the cooling towers outlet temperature decreased despite the power increase. This behavior is shown in Figure 5.2.1-2. Both the power and the cooling tower outlet temperature are input forcing functions to the simulation code.

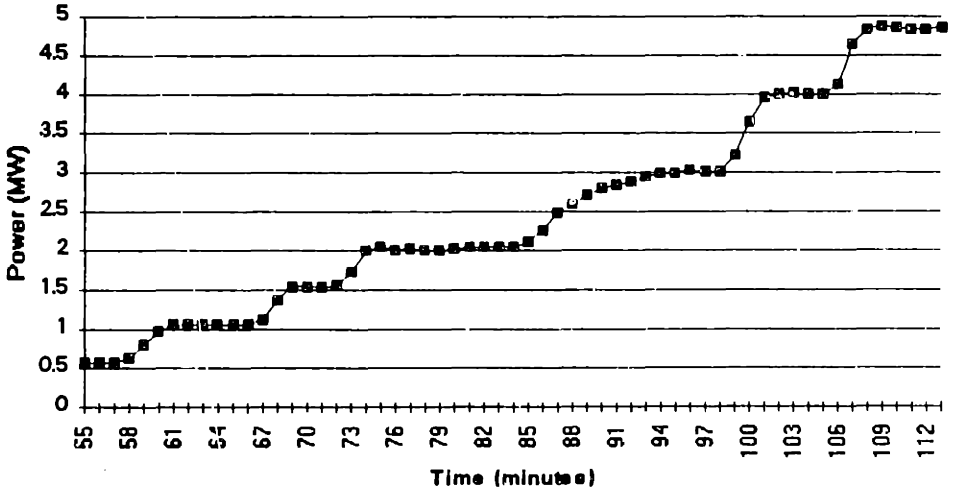

Figure 5.2.1-1. Power in Startup Transient

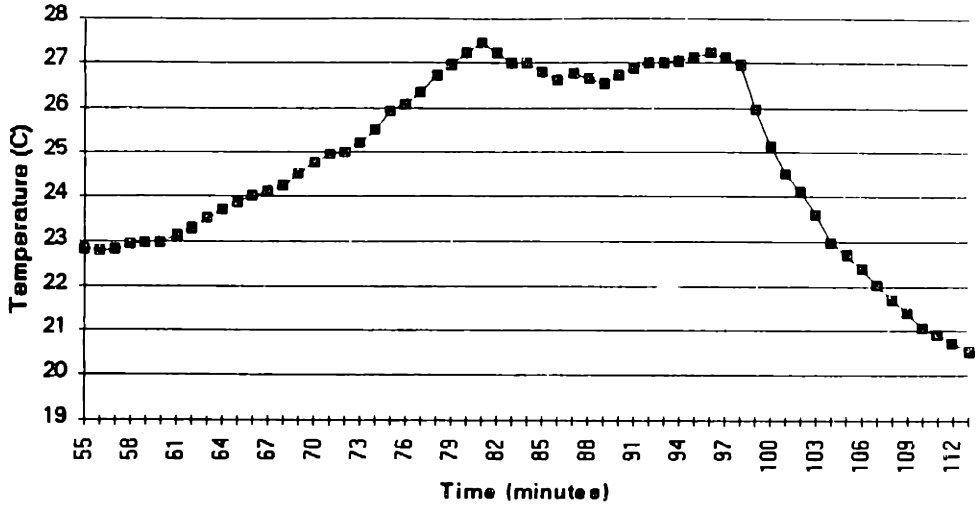

Figure 5.2.1-2. Cooling Towers Outlet Temperature in Startup Transient

The following figures show a comparison between the measured and simulated behavior of the cold leg, hot leg, and heat exchanger secondary outlet temperatures. The input data is given in Appendix D. The simulation follows the measured data closely throughout the entire transient.

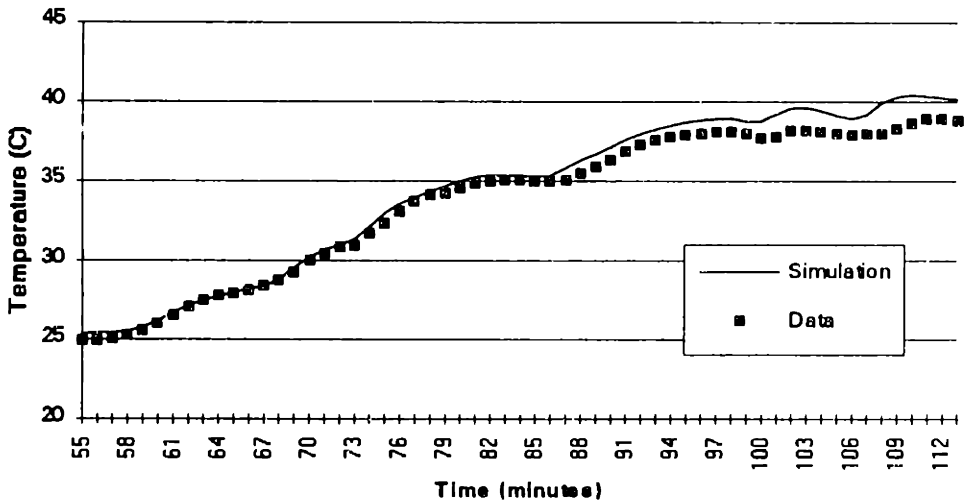

Figure 5.2.1-3. Cold Leg Temperature in Startup Transient

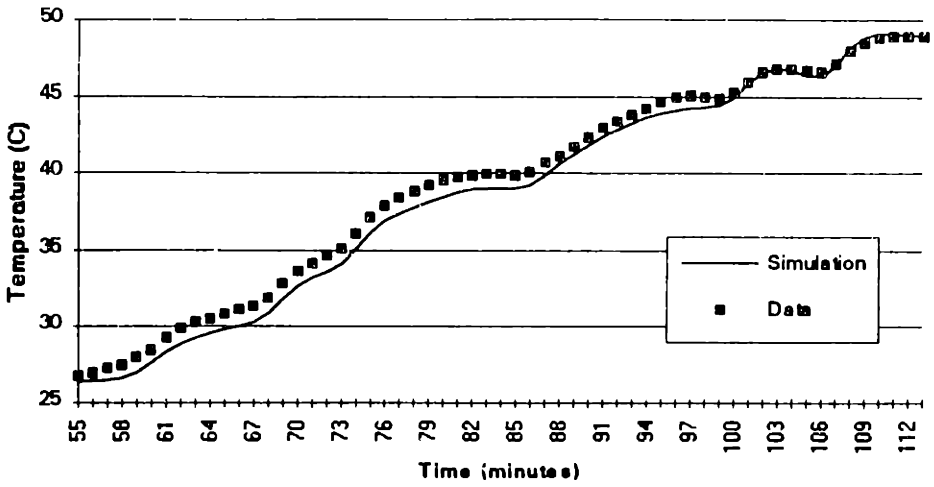

Figure 5.2.1-4. Hot Leg Temperature in Startup Transient

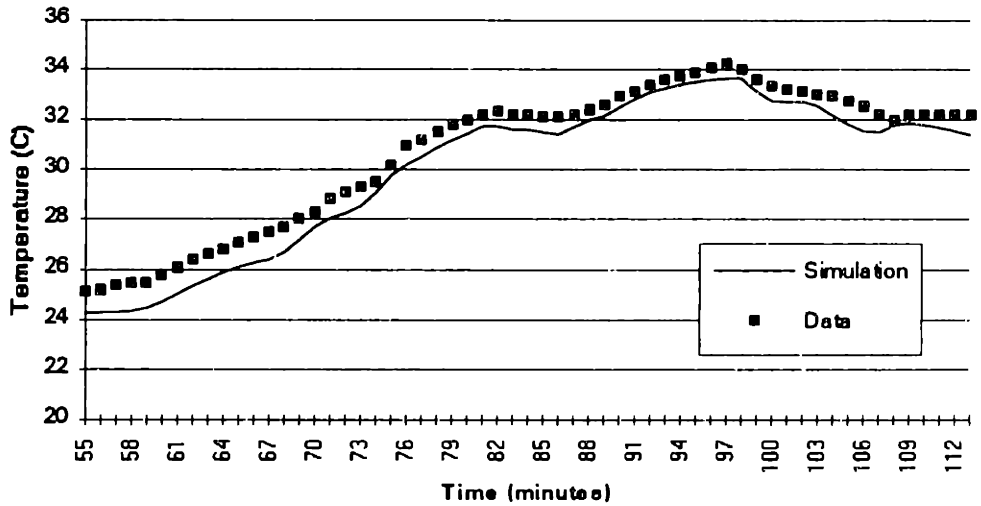

Figure 5.2.1-5. Heat Exchangers Secondary Outlet Temperature in Startup Transient

5.2.2 REACTOR SHUTDOWN

The reactor shutdown data were taken after five days of full power operation. The decrease in power was in the stepwise manner shown in Figure 5.2.2-1. Due to the decrease in power, the cooling towers outlet temperature decreased from 20°C to 14°C

approximately in 85 minutes. Thereafter, the cooling towers fan was turned off to prevent overcooling of the heavy-water reflector. This behavior is shown in Figure 5.2.2-2. As in the reactor startup case, both the power and the cooling tower outlet temperature are input forcing functions.

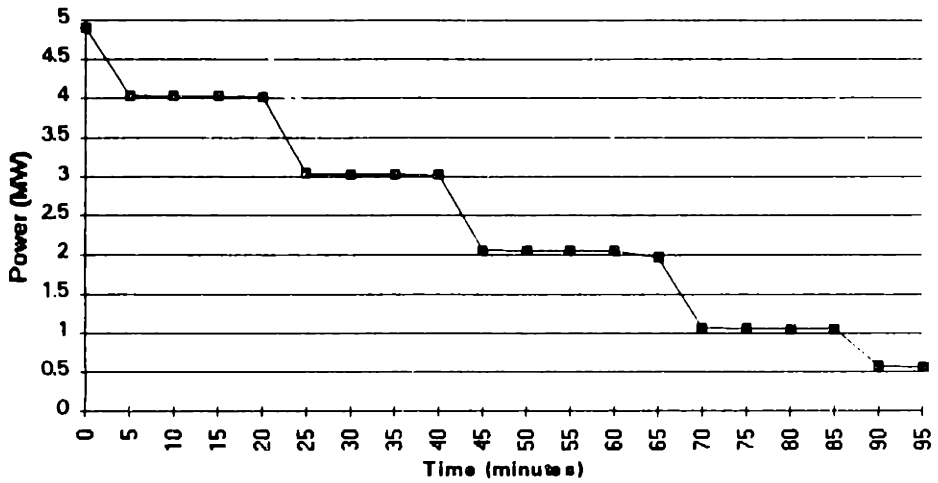

Figure 5.2.2-1. Reactor Power in Shutdown Transient

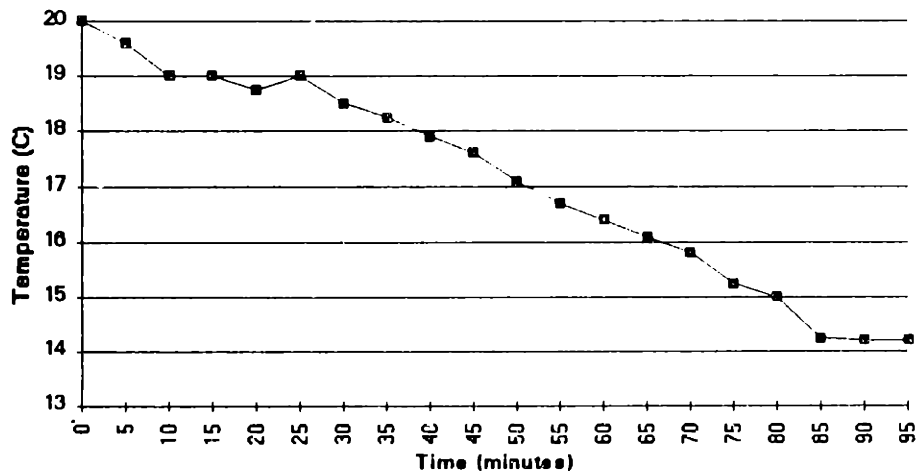

Figure 5.2.2-2. Cooling Towers Outlet Temperature in Shutdown Transient

The following figures show the measured and simulated behavior of the cold leg, hot leg, and heat exchanger secondary outlet temperatures. As for the startup case, the simulated results and the measured data are in good agreement throughout the entire transient. The biggest discrepancy occu for the heat exchanger secondary outlet temperature (Figure 5.2.2-5). However, this discrepancy is within 2°C and any closer results would not be expected.

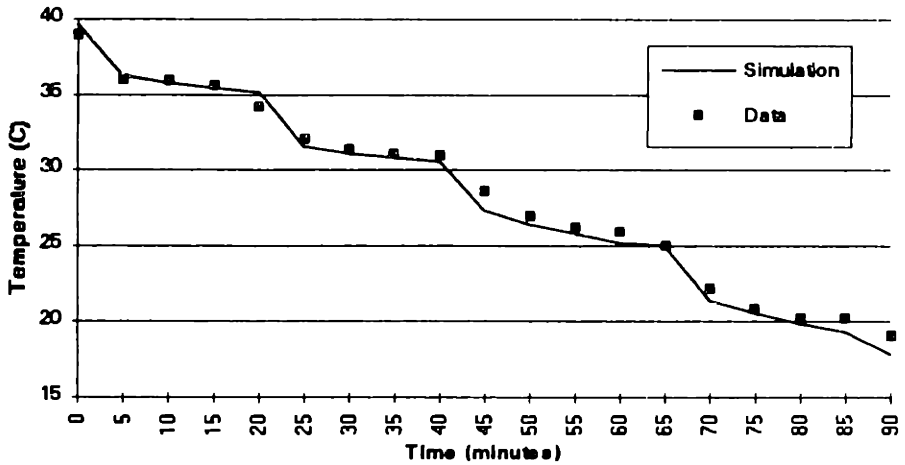

Figure 5.2.2-3. Cold Leg Temperature in Shutdown Transient

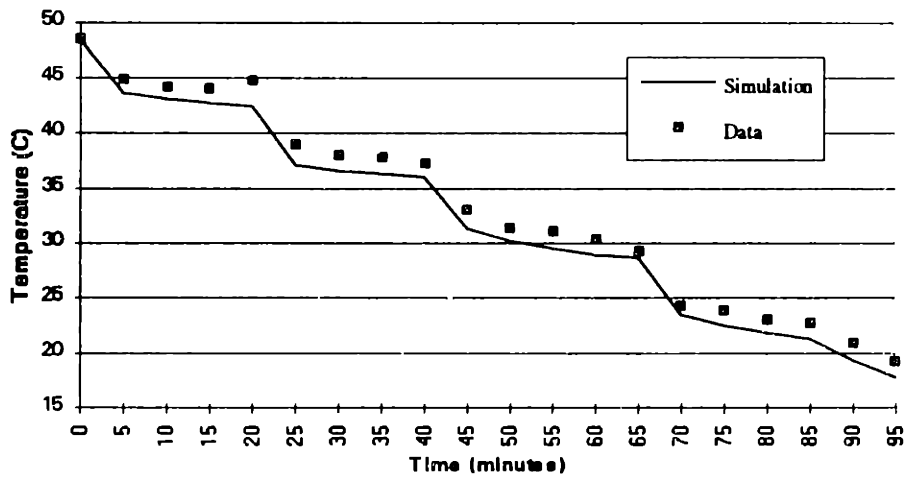

Figure 5.2.2-4. Hot Leg Temperature in Shutdown Transient

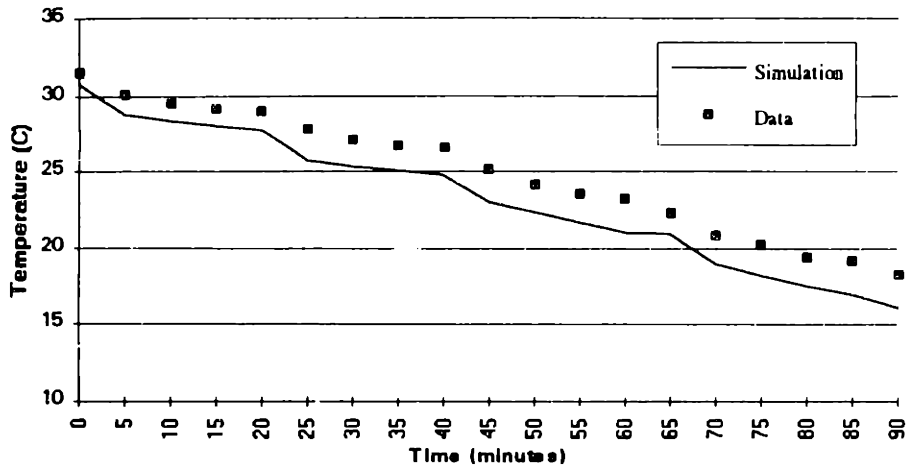

Figure 5.2.2-5. Heat Exchangers Secondary Outlet Temperature in Shutdown Transient

5.2.3. PUMP COASTDOWN

A series of pump trip transient temperature measurements were made during the MITR-II step-wise startup to full power to demonstrate that the decay heat resulting from long-term operation at 5 MW can be removed by natural convective cooling[32]. In addition, the flow behavior in a pump coastdown has been experimentally measured by K. B. Terry[33].

The comparison between the simulation and the available data is shown in Figures 5.2.3-1, 5.2.3-2, and 5.2.3-3. The input data used in simulating the pump coastdown is found in Appendix D. The simulation results are in good agreement with the experimental values except for the core inlet temperature. The discrepancy can be due to the definition of the core inlet. In the simulation, the core inlet is taken as the

---

[32] Bamdad-Haghighi, F., "Natural Convection analysis of the MITR-II During Loss of Flow Accident," Nucl. E. and S.M. Thesis, MIT Department of Nuclear Engineering, page 100, 1977.

[33] Terry, K. B., "Flow Coastdown and Time to Scram for MITR-II," 22.39 Term Project, MIT Department of Nuclear Engineering, 1993.

temperature entering the core. In a pump coastdown transient, this temperature will behave significantly different from the cold leg exit temperature.

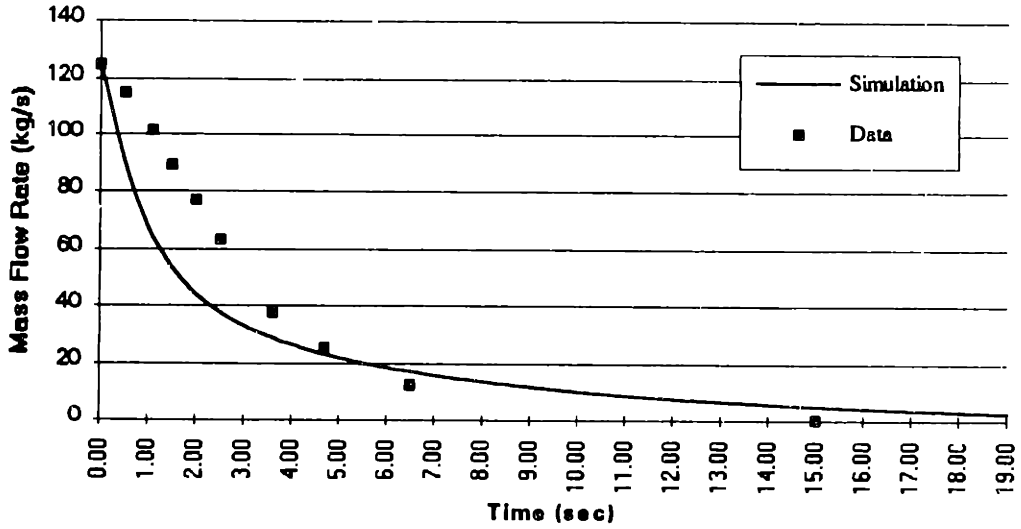

Figure 5.2.3-1. Mass Flow Rate in Pump Coastdown Transient

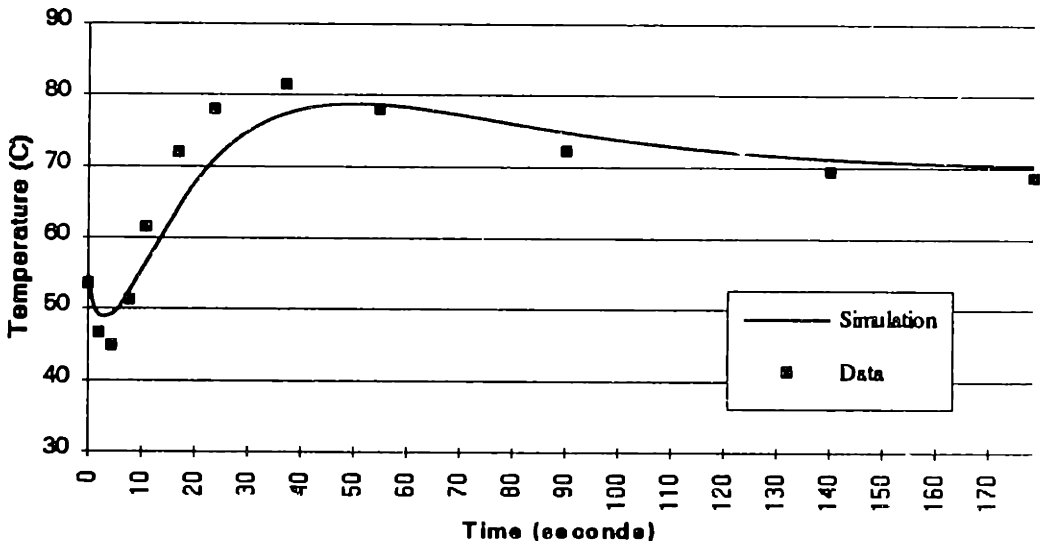

Figure 5.2.3-2. Core Outlet Temperature in Pump Coastdown Transient

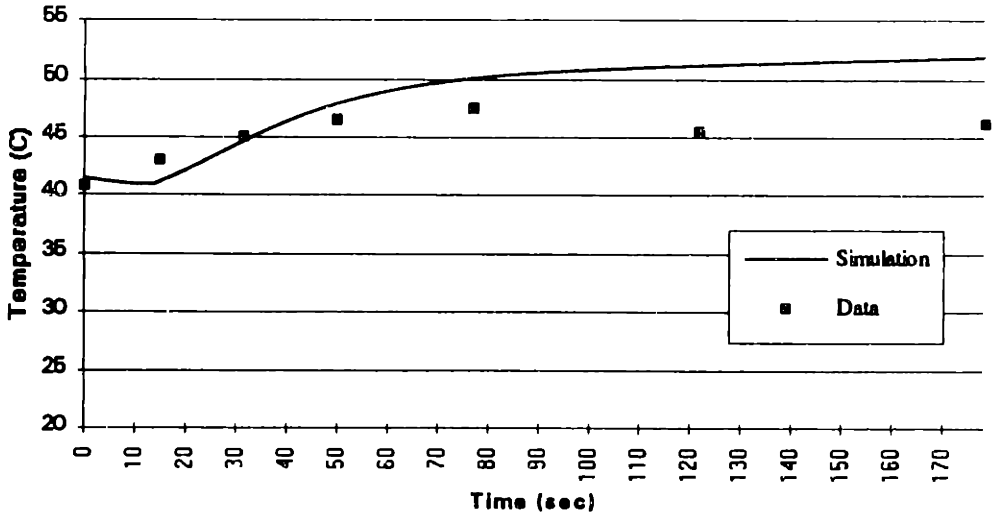

Figure 5.2.3-3. Core Inlet Temperature in Pump Coastdown Transient

Once the loop mass flow rate reaches about six percent of rated flow, the natural circulation valves are expected to open. At that instant the static pressure below the natural circulation valve exceeds that of the top, creating an upward flow through the valves bypassing the core. However, the rapidly decreasing pressure below the natural circulation valves produces a calculated reversal of flow through the valves 10 seconds later. Thereafter, the calculated natural circulation increases and reaches a maximum of approximately 1.8 kg/s in about 150 seconds from the initiation of the pump coastdown. Then, the natural circulation flow rate decreases as the heat slowly decays away. The natural circulation mass flow rate simulation is shown in the following figure.

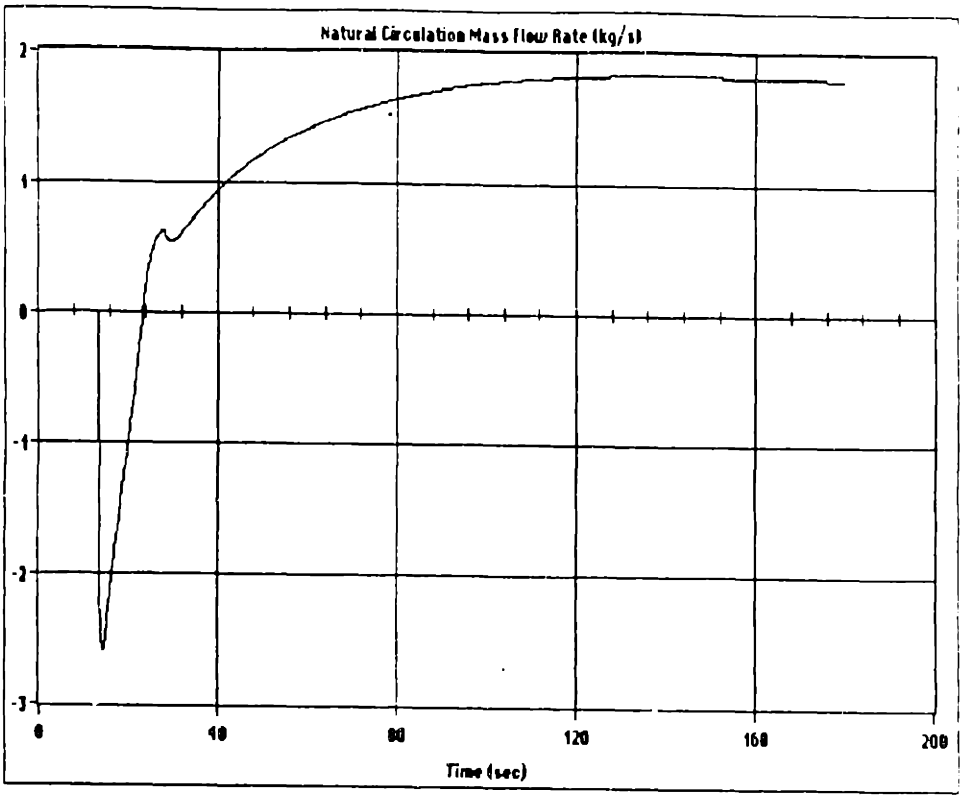

Figure 5.2.3-4. Natural Circulation Mass Flow Rate in Pump Coastdown Transient

Immediately after the pumps begin to coast down, the core outlet temperature increases sharply from approximately 51 °C to 53 °C due to the decrease in core mass flow rate (this is not shown in Figure 5.2.3-2 due to low printing resolution). However, the 1800 gpm trip setting is reached very quickly interrupting this temperature increase. For a short period of time (about 3 seconds), the sudden decrease in power due to the reactor scram outweighs the decrease in mass flow rate, thus lowering the core outlet temperature. Eventually, the mass flow rate through the core reaches a minimum and the core outlet temperature begins to increase once again. In addition, the core inlet temperature increases since the source of coolant for natural circulation is the mixing pool above the core which is hotter than the coolant previously received from the cold

leg. As a consequence of these two effects combined, the core outlet temperature increases at a rapid rate. Since the natural circulation mass flow rate increases and the decay heat decreases, the core outlet temperature reaches a maximum of approximately 81 °C at about 37 seconds from the pump coastdown initiation. The calculated clad temperature follows a similar trend as the core outlet temperature as shown in Figure 5.2.3-5. Note that the clad temperature never reaches the onset-of-nucleate-boiling temperature.

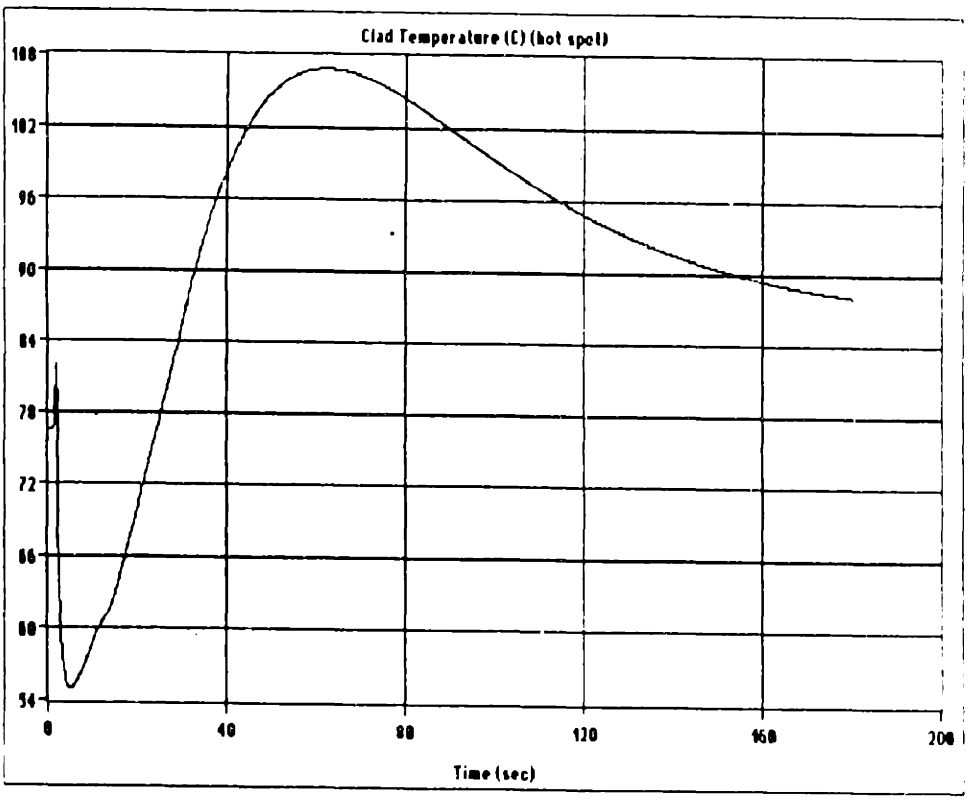

Figure 5.2.3-5. Clad Temperature (hot-spot) in Pump Coastdown Transient

5.3 MITR-II SIMULATION RESULTS

The postulated accidents studied include a loss of heat sink and continuous rod withdrawal at various speeds. The simulations were performed with reactor trips set according to the Limiting Safety System Settings (LSSS): 60°C hot leg temperature, 112.7 kg/s (1800 gpm) mass flow rate, 10 second reactor period, 6 MW power, and 2.9 m water level. In the MITR-II, the actual trip settings (operating limits) are set conservative relative to the LSSS (i.e., 55°C, 1960 gpm, 5.5 MW, 11 sec. period). Although the present design includes a secondary flow rate trip, it was not included in the model.

In modeling the present reactor design, two identical shell-and-tube heat exchangers were used due to lack of detailed information about the lamella heat exchangers. However, this approximation did not affect the results much as shown in Section 5.2. The input data used in modeling the MITR-II system is given in Appendix D. The first transient analyzed is a loss of heat sink described in the following section.

5.3.1 LOSS OF HEAT SINK

The loss of heat sink under study involves a complete loss of secondary pumping power (secondary mass flow rate). To simulate this postulated accident, the flow in the secondary side of the heat exchangers was reduced from the rated volumetric flow rate (1660 gpm) to zero flow rate in a five second interval. A power of 5 MW and a primary volumetric flow rate of 2050 gpm were assumed as the initial conditions.

Due to the decrease in secondary flow rate, the heat exchangers energy removal rate drops significantly in a short period of time as shown in Figure 5.3.1-1. As a

consequence, the heat exchangers primary outlet temperature rises from approximately 46°C to 58°C in about a minute as shown in Figure 5.3.1-2. This sharp increase in the core inlet temperature produces a negative reactivity feedback decreasing the power from about 5.0 MW to 3.6 MW in approximately 50 seconds as shown in Figure 5.3.1-3.

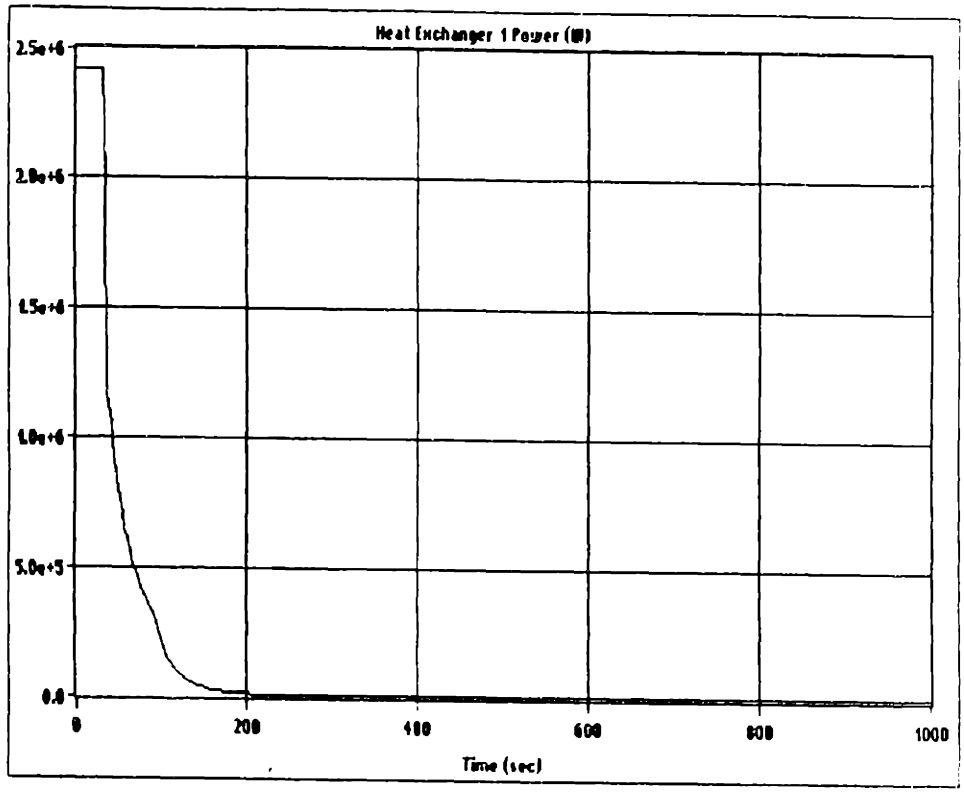

Figure 5.3.1-1. Heat Exchangers Power in Loss of Heat Sink Transient

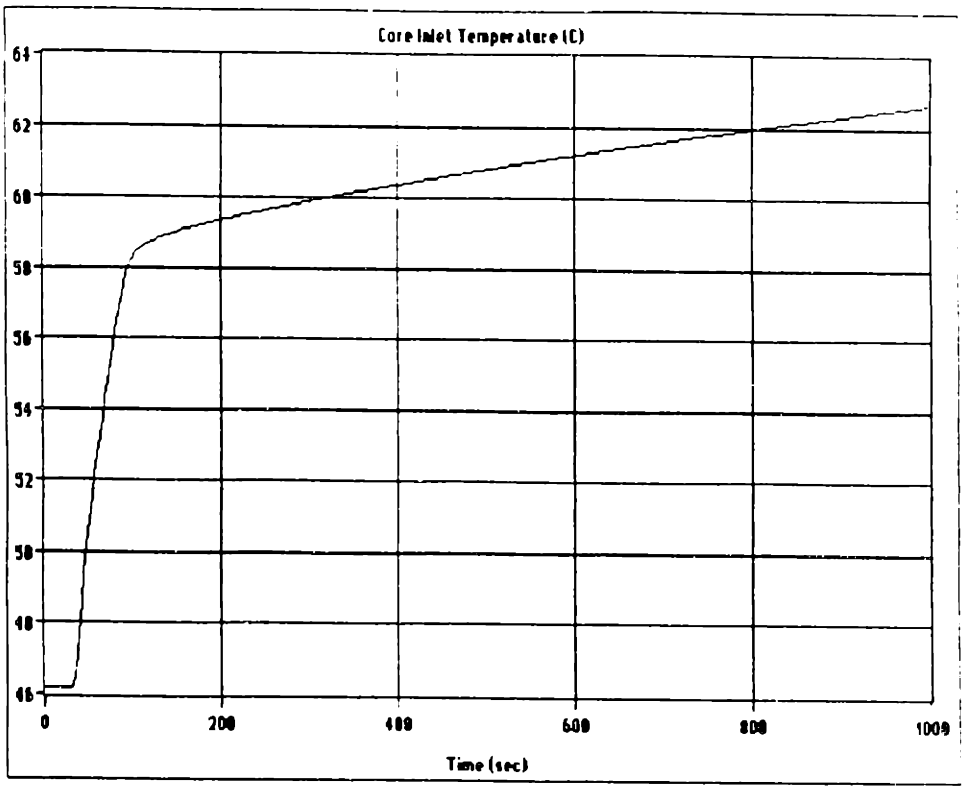

Figure 5.3.1-2. Core Inlet Temperature in Loss of Heat Sink Transient

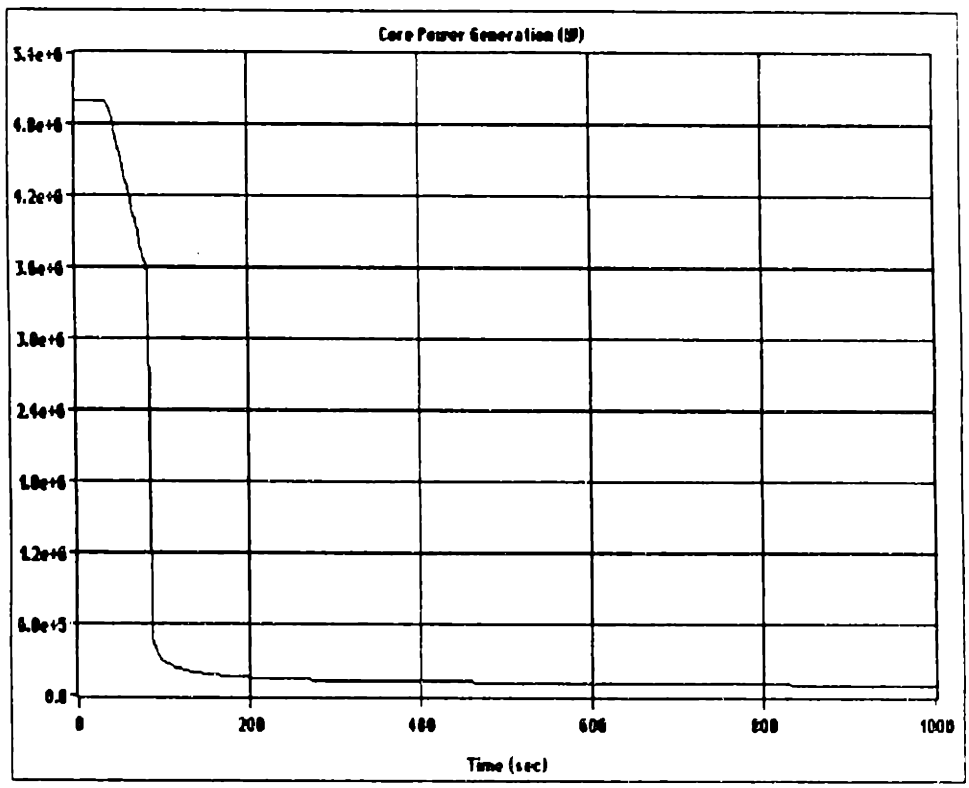

Figure 5.3.1-3. Core Power Generation in Loss of Heat Sink Transient

However, since the energy removal rate decreases more rapidly than the feedback effects, the core outlet temperature rises sharply from approximately 56°C to 63°C in about 50 seconds. During this time interval, the water leaving the mixing pool above the core into the hot leg piping rises from approximately 55°C to 60°C reaching the hot leg temperature trip setting and, consequently, scramming the reactor 50 seconds after the transient was initiated. Therefore, the core outlet and hot leg temperatures drop sharply. However, due to the decay heat generated in the core both temperatures slowly increase thereafter. The same phenomenon is responsible for the slow increase in the core inlet temperature. The core outlet and hot leg inlet temperatures behavior are shown in Figures 5.3.1-4 and 5.3.1-5, respectively. The clad temperaure stays well below the value necessary for the onset of nucleate boiling.

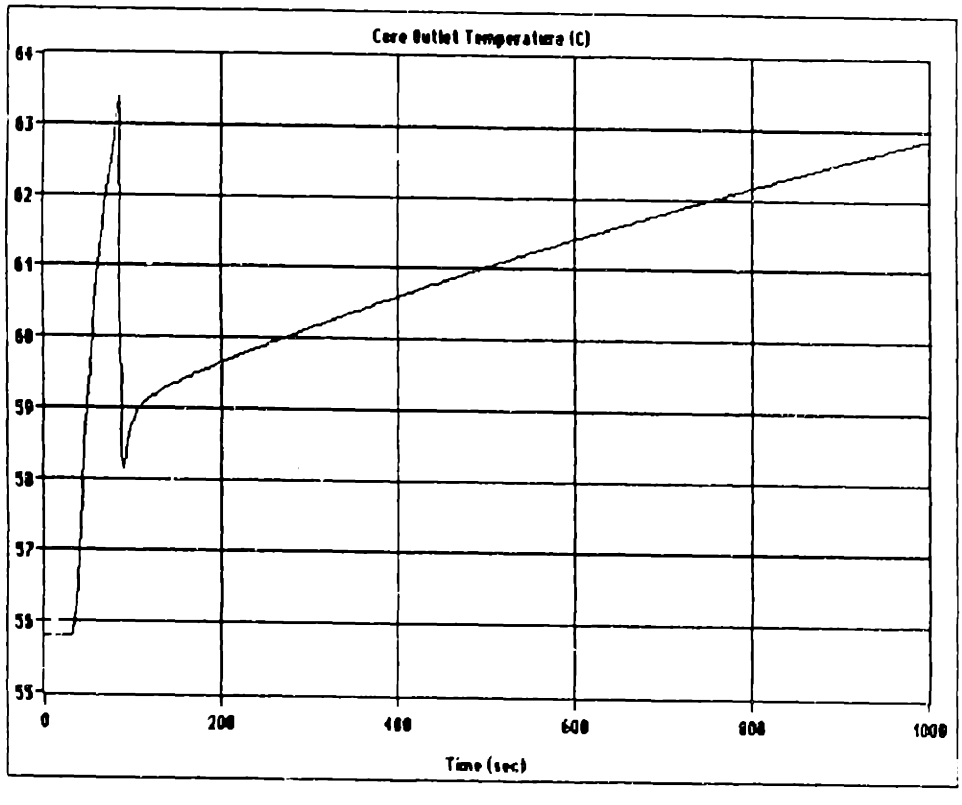

Figure 5.3.1-4. Core Outlet Temperature in Loss of Heat Sink Transient

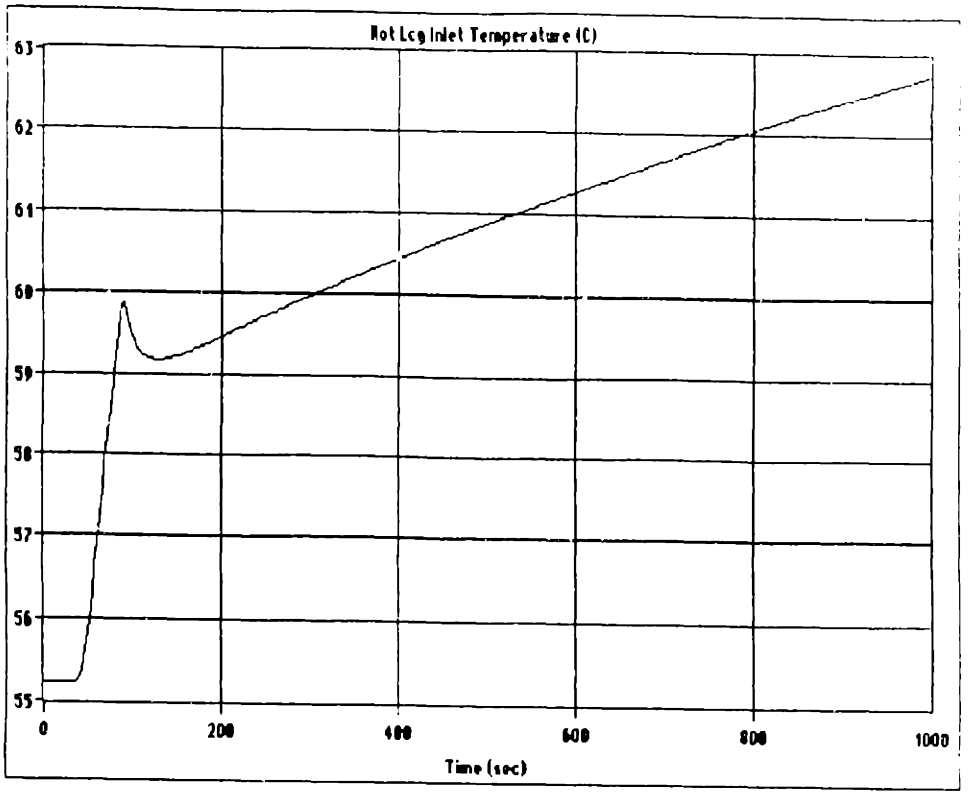

Figure 5.3.1-5. Hot Leg Inlet Temperature in Loss of Heat Sink Transient

It is important to note that the heavy-water tank has not been modeled here. This would contribute to the decay heat removal by conduction through the core tank. In addition, the secondary system was designed so that natural circulation can exist in the case of a loss of secondary pumping power. This occurrence was also excluded from the modeling of the transient. As a consequence, the long term results are believed to be conservative.

5.3.2 CONTINUOUS CONTROL BLADE WITHDRAWAL

The continuous single blade withdrawal simulation was simplified by assuming that the differential worth of the control blade is uniform and equal to the maximum

differential worth for the most reactive control blade (0.147 β/inch). The maximum control blade velocity is 4.25 inches/min and an approximate total reactivity worth of two dollars was used[34]. This is equivalent to inserting two dollars of reactivity in a ramp of approximately 192 seconds. A power of 5 MW (4.83 MW deposited in primary system) and a volumetric flow rate of 2050 gpm were assumed for the initial conditions. The secondary volumetric flow rate was assumed to be 1660 gpm. Any additional information used in simulating this transient can be found in Appendix D.

Figure 5.3.2-1 shows the trend of the core power generation. Note that the reactivity insertion begins after 10 seconds of steady-state operation. The nuclear power rises from approximately 5.0 MW to 6 MW in about 10 seconds where it reaches the overpower trip setting and consequently scrams. The core outlet temperature experiences a sharp increase that is abruptly interrupted by the decrease in power as shown in Figure 5.3.2-2. The hot leg inlet temperature (Figure 5.3.2-3) experiences a slight increase and then it decreases sharply following the reactor scram. The clad temperature (hot-spot) increases from 81°C to 88°C approximately in 10 seconds. Once the reactor scrams, the clad temperature drops quickly as shown in Figure 5.3.2-4. Note that the clad temperature (hot-spot) stays well below the onset-of-nucleate-boiling temperature. The inlet temperature to the core stays practically constant throughout the transient.

---

[34] "MITR-II Integral and Differential Reactivity Worth Curves," Nuclear Reactor Laboratory.

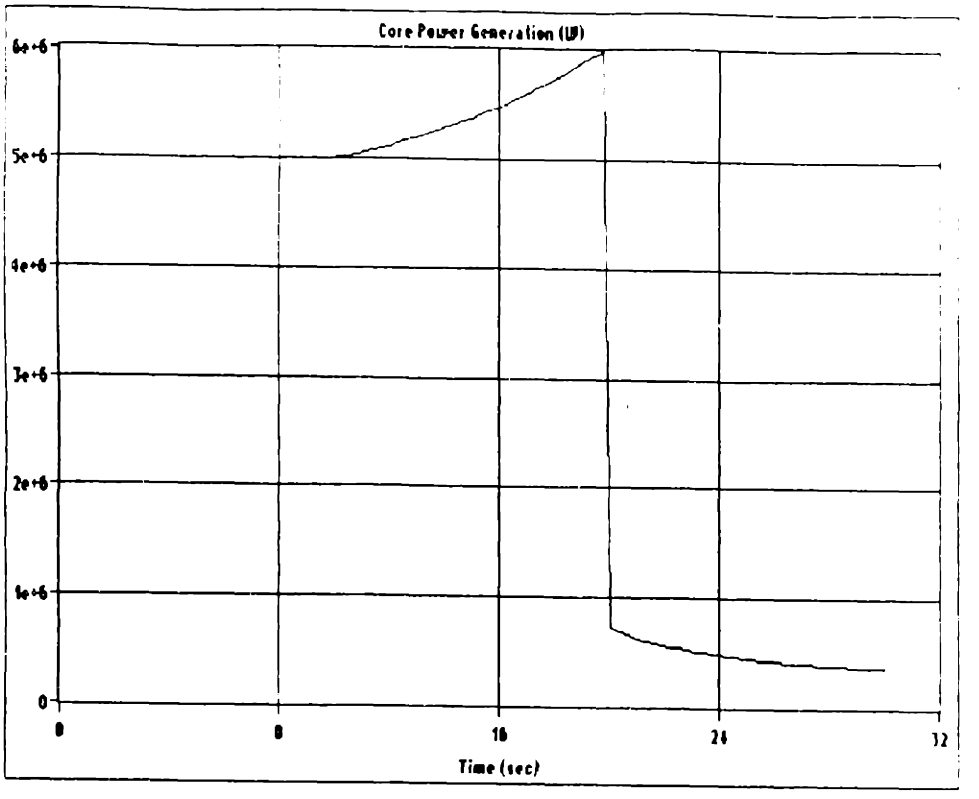

Figure 5.3.2-1. Core Power Generation in Blade Withdrawal Transient (4.25 in/min)

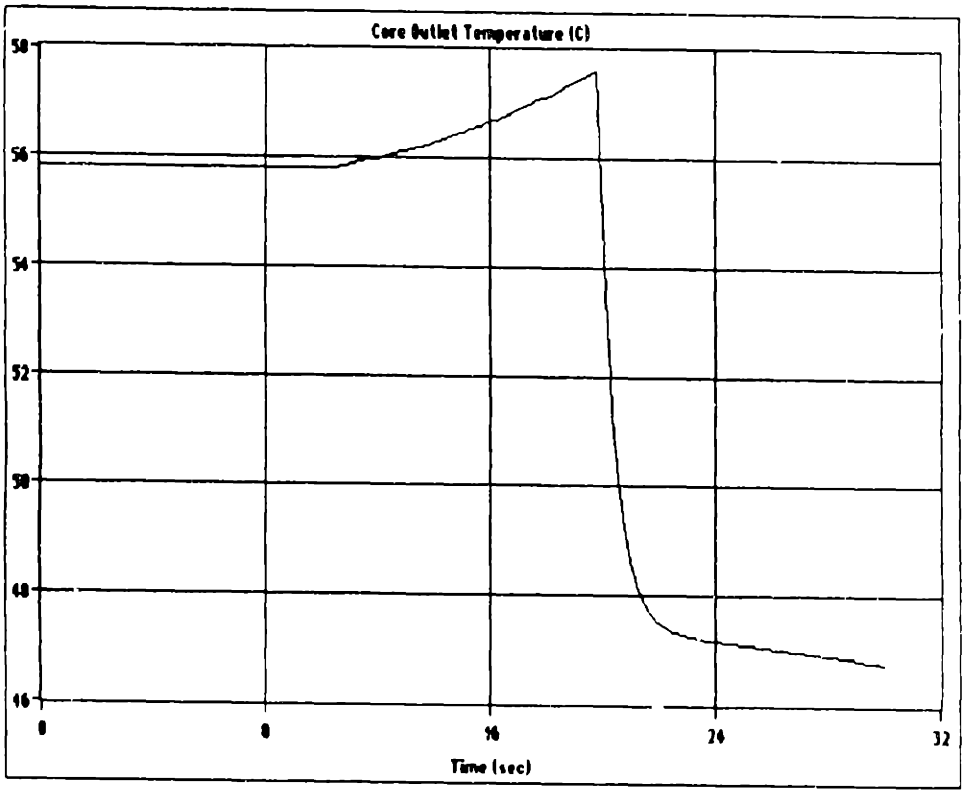

Figure 5.3.2-2. Core Outlet Temperature in Blade Withdrawal Transient (4.25 in/min)

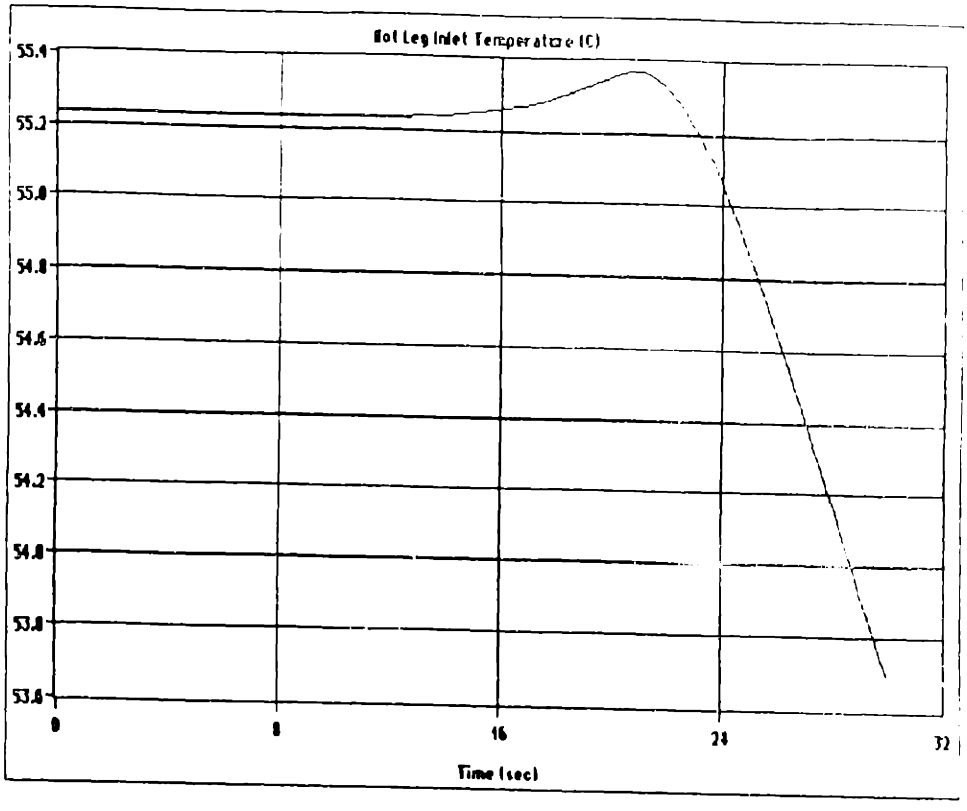

Figure 5.3.2-3. Hot Leg Temperature in Blade Withdrawal Transient (4.25 in/min)

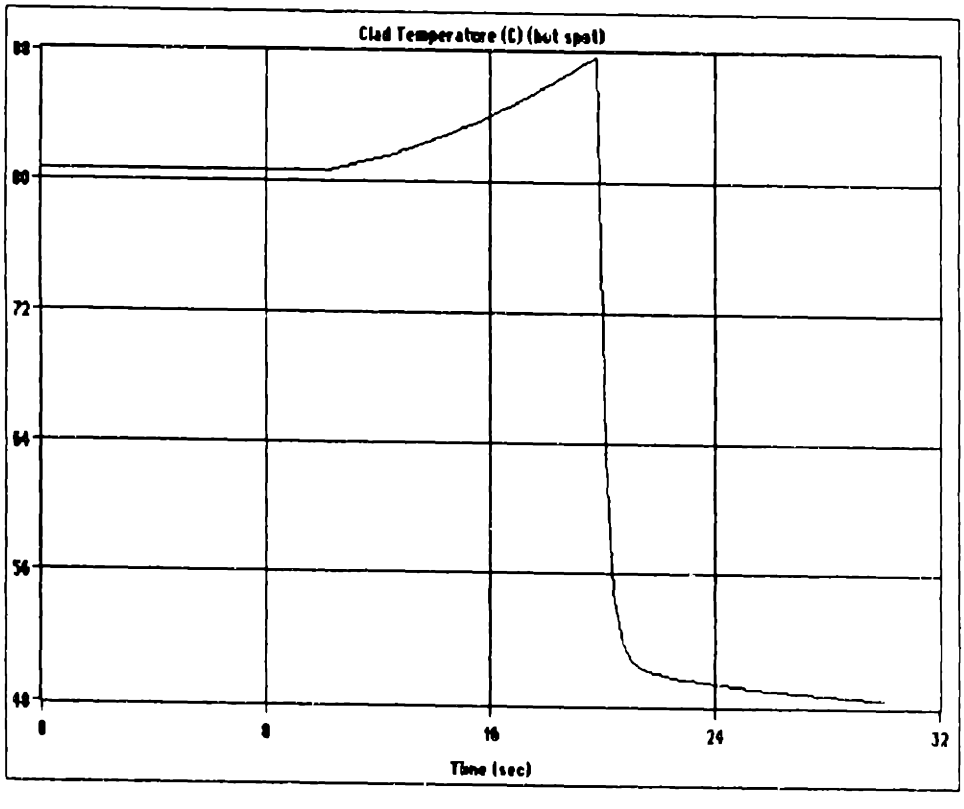

Figure 5.3.2-4. Clad Temperature (hot-spot) in Blade Withdrawal Transient (4.25 in/min)

A control blade velocity of twice the maximum velocity (8.50 in/min) was also studied. The nuclear power increases from 5 MW to 6 MW in approximately 5.5 seconds as shown in the following figure. The core outlet, hot leg inlet, and clad (hot-spot) temperatures are shown in Figures 5.3.2-6, 5.3.2-7, and 5.3.2-8, respectively. The clad temperature never reaches the onset-of-nucleate-boiling temperature.

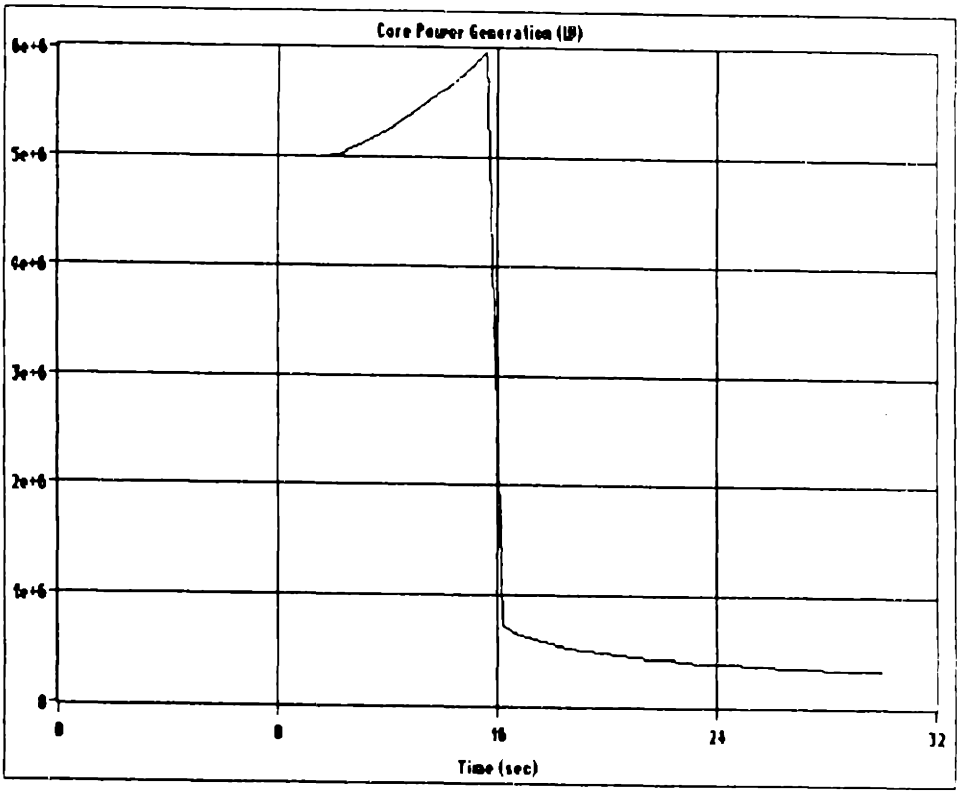

Figure 5.3.2-5. Core Power Generation in Blade Withdrawal Transient (8.50 in/min)

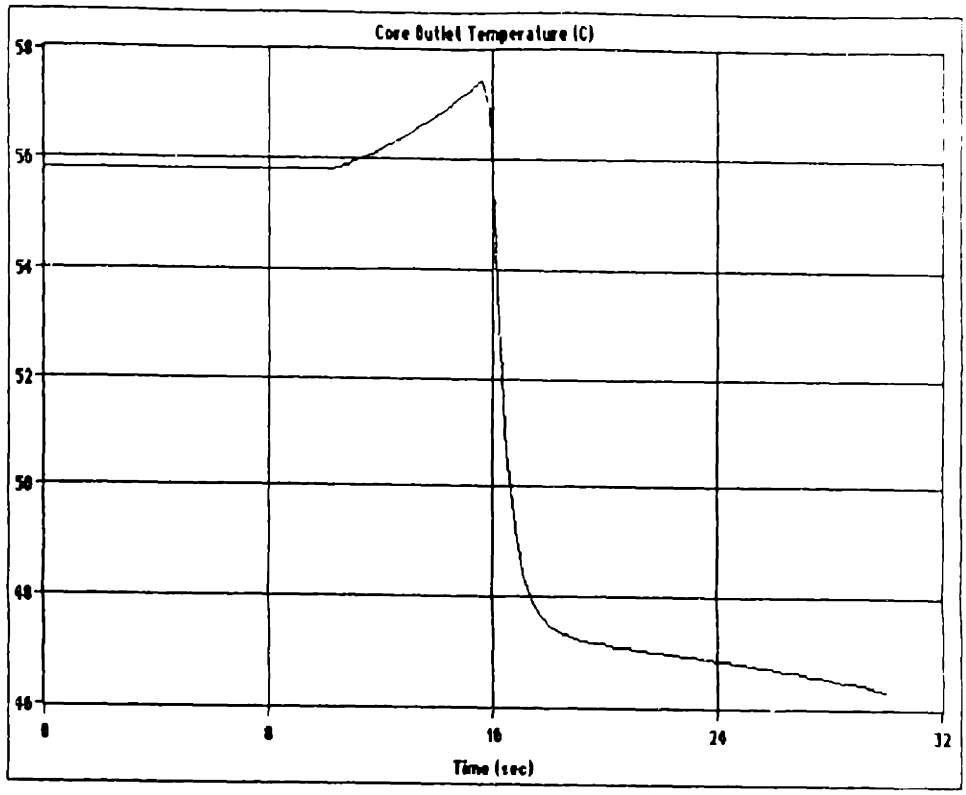

Figure 5.3.2-6. Core Outlet Temperature in Blade Withdrawal Transient (8.50 in/min)

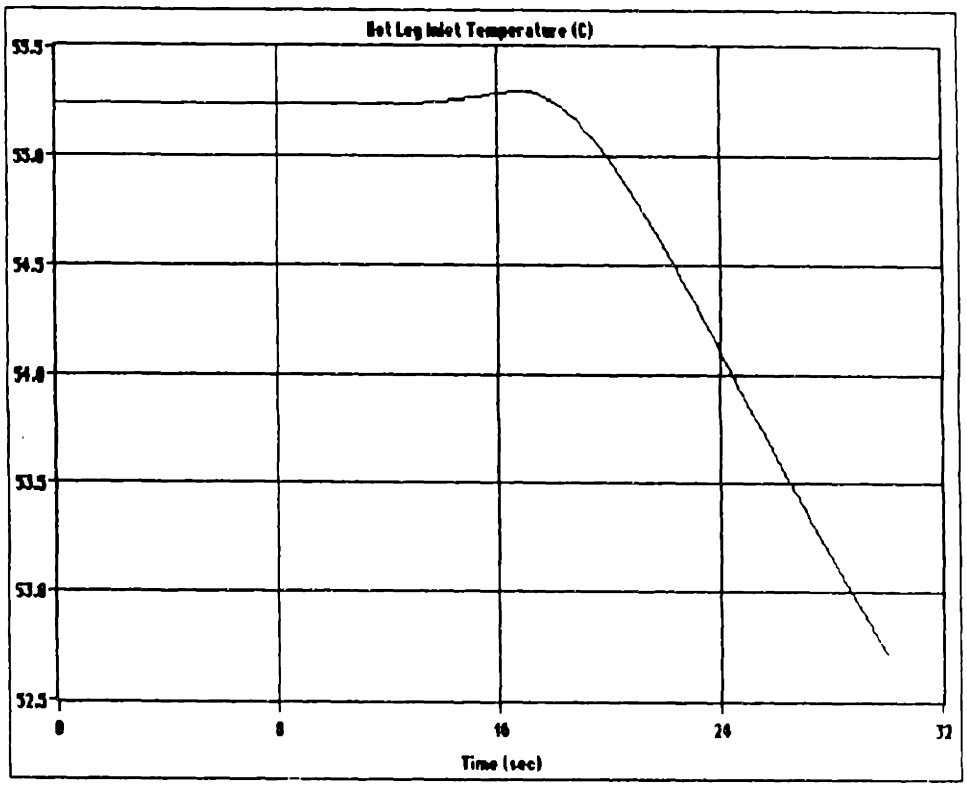

Figure 5.3.2-7. Hot Leg Temperature in Blade Withdrawal Transient (8.50 in/min)

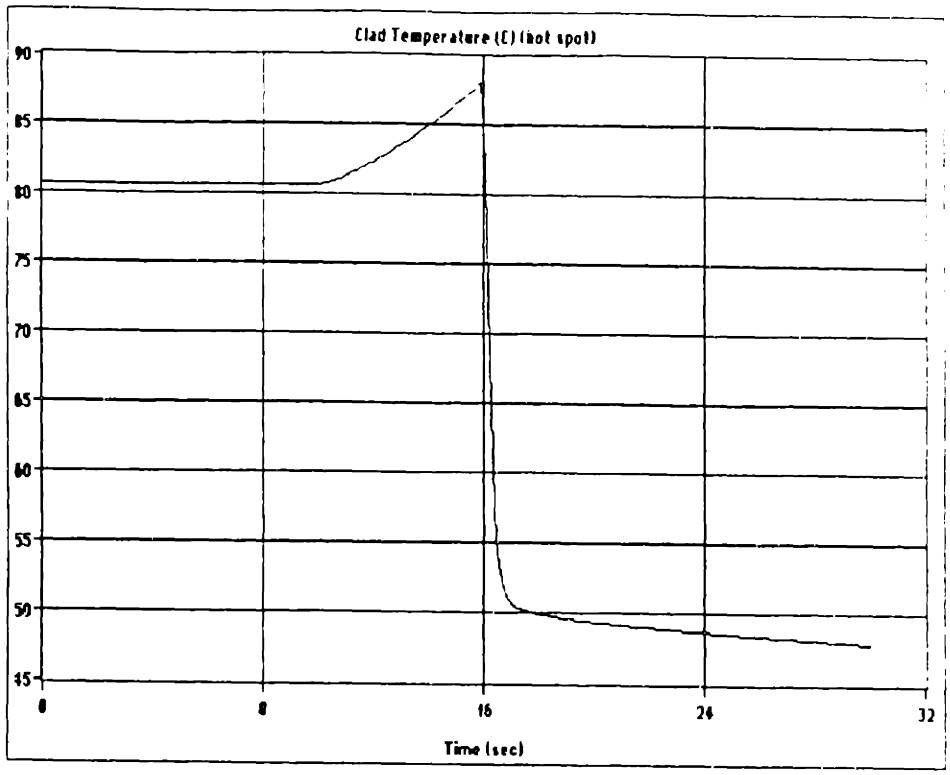

Figure 5.3.2-8. Clad Temperature (hot-spot) in Blade Withdrawal Transient (8.50 in/min)

5.4 MITR-III SIMULATION RESULTS (10 MW Operating Power)

The MITR-III simulations are first performed without any trips. From these results, preliminary trip settings are chosen and the transient simulations are repeated. The same postulated accidents of Section 5.3 as well as a pump coastdown are analyzed. In modeling the MITR-III system, two identical plate type heat exchangers are used. The dimensions of the heat exchangers were gathered by Michael Turek[35]. The primary pumps used in the model provide approximately 2500 gpm of primary volumetric flow rate. The secondary volumetric flow rate used is 2290 gpm with a heat exchanger secondary inlet temperature between 25 and 27°C.

---

[35] Turek, M., "Summary of MITR-III Upgrade Studies," 22.902 Special Project, MIT Department of Nuclear Engineering, 1994.

The power shapes for every assembly and the engineering hot channel factors have been calculated by S. A. Parra[36]. In the following simulations, three clad locations were studied: top and bottom of assembly A-1, and bottom of assembly C-1. The radial peaking factors of assembly A-1 and C-1 are 1.388 and 1.131, respectively. At the top and bottom of assembly A-1 the axial peaking factors are 1.05 and 1.67, respectively. The axial peaking factor at the bottom of assembly C-1 is 2.475. To account for fuel axial conductivity and entrance effects, the local (bottom) peaking factors were reduced by 15 percent. Note that when clad temperature results are stated, they are the most limiting of these three locations. In addition, a hot channel flow disparity of 0.916 was used.

5.4.1 LOSS OF HEAT SINK (no scram)

As in the MITR-II simulation, the loss of heat sink involves a complete loss of secondary pumping power. The flow in the secondary side of the heat exchangers was reduced from the rated volumetric flow rate (2290 gpm) to zero flow rate in a thirty second interval. An initial power of 10 MW was assumed.

Due to the decrease in secondary flow rate, the heat exchangers energy removal rate drops significantly in a short period of time as shown in Figure 5.4.1-1. As a consequence, the heat exchangers primary outlet temperature (core inlet temperature) rises as shown in Figure 5.4.1-2. Although the reactor does not scram, the increase in the core inlet temperature produces a negative reactivity feedback effectively shutting down the reactor. The behavior of the core power generation is shown in Figure 5.4.1-3.

---

[36] Parra, S. A. ibid., page 46-48 & page 89.

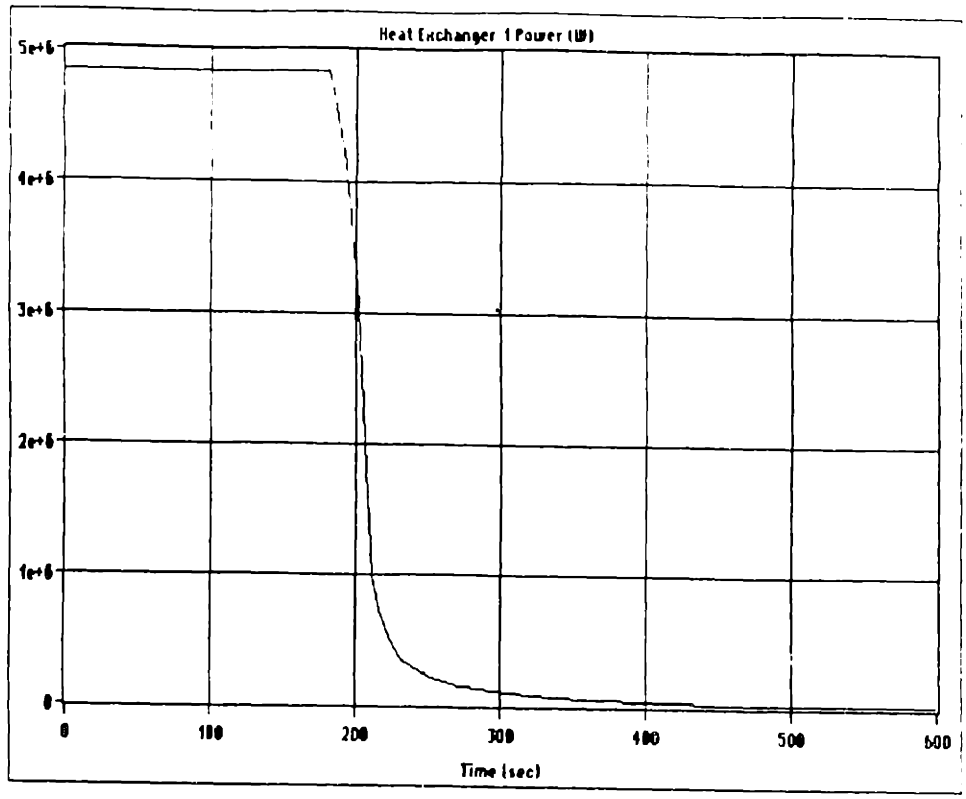

Figure 5.4.1-1. Heat Exchangers Power in Loss of Heat Sink Transient

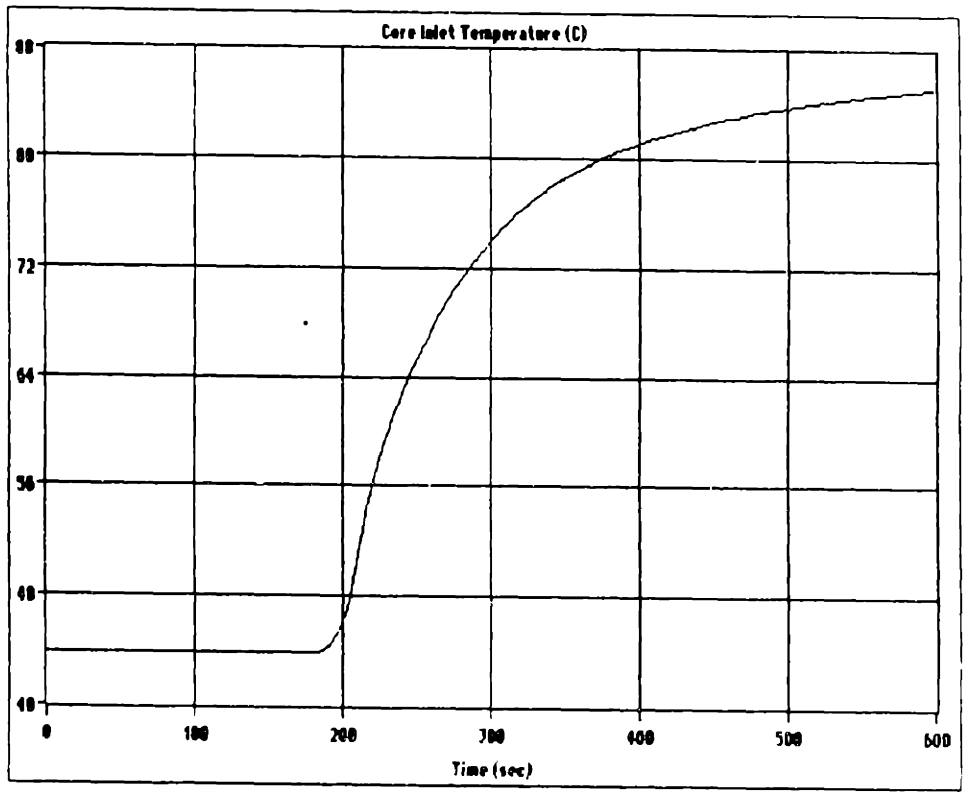

Figure 5.4.1-2. Core Inlet Temperature in Loss of Heat Sink Transient

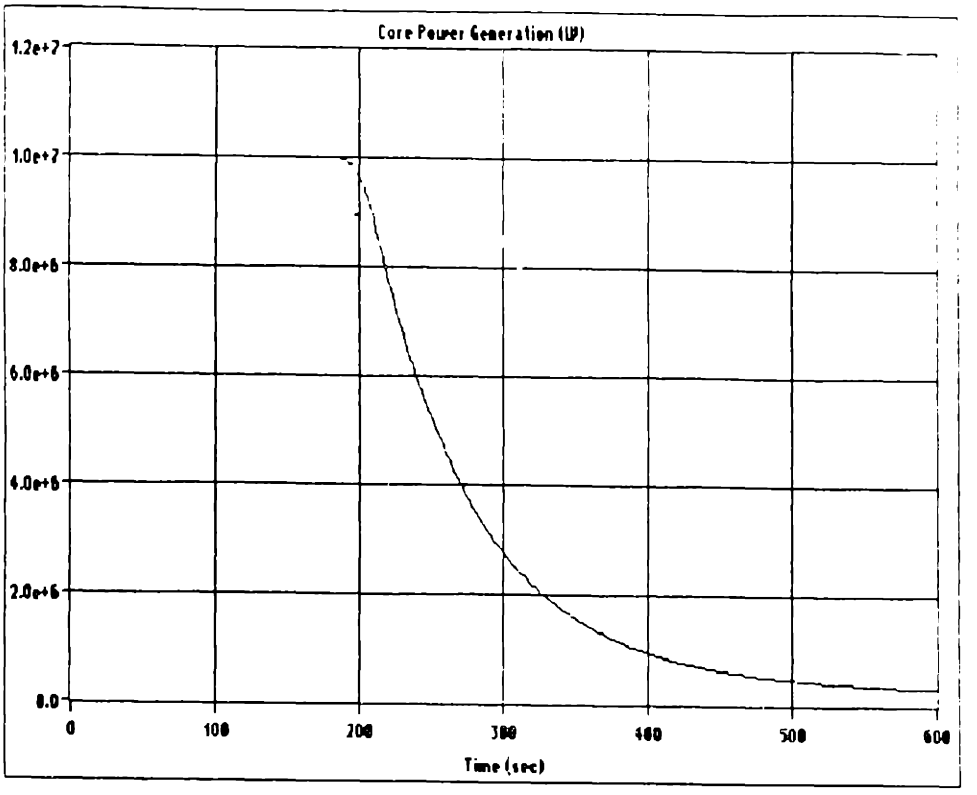

Figure 5.4.1-3. Core Power Generation in Loss of Heat Sink Transient

However, since the energy removal rate decreases faster than the core power, the core outlet temperature also rises sharply as shown in Figure 5.4.1-4. Thus, the water leaving the mixing pool above the core into the hot leg piping rises also. The hot leg inlet temperature is shown in Figure 5.4.1-5. As can be observed from all of the temperature figures, the rate at which the temperatures increase (post-shutdown) continually decreases due to the slow decay of the heat generation within the core.

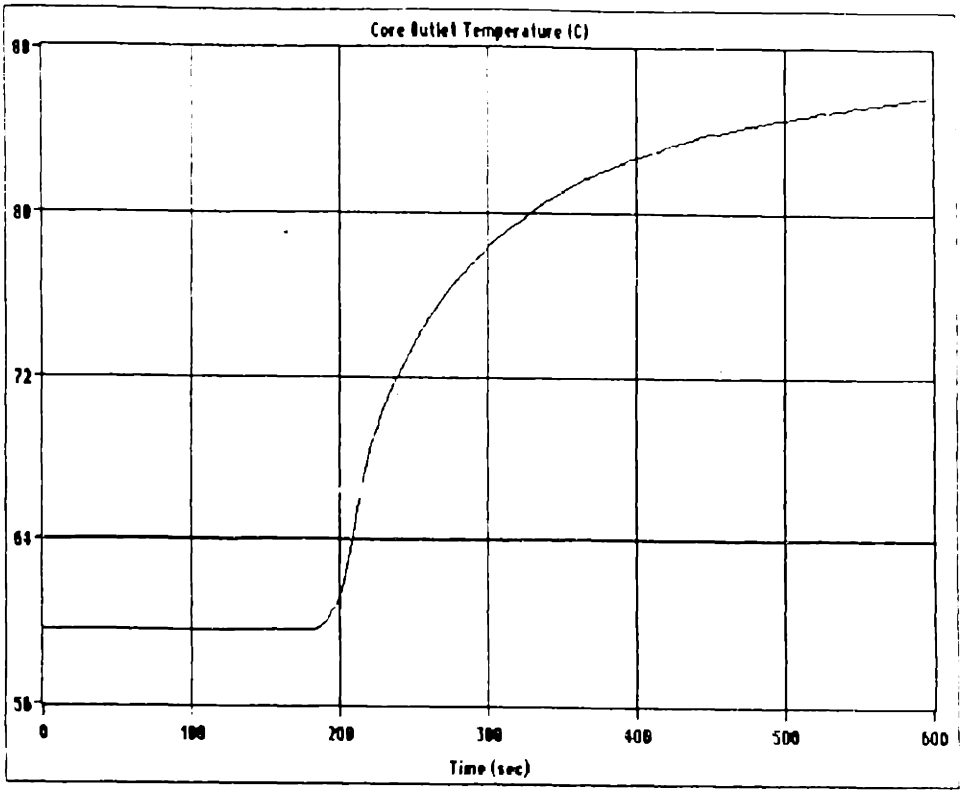

Figure 5.4.1-4. Core Outlet Temperature in Loss of Heat Sink Transient

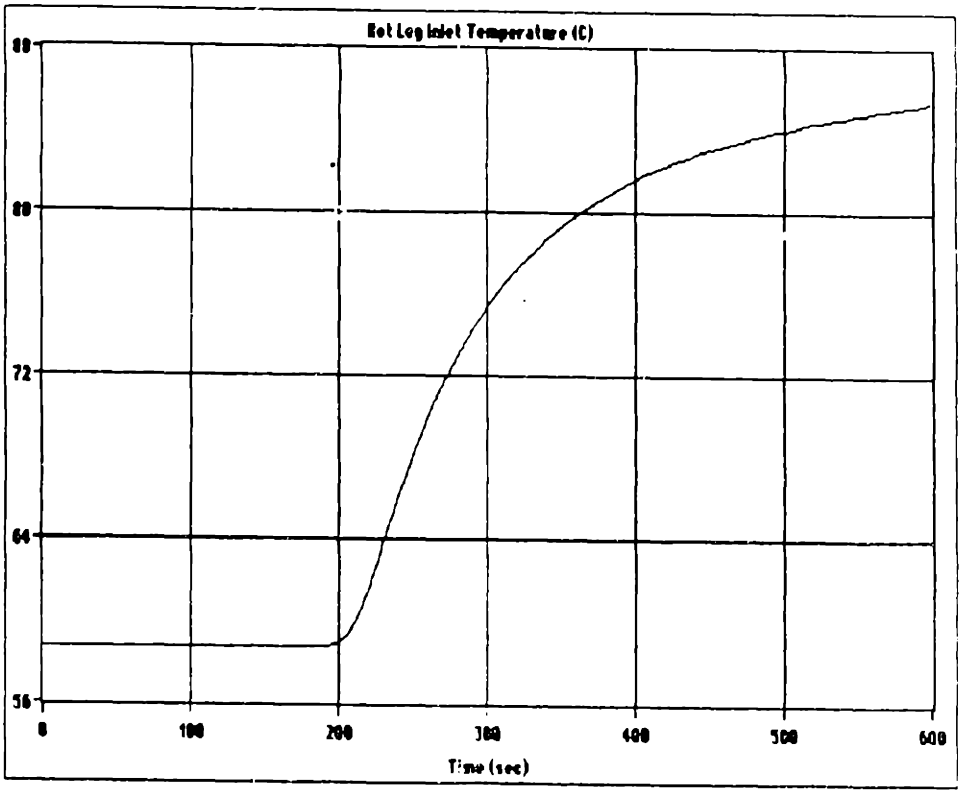

Figure 5.4.1-5. Hot Leg Inlet Temperature in Loss of Heat Sink Transient

Although the heat slowly decays away, there isn't any heat transfer in the heat exchangers to remove this heat. Therefore, the entire primary system heats up and eventually (about an hour and a half into the transient) subcooled nucleate boiling is predicted to occur.

As noted in Section 5.3.1, the heavy-water tank was not modeled here. In addition, natural circulation effects on the secondary system have also been neglected. Therefore, the long range results are believed to be conservative.

5.4.2 CONTINUOUS CONTROL BLADE WITHDRAWAL (no scram)

For simplicity, the MITR-III control blade worth curves were assumed identical to the MITR-II curves. Two control blade velocities were studied: 4.25 and 8.50 inches/min. This is equivalent to inserting two dollars of reactivity in approximately 192 and 96 seconds, respectively. A power of 10 MW and a primary volumetric flow rate of 2500 gpm were assumed as the initial conditions. As in the MITR-II simulations, the reactivity insertions begin after 10 seconds of steady-state operations. The calculations were followed until subcooled nucleate boiling was predicted. Any predictions beyond the onset of nucleate boiling may not be accurate due to the possibility of flow instabilities within the core which is a phenomenon not included in the simulation model. It is important to remember that these calculations were done without trips with intent to subsequently select adequate preliminary trip settings for the MITR-III design. For the 4.25 in/min case, the power behavior is shown in Figure 5.4.2-1. Due to the continuous reactivity insertion, the power rises with an approximate 30 second period. This causes a

rapid increase in the core outlet temperature as shown in Figure 5.4.2-2. Due to the increase in core outlet temperature, the hot leg inlet temperature increases as shown in Figure 5.4.2-3. The core inlet temperature does not change significantly during the first 14 seconds due to the delay caused by the transport time through the loop. The core inlet temperature is shown in Figure 5.4.2-4. Due to the increase in heat generation, the clad temperature (hot-spot) increases rapidly as shown in Figure 5.4.2-5. The clad temperature required for the onset of nucleate boiling is predicted to occur 11.2 seconds after the transient initiation.

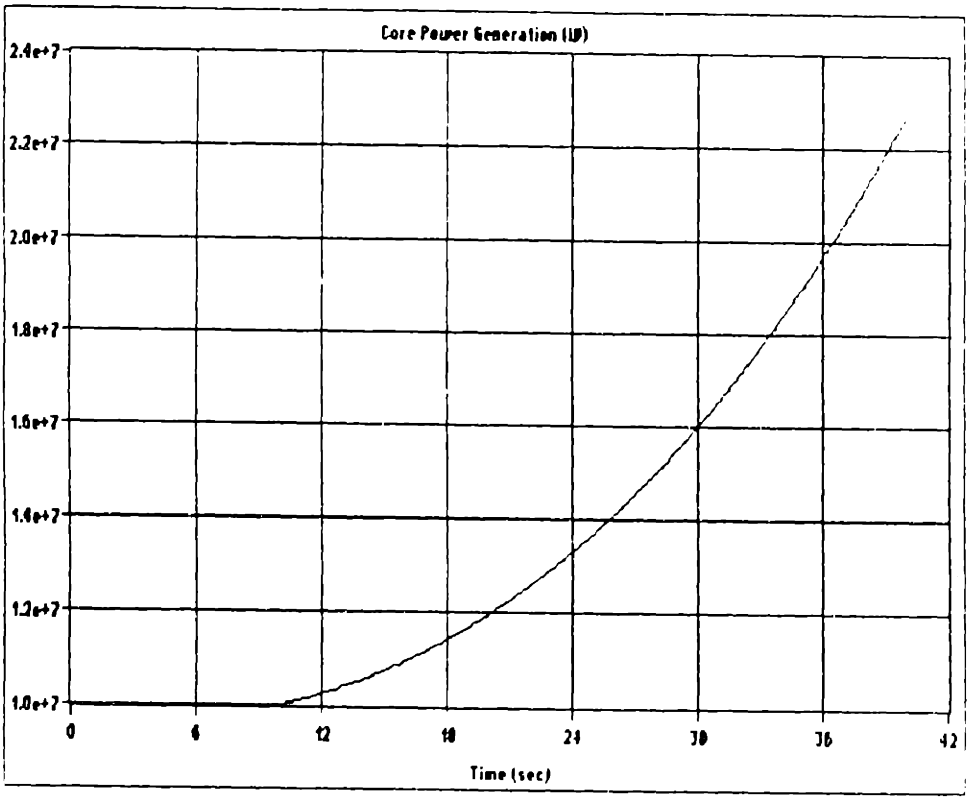

Figure 5.4.2-1. Core Power Generation in Blade Withdrawal Transient (4.25 in/min)

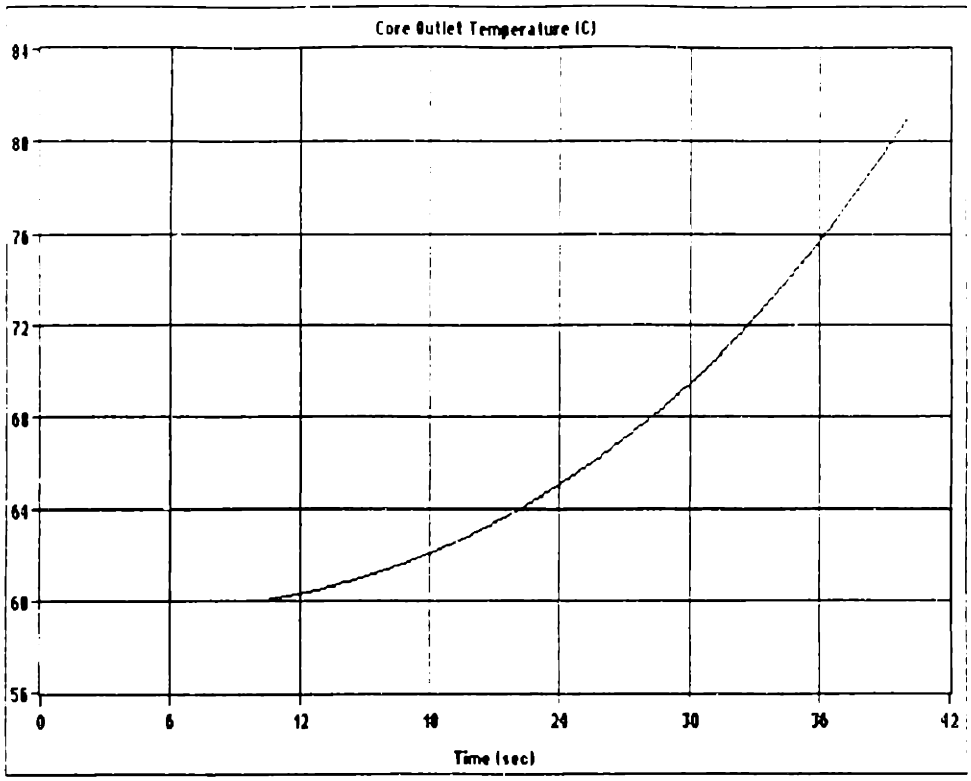

Figure 5.4.2-2. Core Outlet Temperature in Blade Withdrawal Transient (4.25 in/min)

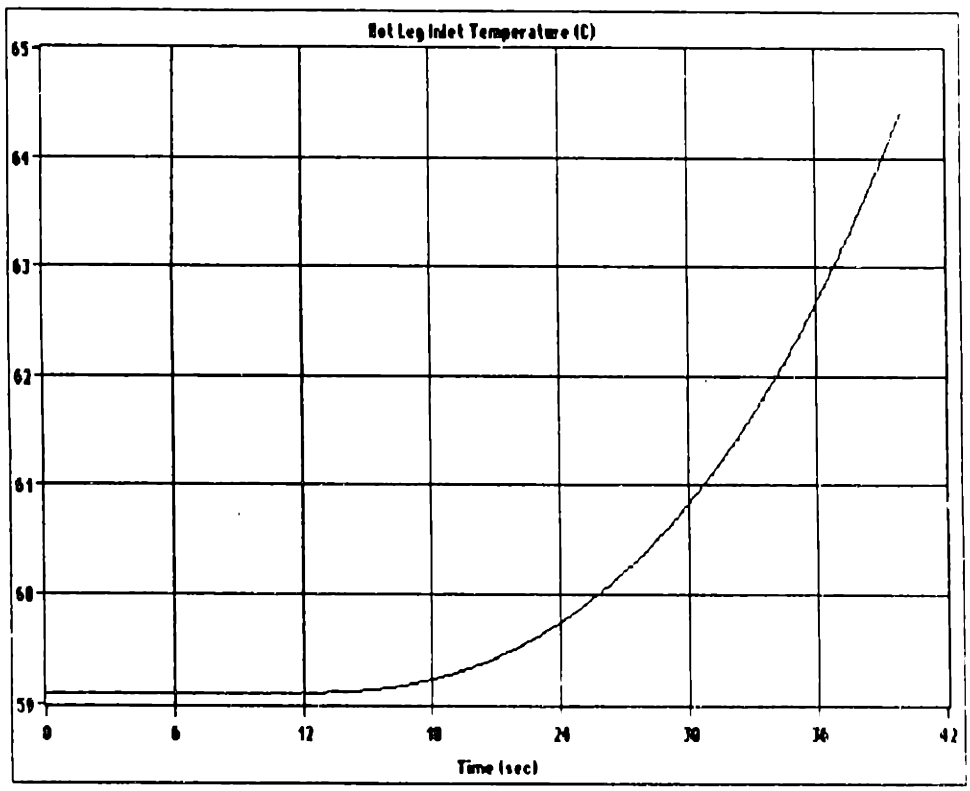

Figure 5.4.2-3. Hot Leg Temperature in Blade Withdrawal Transient (4.25 in/min)

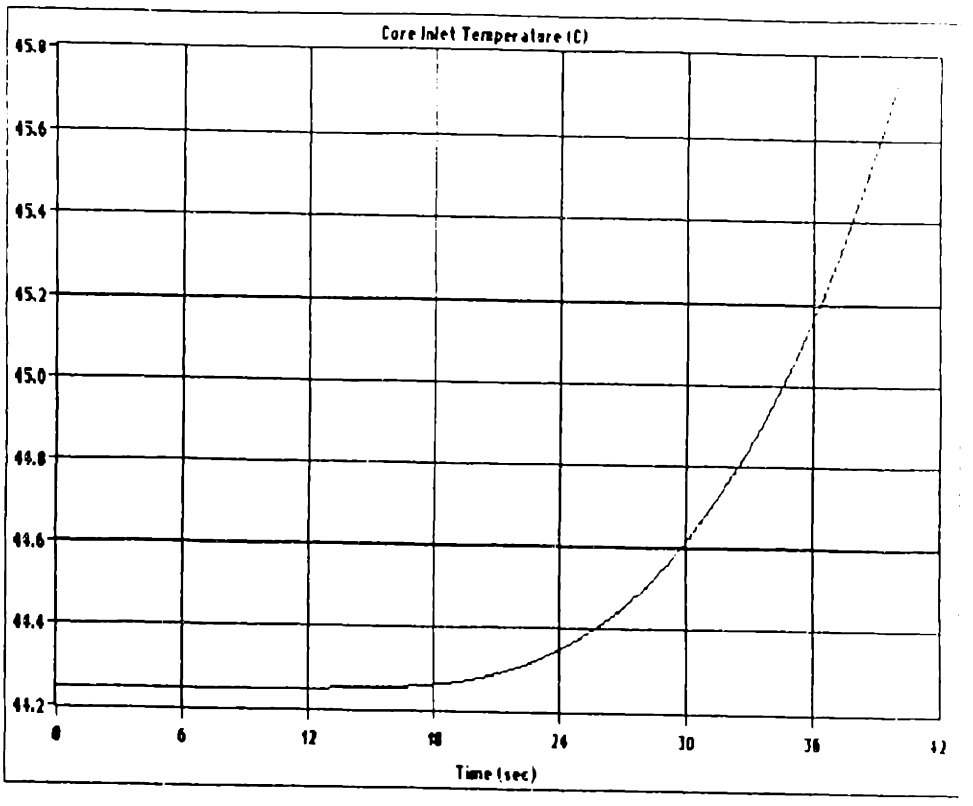

Figure 5.4.2-4. Core Inlet Temperature in Blade Withdrawal Transient (4.25 in/min)

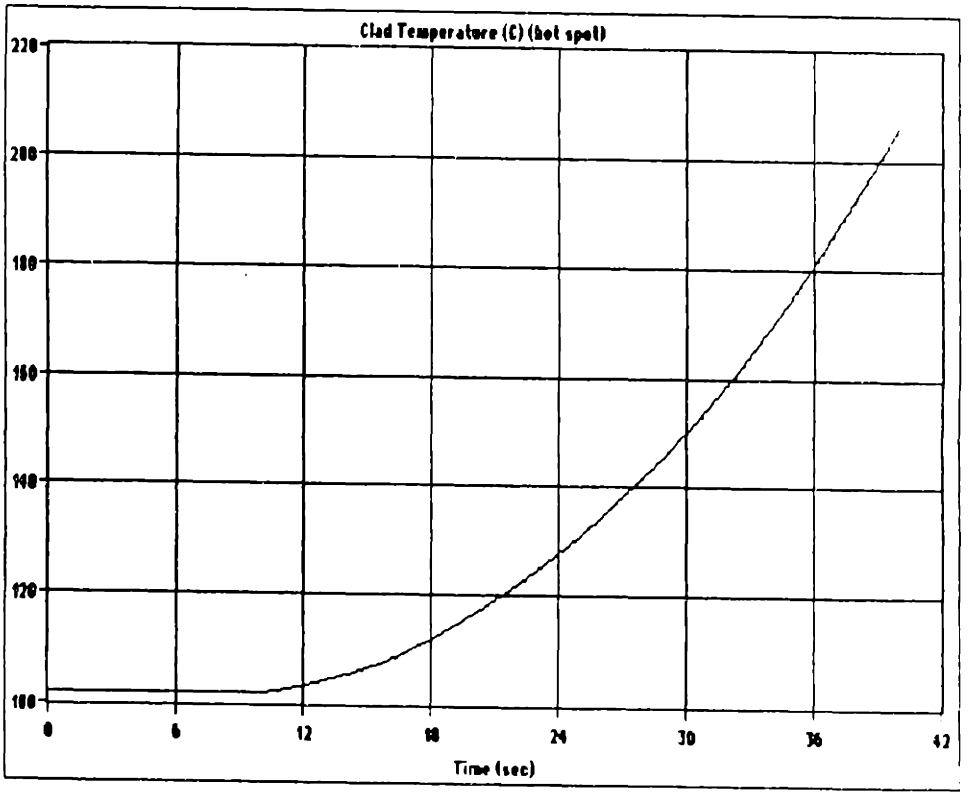

Figure 5.4.2-5. Clad Temperature (hot-spot) in Blade Withdrawal Transient (4.25 in/min)

For the 8.50 in/min control blade velocity case, the power increases with an approximate 16 second period as shown in Figure 5.4.2-6. The transient results do not differ much from the previous case, except the rates at which the temperatures increase are larger, and the onset of nucleate boiling is predicted to occur 6.7 seconds after the transient begins. The core outlet and hot leg inlet temperatures are shown in Figures 5.4.2-7 and 5.4.2-8, respectively. The core inlet and clad (hot-spot) temperatures are shown in Figures 5.4.2-9 and 5.4.2-10, respectively.

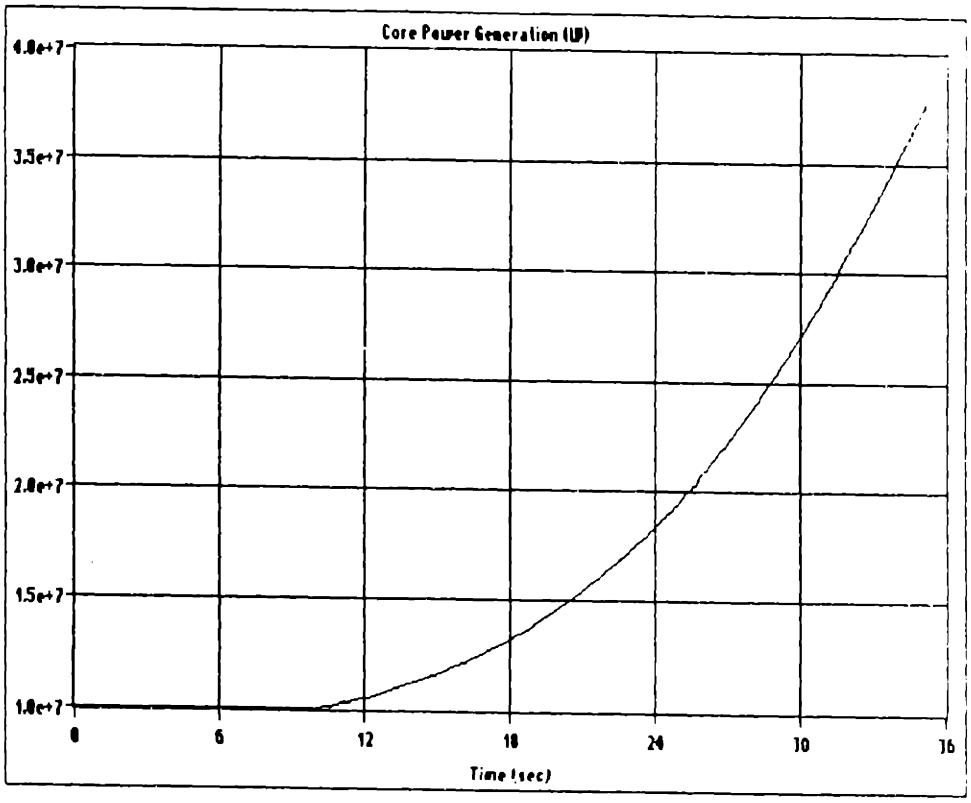

Figure 5.4.2-6. Core Power Generation in Blade Withdrawal Transient (8.50 in/min)

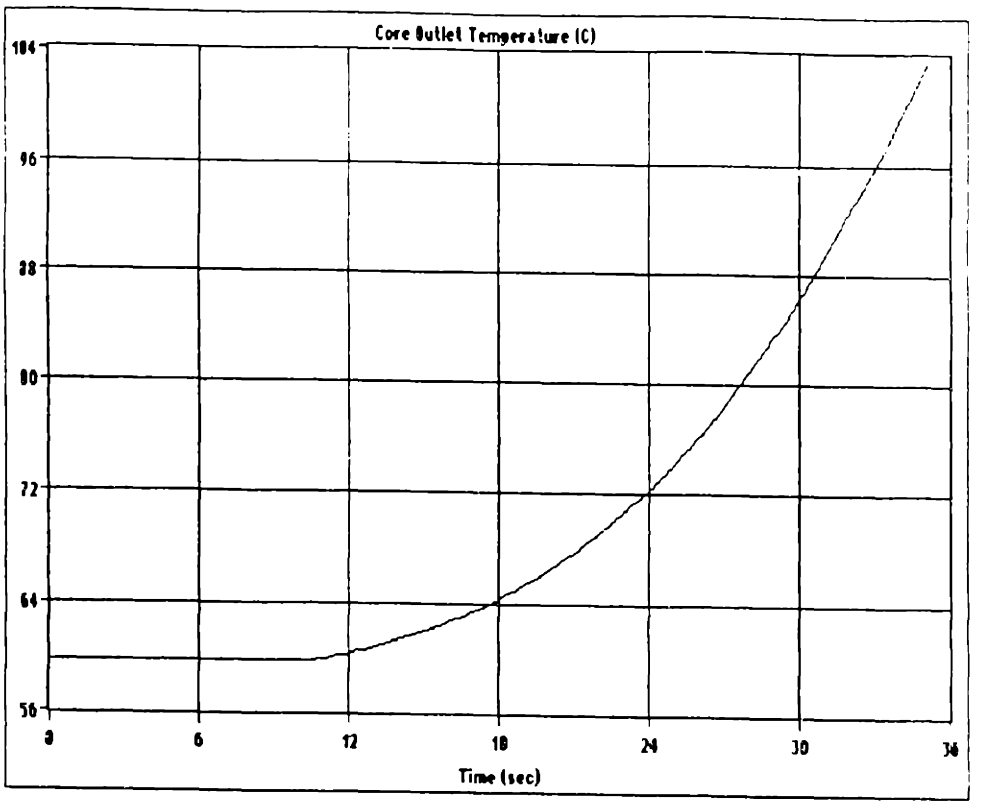

Figure 5.4.2-7. Core Outlet Temperature in Blade Withdrawal Transient (8.50 in/min)

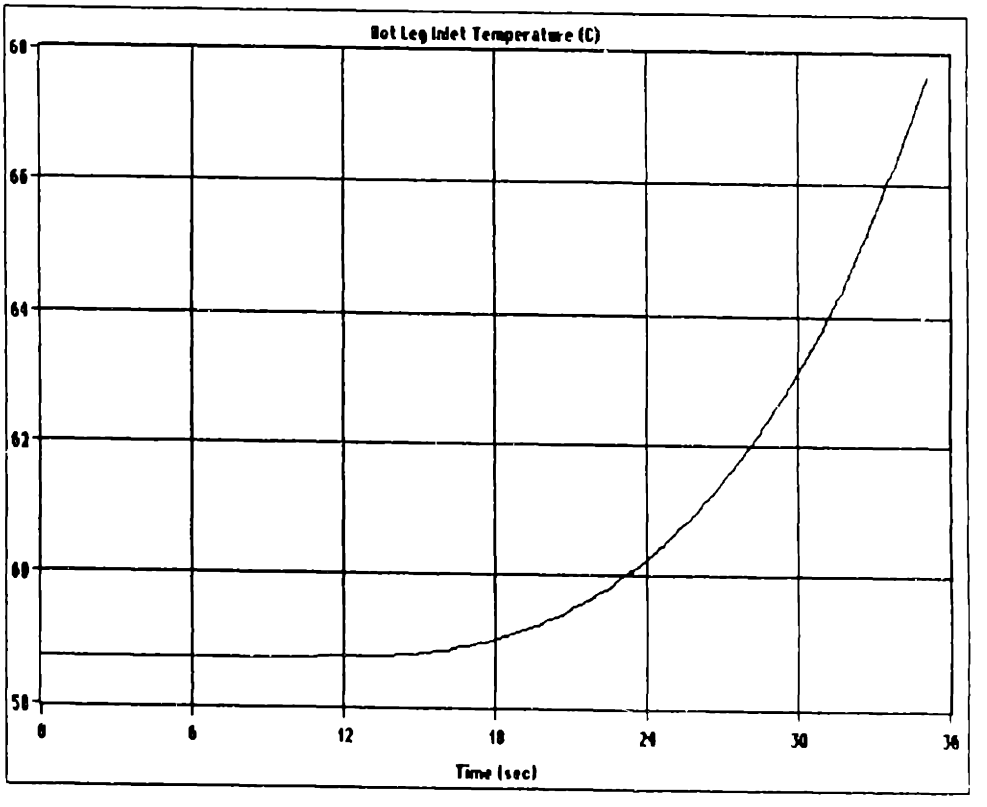

Figure 5.4.2-8. Hot Leg Temperature in Blade Withdrawal Transient (8.50 in/min)

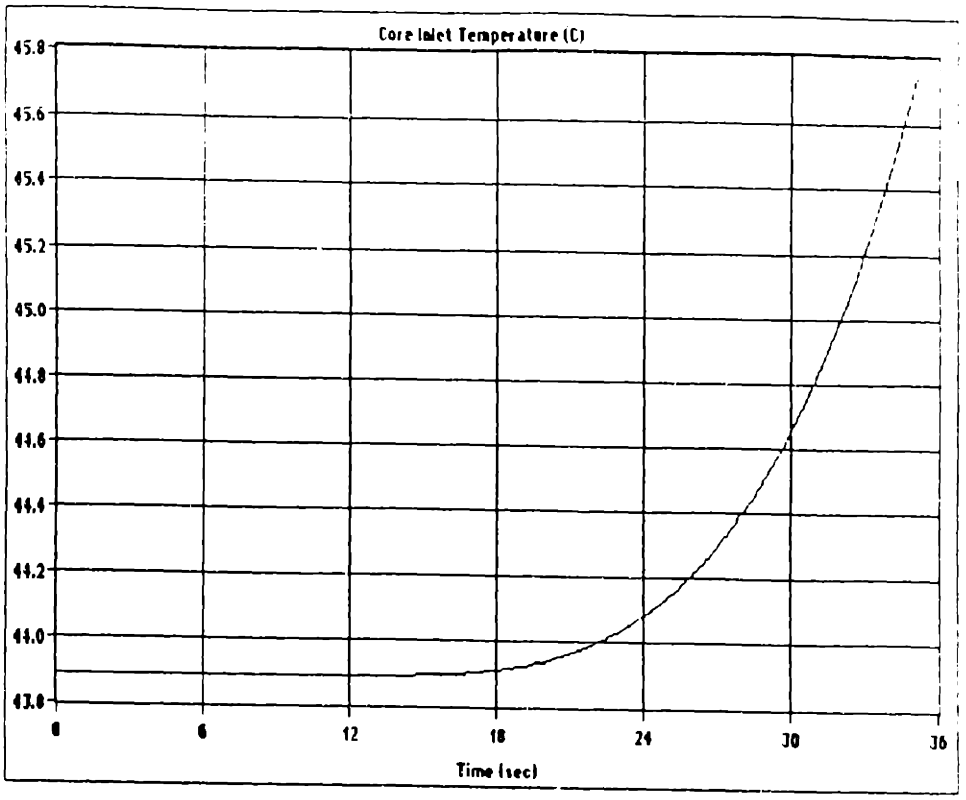

Figure 5.4.2-9. Core Inlet Temperature in Blade Withdrawal Transient (8.50 in/min)

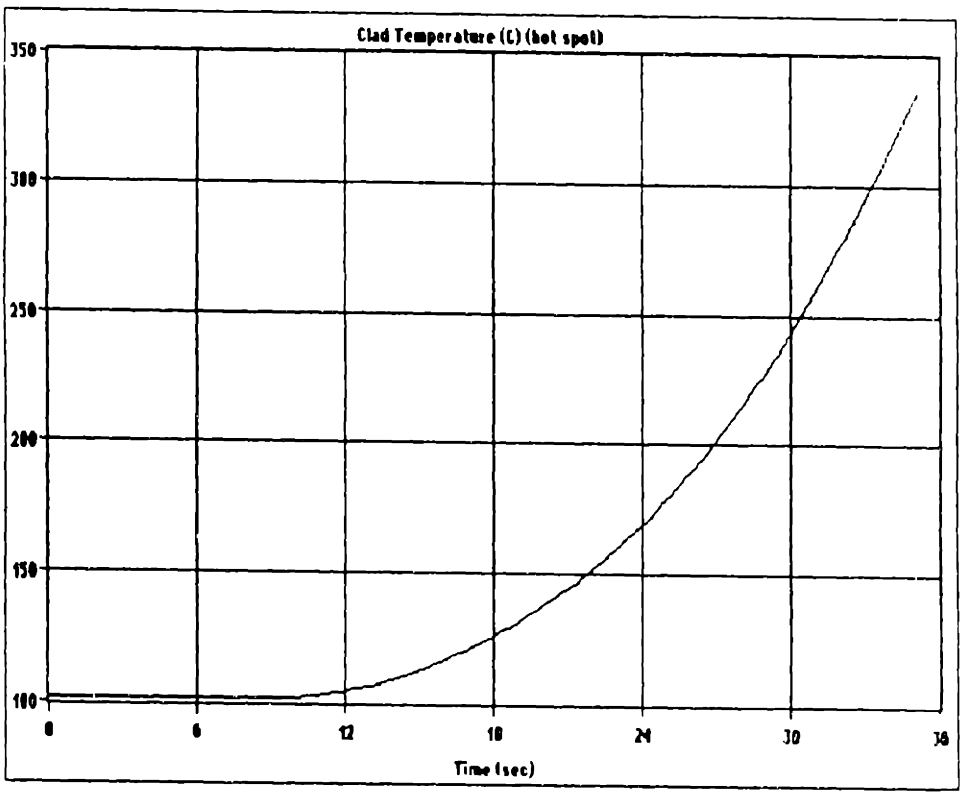

Figure 5.4.2-10. Clad Temp. (hot-spot) in Blade Withdrawal Transient (8.50 in/min)

5.4.3 PUMP COASTDOWN (no scram)

In a loss of flow accident without a reactor trip, subcooled nucleate boiling is inevitable. As the flow decreases (Figure 5.4.3-1), the core power decreases significantly due to the negative coolant reactivity feedback as shown in Figure 5.4.3-2. However, the decrease in flow dominates, and the core outlet and clad (hot-spot) temperatures increase sharply as shown in Figures 5.4.3-3 and 5.4.3-4, respectively. The clad temperature required to cause nucleate boiling is reached 0.38 seconds after the pumps begin to coast down. During the first few seconds (3-4 seconds) of the transient, the hot leg inlet and the core inlet temperatures remain approximately constant. Note that a one second of steady-state operation is shown in all figures except for Figure 5.4.3-1.

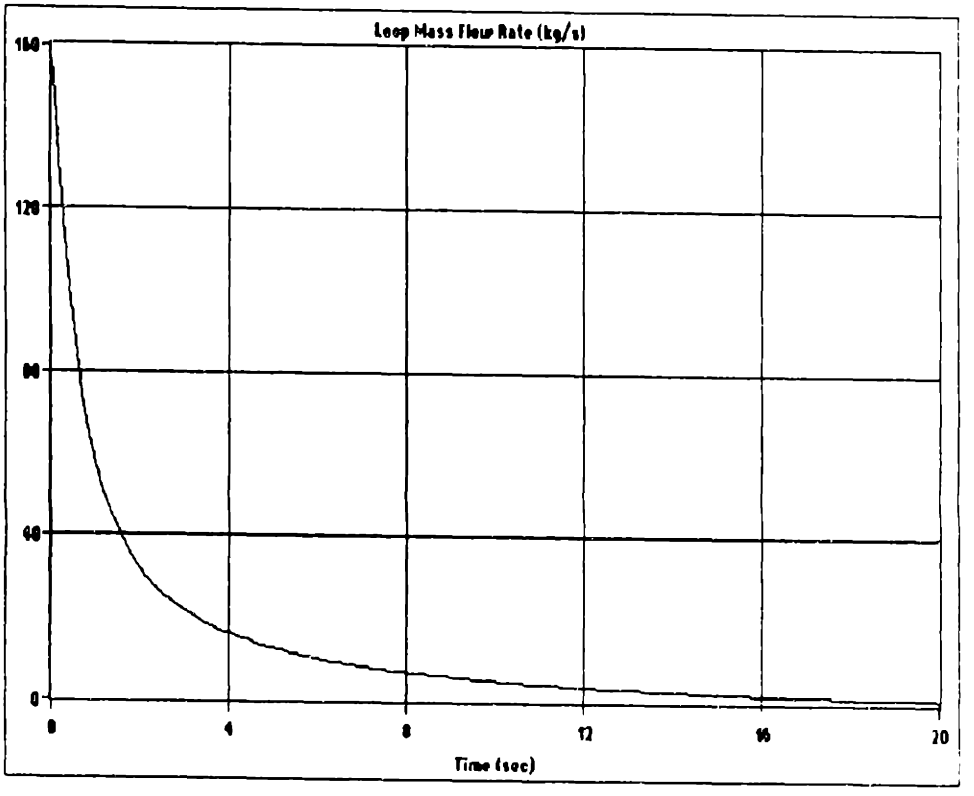

Figure 5.4.3-1. Loop Mass Flow Rate in Pump Coastdown Transient

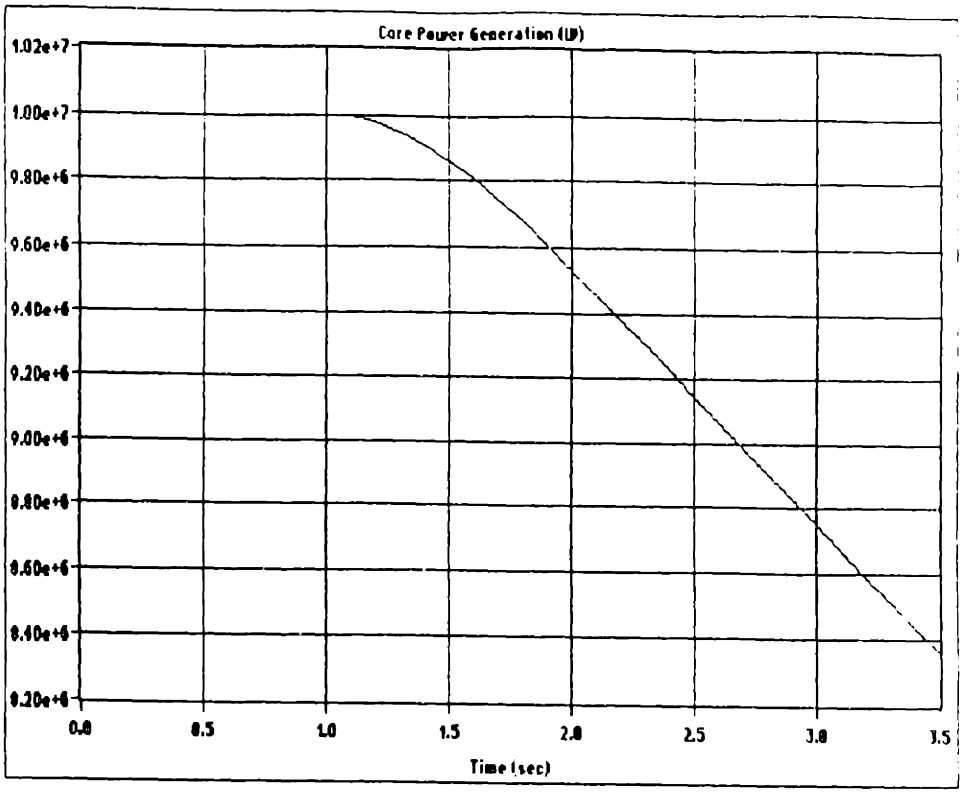

Figure 5.4.3-2. Core Power Generation in Pump Coastdown Transient

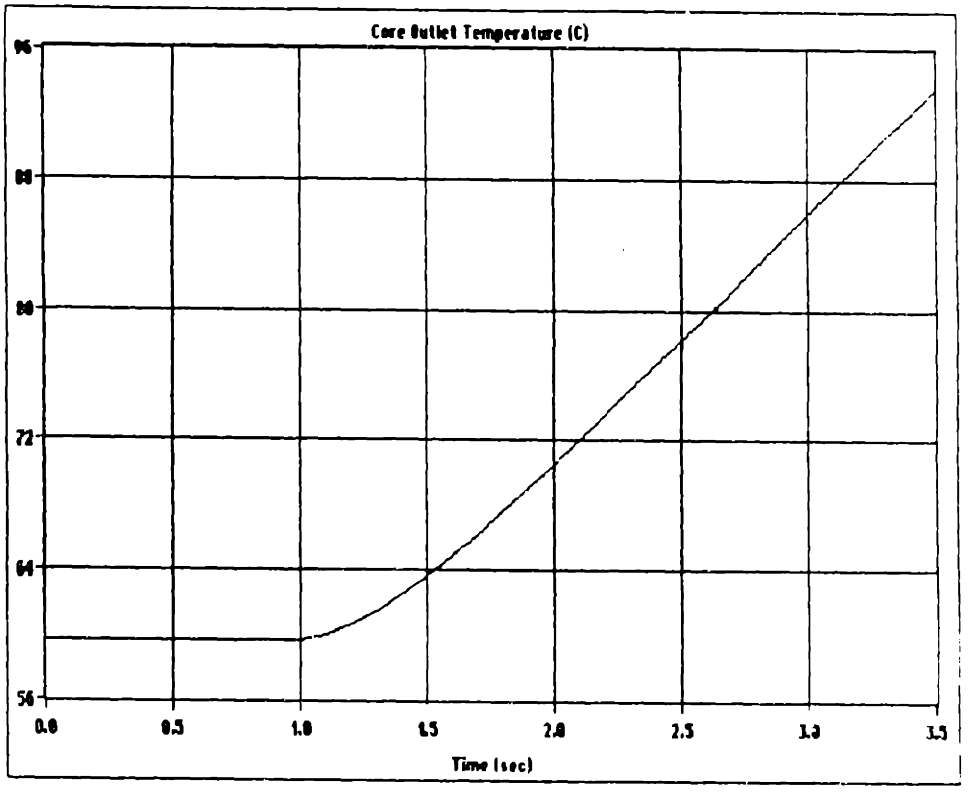

Figure 5.4.3-3. Core Outlet Temperature in Pump Coastdown Transient

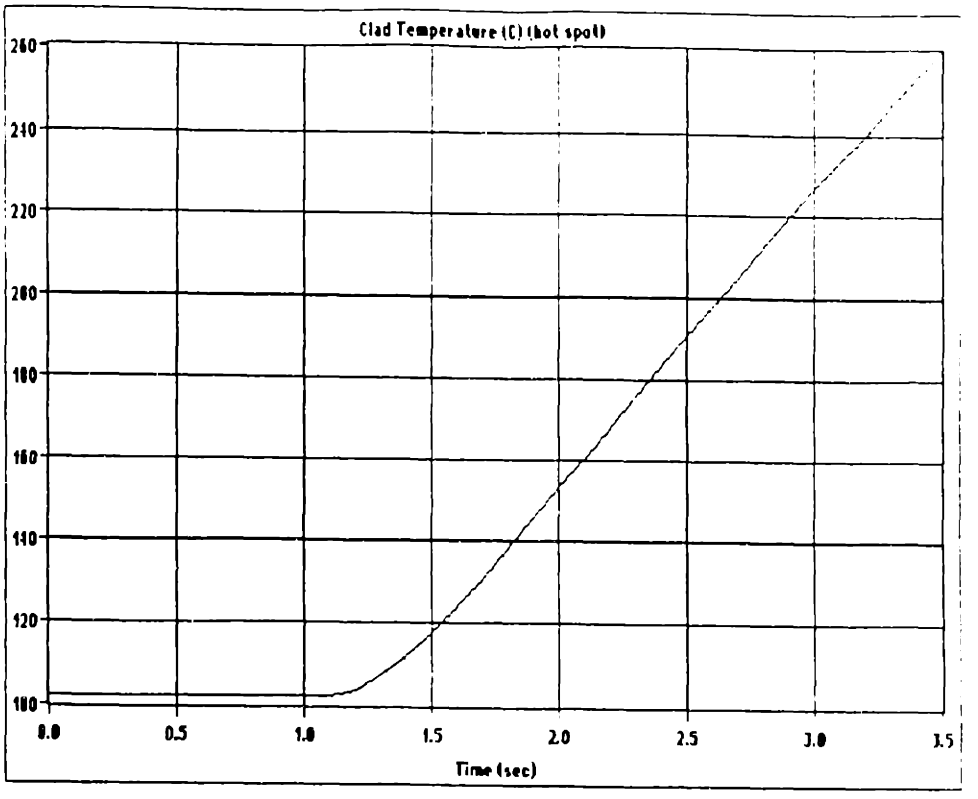

Figure 5.4.3-4. Clad Temperature (hot-spot) in Pump Coastdown Transient

5.4.4 TRIP SETTINGS

Like the MITR-II system, the MITR-III system will have trip settings that include overpower, minimum flow rate, maximum hot leg temperature, minimum reactor period, and water level trips. The operational trip settings are set conservative related to the Limiting Safety System Setting (LSSS). The LSSS for MITR-II involved the determination of the maximum outlet temperature, minimum flow rate, and maximum power such that if operations are constrained to within this envelope, subcooled nucleate boiling does not occur.

Following the same approach as for MITR-II, the MITR-III power LSSS is taken to be 120 % of nominal power (12 MW). This leaves enough margin to set the power operational limit and the power trip setting. The flow LSSS is arbitrarily chosen to be

2500 gpm. The hot leg inlet temperature LSSS is set by determining the minimum temperature that would produce subcooled nucleate boiling within the core at 2500 gpm and 12 MW. This temperature is calculated to be 68°C. The corresponding core outlet temperature is 69°C. The difference in the hot leg and core outlet temperature is due to the core bypass flow. This calculation included the following engineering hot-channel factors: enthalpy rise hot-channel factor (1.146), and heat flux hot channel factor (1.527). The following table summarizes the Limiting Safety System Setting.

Table 5.4.4-1

Proposed Limiting Safety System Setting

Maximum Power (*MW*)	12
Minimum Flow Rate (*gpm*)	2,500
Maximum Average Core Outlet Temperature (°*C*)	69
Maximum Core Inlet Temperature (°*C*)	50

To determine the operational limits, three transients were investigated: (1) a loss of heat sink, (2) a reactivity insertion, and (3) a loss of flow. An initial power of 10 MW has been taken for all three cases. The initial core inlet and outlet temperatures are 45.7 °C and 59.7°C, respectively. The initial primary mass flow rate is taken to be 2800 gpm for all three cases. Although, pump data has been obtained for two pumps which provide a maximum of 2500 gpm, the same head-capacity curve shape is assumed and a rated pump "head" capacity of about 400 kPa (at rated flow of 1400 gpm) is taken.

The loss of heat sink accident was modeled as a rapid (less than 3 seconds) decrease in the secondary flow. From this calculation, the hot leg temperature operational limit is determined as the maximum hot leg temperature at which the reactor should

scram to prevent the core outlet temperature from exceeding the LSSS (69°C). This temperature (hot leg) is calculated to be 62°C.

A reactivity insertion accident was postulated to determine the power operational limit. The accident postulated is a full shim bank withdrawal at maximum speed (4.25 in/min). This is approximated as a ramp reactivity insertion of $12 in 207 seconds. The power operational limit has been determined as the maximum power at which the reactor should scram to prevent the power overshoot (due to the rod insertion time) from exceeding the power LSSS (12 MW). The power operational limit is calculated to be 11.5 MW based on a maximum control blade insertion time (from full out to 80 percent insertion) of 0.8 seconds.

The loss of flow accident was postulated to determine the flow rate operational limit. In addition, restrictions on the maximum control blade insertion time and the maximum shim bank elevation have been determined from the results of this accident simulation. The flow rate operational limit has been determined as the minimum mass flow rate at which the reactor should scram as to prevent nucleate boiling prior to reactor shutdown. This accident scenario is the most limiting of the accidents studied thus far. A compromise between the maximum (initial) control shim bank height, maximum control blade insertion time, and minimum mass flow rate is required. The results indicate that a maximum control blade insertion time (from full out to 80 percent insertion) of 0.8 seconds, a maximum shim bank height of 19 inches (out of the core) and a minimum volumetric flow rate of 2650 gpm is a good compromise.

It is important to note that for the MITR-II pump coastdown, the simulation under-predicted the mass flow rate in the early portion of the transient (as shown in

Figure 5.2.3-1). If data become available proving that a similar mass flow rate under-prediction occurs for the MITR-III pump coastdown simulation, the 0.8 maximum blade drop time and the 19 inches maximum shim bank height restrictions can be relaxed. The following table summarizes the operational limits.

Table 5.4.4-2

Proposed Operational Limits

		Based on
Maximum Power (*MW*)	11.5	Overshoot from reactivity insertion not to exceed 12 MW (LSSS)
Minimum Flow Rate (*gpm*)	2650	No nucleate boiling prior to scram on a loss of flow accident
Maximum Hot leg Temperature (°C)	62	Core outlet temperature not to exceed 69 (LSSS) on a loss of heat sink accident
Maximum Control Blade Insertion time (full out to 80 % insertion, *sec.*)	0.8	No nucleate boiling prior to scram on a loss of flow accident
Maximum Shim Bank Height at Full-Power (*inches* above full insertion)	19	No nucleate boiling prior to scram on a loss of flow accident

The following sections present the simulated behavior of the MITR-III system for the transients analyzed in Sections 5.4.1, 5.4.2, and 5.4.3 with the proposed trip settings of Table 5.4.4-2.

5.4.5 LOSS OF HEAT SINK (with scram)

The loss of heat sink accident simulated is identical to the one studied in Section 5.4.1 in that the secondary flow rate is reduced from rated flow (2290 gpm) to zero flow rate in a thirty second interval. In this case, however, a primary flow rate of 2800 gpm is assumed. The input data used in simulating this transient is given in Appendix D. Note that the reactor is scrammed upon reaching a 62°C hot leg temperature preventing the core outlet temperature from reaching 69°C (LSSS).

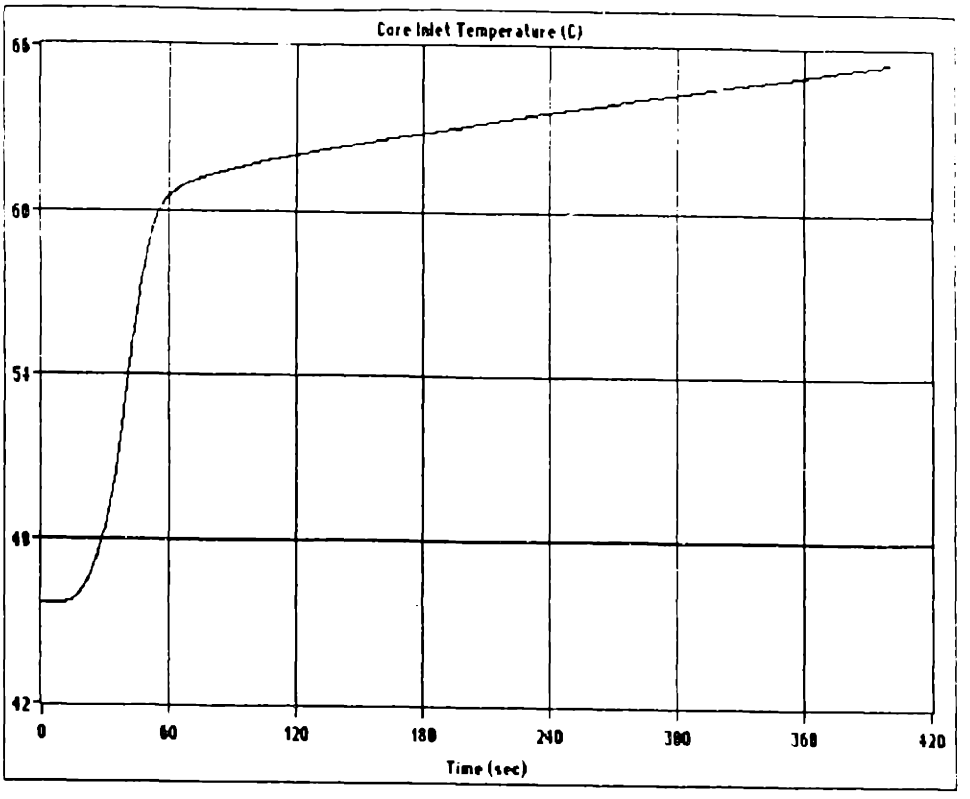

Figure 5.4.5-1. Core Inlet Temperature in Loss of Heat Sink Transient

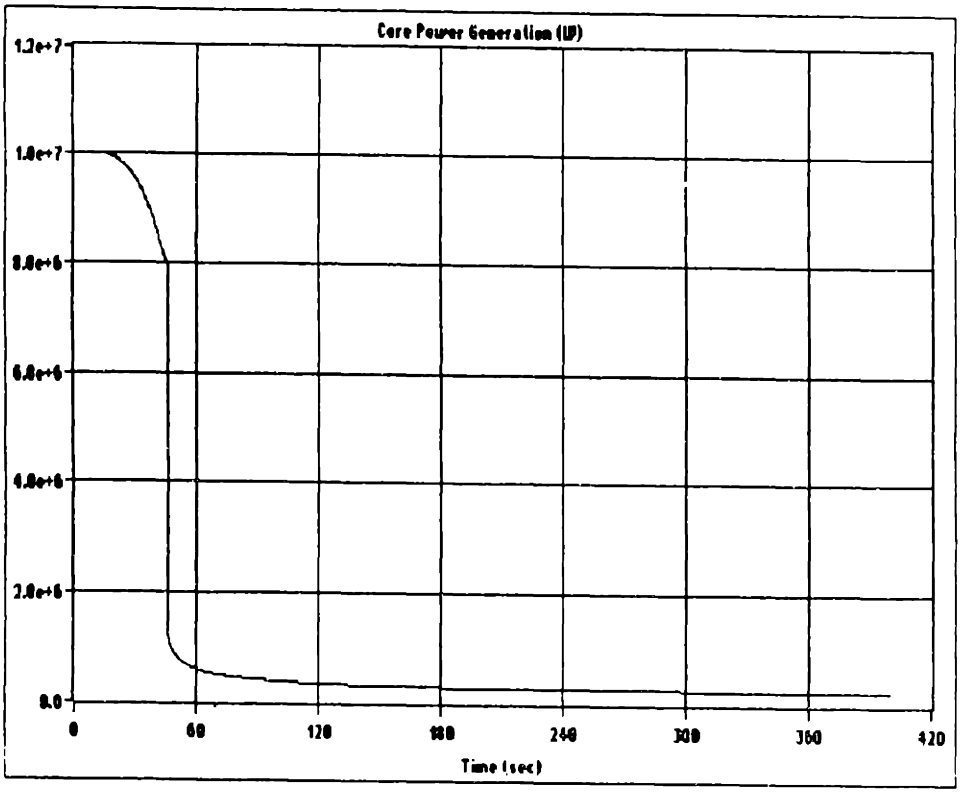

Figure 5.4.5-2. Core Power Generation in Loss of Heat Sink Transient

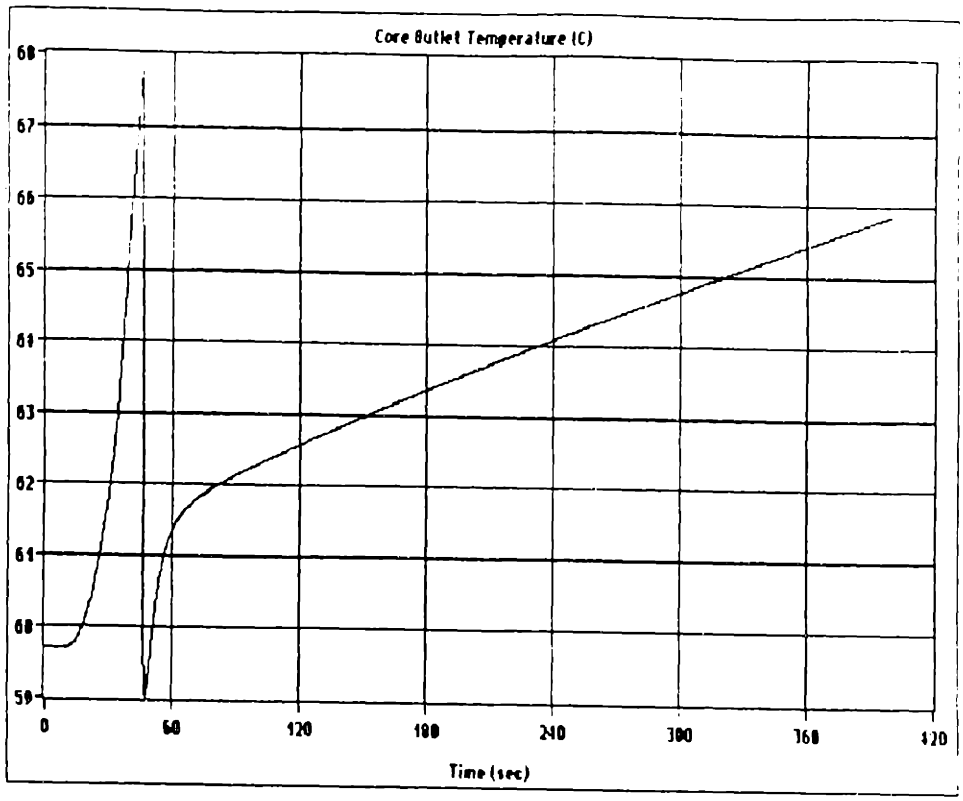

Figure 5.4.5-3. Core Outlet Temperature in Loss of Heat Sink Transient

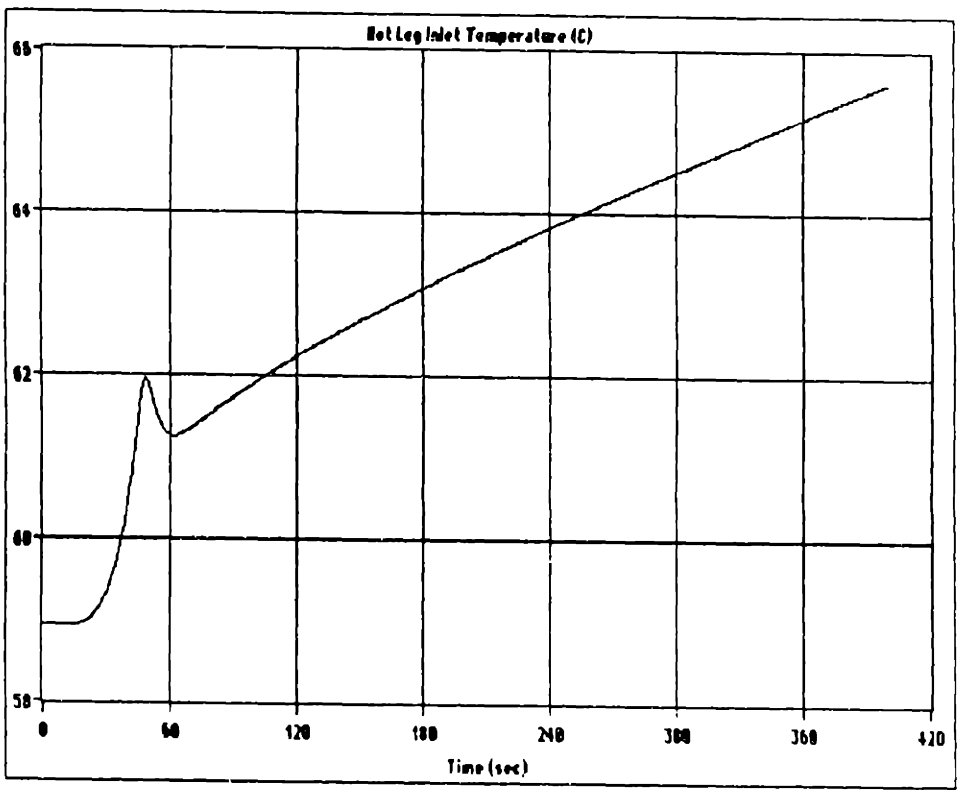

Figure 5.4.5-4. Hot Leg Temperature in Loss of Heat Sink Transient

5.4.6 CONTINUOUS CONTROL BLADE WITHDRAWAL (with scram)

The control blade withdrawal transients studied are identical to the transients of Section 5.4.2. These are a single control blade withdrawal at two speeds: 4.25 and 8.50 inches/min. In this case, however, a primary flow rate of 2800 gpm is assumed. The input data used in simulating this transient is given in Appendix D.

Note that the reactor scrams upon reaching 11.5 MW. For both control blade speed cases, the power overshoot does not reach the LSSS (12 MW). The results of both cases are shown in the following figures. The core inlet temperature and the hot leg temperature remain practically constant until the reactor scrams. Figures 5.4.6-1 and 5.4.6-2 show that the clad temperature stays below the onset-of-nucleate-boiling temperature for both cases.

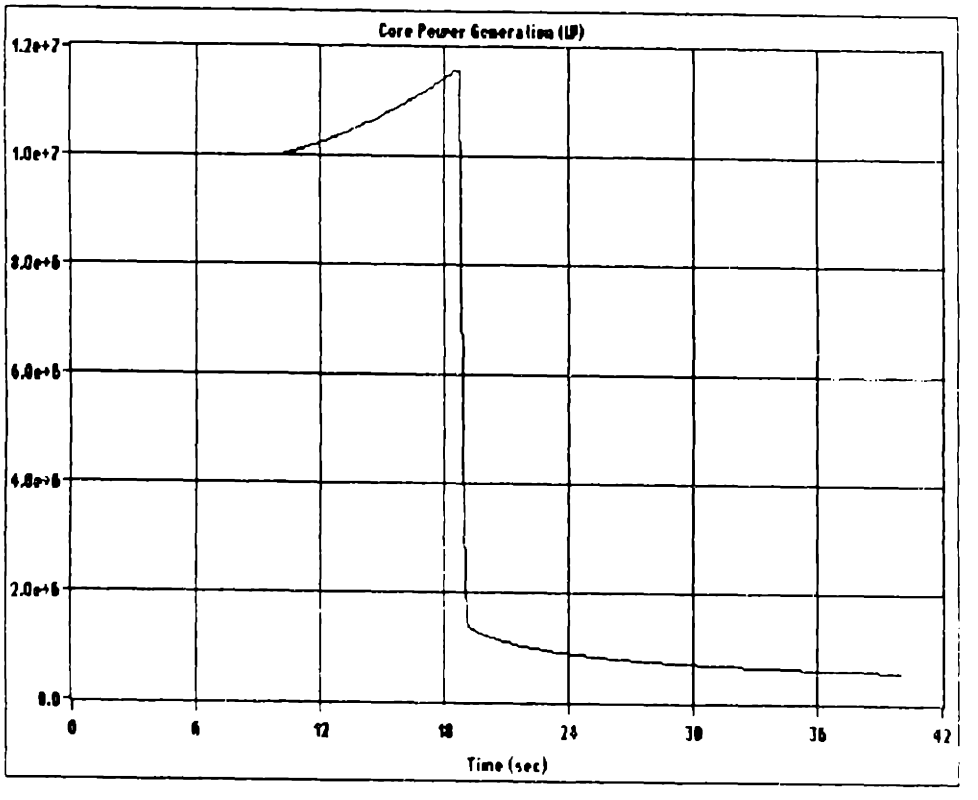

Figure 5.4.6-1. Core Power Generation in Blade Withdrawal Transient (4.25 in/min)

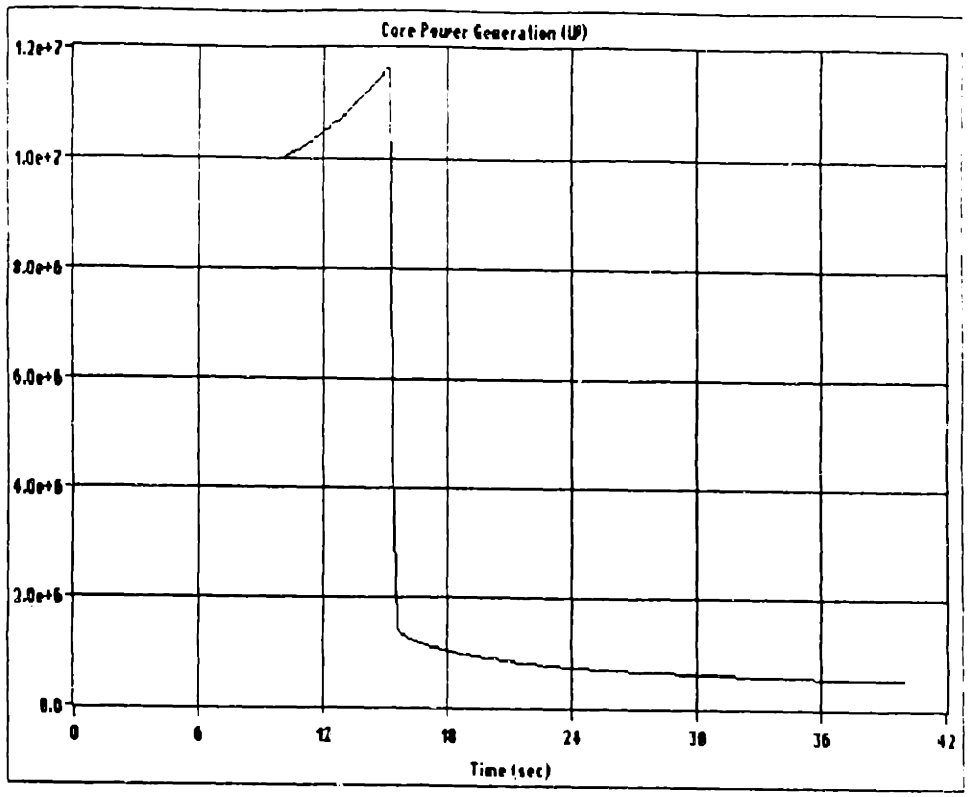

Figure 5.4.6-2. Core Power Generation in Blade Withdrawal Transient (8.50 in/min)

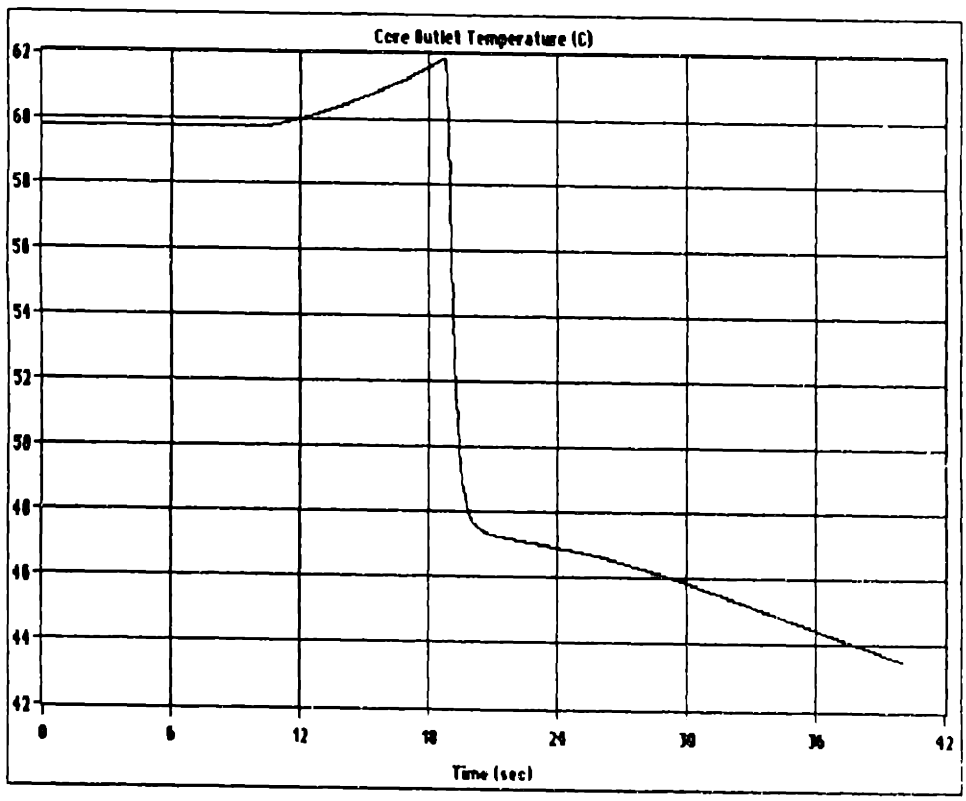

Figure 5.4.6-3. Core Outlet Temperature in Blade Withdrawal Transient (4.25 in/min)

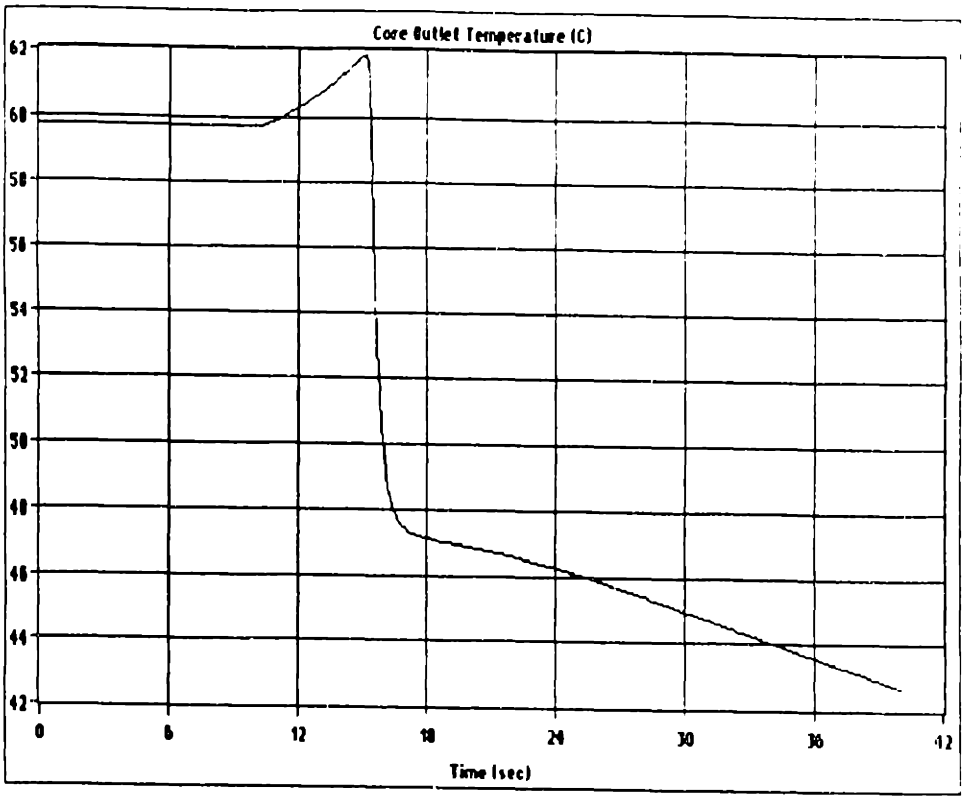

Figure 5.4.6-4. Core Outlet Temperature in Blade Withdrawal Transient (8.50 in/min)

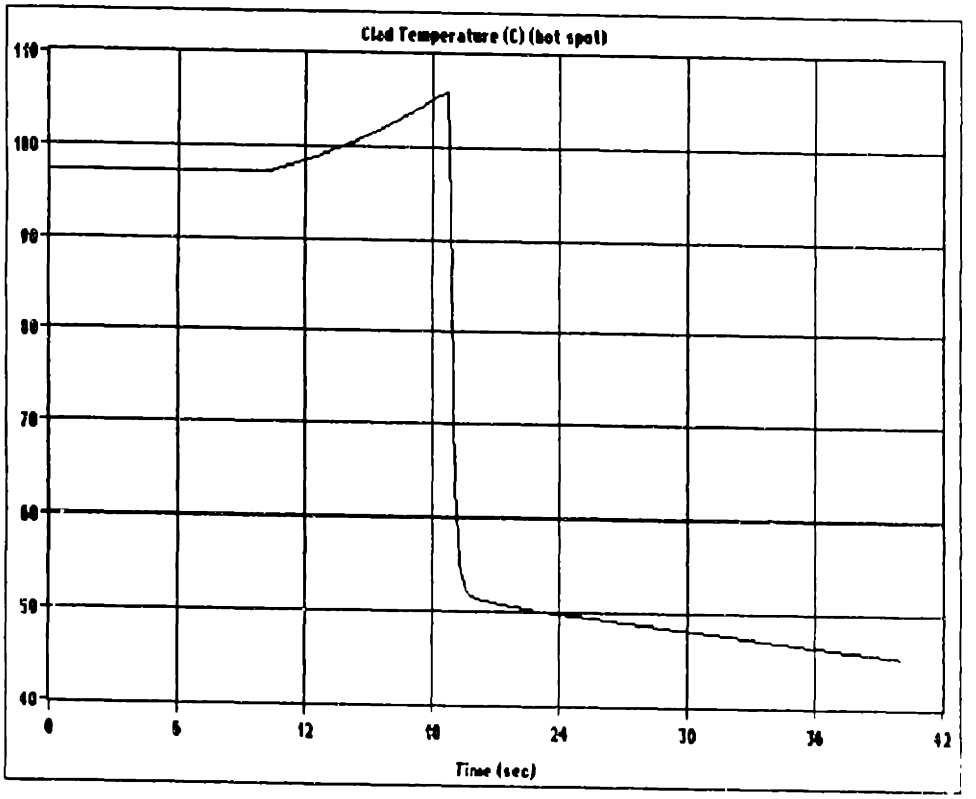

Figure 5.4.6-5. Clad Temperature (hot-spot) in Blade Withdrawal Transient (4.25 in/min)

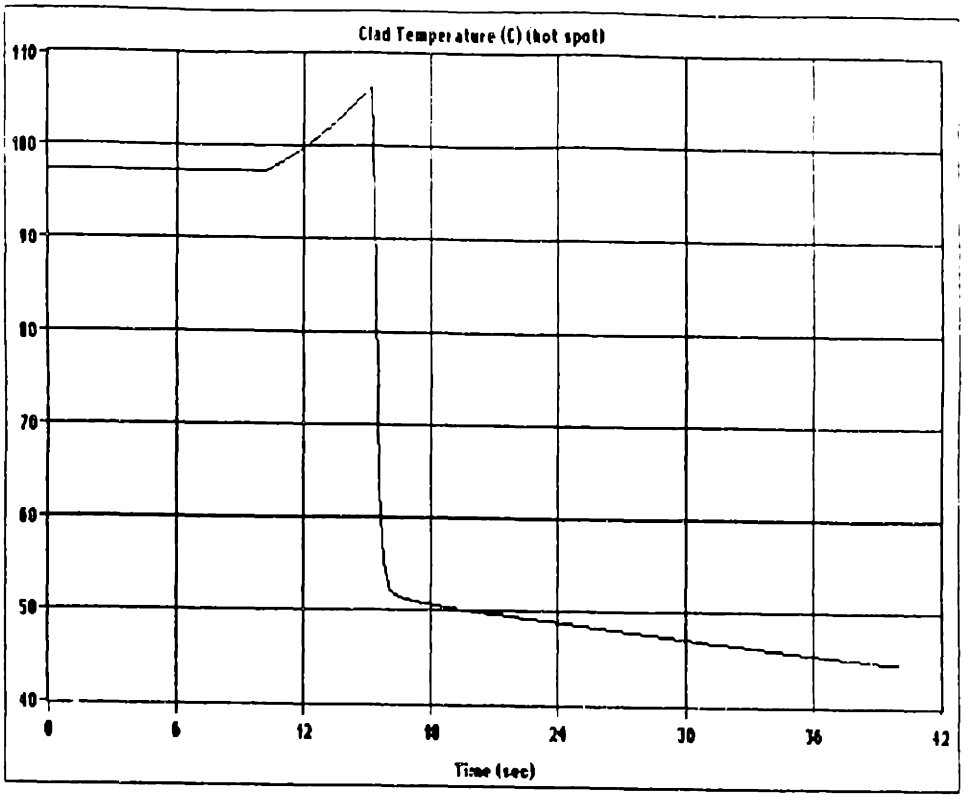

Figure 5.4.6-6. Clad Temperature (hot-spot) in Blade Withdrawal Transient (8.50 in/min)

5.4.7 PUMP COASTDOWN (with scram)

The pump coastdown simulated is identical to the one of Section 5.4.3 except that the reactor is scrammed when the flow reaches 2650 gpm. During a pump coastdown, both fluid and clad experience two temperature peaks. The first temperature peak is due to the rapidly decreasing flow while the control blades are not yet inserted in the core. The results of the simulation indicate that for the first peak the most limiting clad temperature occurs at the bottom of assembly C-1. This clad temperature is shown in Figure 5.4.7-1. The second peak occurs after the reactor scrams and it is due to the core flow reaching a minimum value while in transition between forced flow and natural circulation while the decay heat is still relatively large. The most limiting clad

temperature for this case occurs at the top of assembly A-1. This clad temperature behavior is shown in Figure 5.4.7.2. Nucleate boiling is predicted to occur 26.5 seconds after the pumps begin to coast down. As previously mentioned, due to possible flow instabilities -- a phenomenon not included in this model --, the calculations are followed just a few seconds past the point where nucleate boiling occurs. Therefore, due to the short simulation time, the second clad temperature peak is not observed in Figure 5.4.7.2.

The core outlet temperature is shown in Figure 5.4.7.3. The loop mass flow rate is shown in Figure 5.4.7.4. The total coastdown time is approximately 21 seconds. When the flow reaches 2650 gpm, the reactor scrams as shown in Figure 5.4.7.5.

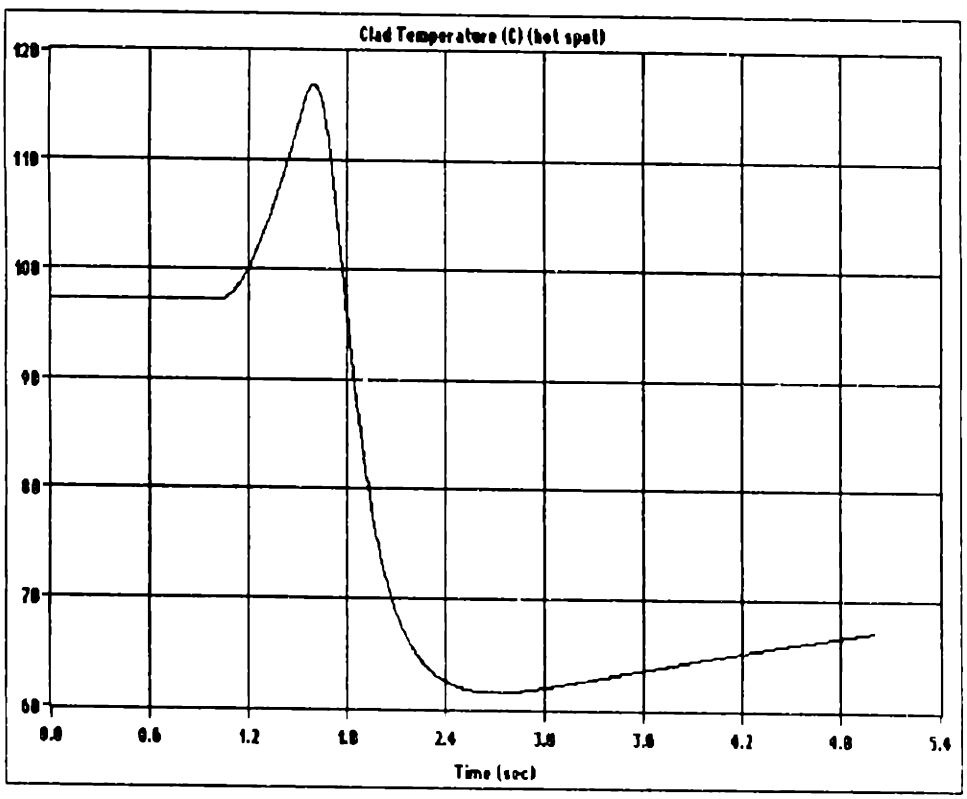

Figure 5.4.7-1. Clad Temperature (hot-spot, C-1) in Pump Coastdown Transient

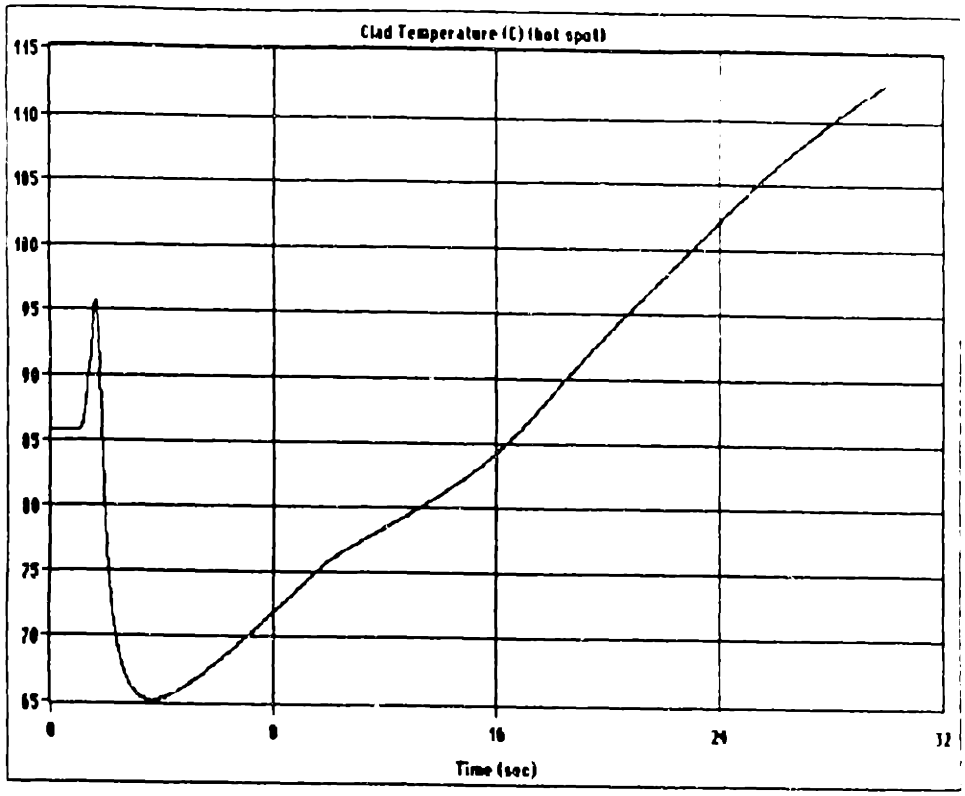

Figure 5.4.7-2. Clad Temperature (hot-spot, A-1) in Pump Coastdown Transient

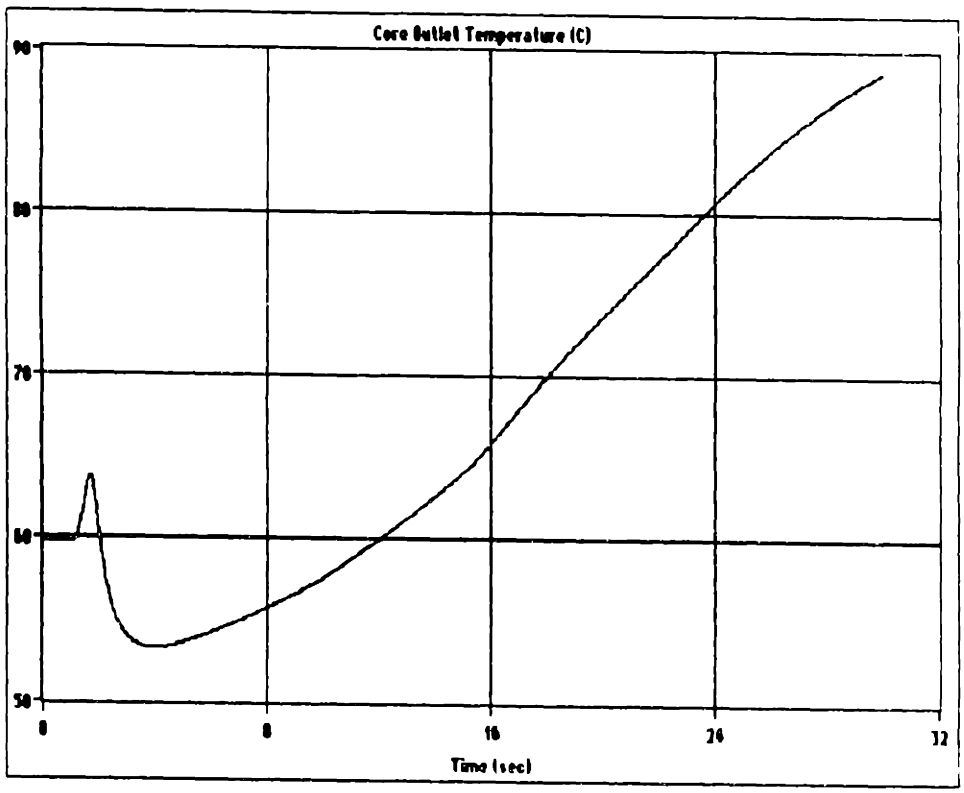

Figure 5.4.7-3. Core Outlet Temperature in Pump Coastdown Transient

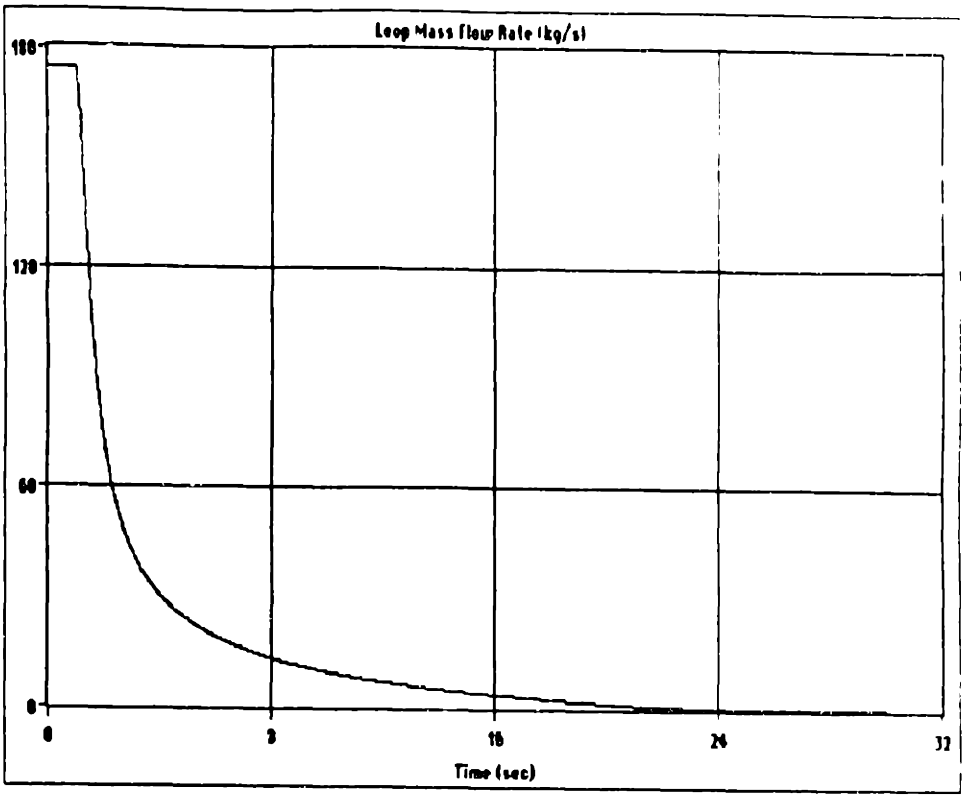

Figure 5.4.7-4. Loop Mass Flow Rate in Pump Coastdown Transient

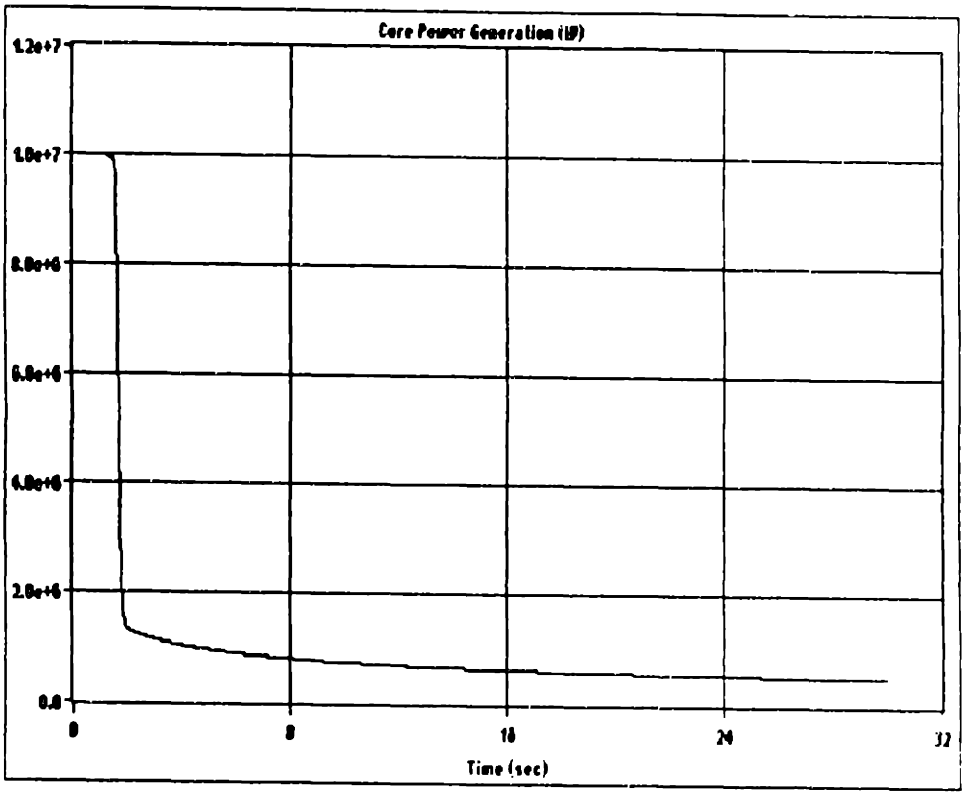

Figure 5.4.7-5. Core Power Generation in Pump Coastdown Transient

The natural circulation valves are predicted to open approximately 11 seconds after the pumps begin to coast down. The natural circulation flow is shown in Figure 5.4.7-6. In the short time of simulation, the natural circulation flow does not reach its maximum value. Ignoring the uncertainty in the validity of the results past onset of nucleate boiling, this maximum value was calculated to be about 3.1 kg/s occurring approximately 90 seconds after the initiation of the transient.

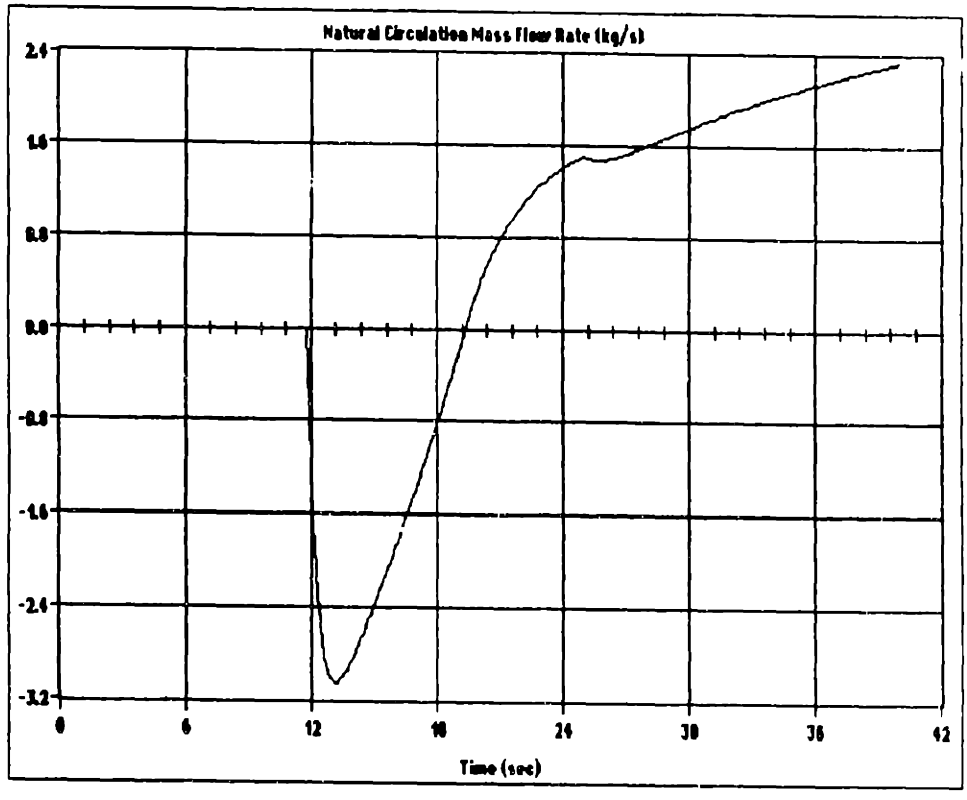

Figure 5.4.7-6. Natural Circulation Mass Flow Rate in Pump Coastdown Transient

5.5 SUMMARY

The code results were compared to available data for a reactor shutdown, startup, and pump coastdown. The simulated results are in acceptable agreement with the experimental values.

For the MITR-II system, three additional transients were simulated: a complete loss of heat sink, and two continuous control blade withdrawal transients. The results indicate that even when the LSSS are used as the trip settings, the reactor has a large margin before nucleate boiling can occur prior to the reactor scram. However, note that nucleate boiling (post-shutdown) is predicted to occur for the loss of heat sink transient about 1.5 hours after the transient begins.

For the MITR-III system, four transients were studied: a complete loss of heat sink, a pump coastdown, and two continuous blade withdrawal transients. First, the transients were simulated without any trips. Then, LSSS and operational limits were proposed and the transients were repeated with the following operational trip settings: 11.5 MW, 2650 gpm, and 62°C (hot leg). The loss of flow accident was shown to be most limiting of the transients under study. Based on this transient, limitations on the maximum blade insertion time and maximum shim bank height were also proposed.

CHAPTER 6: SUMMARY AND RECOMMENDATIONS

6.1 SUMMARY

A computer simulation program (TAMLOC) was developed to study operational transients as well as accident scenarios for the Massachusetts Institute of Technology Research Reactor. The range of applicability includes complete loss of flow with attendant natural circulation, loss of heat sink, reactivity insertions, and small break loss of coolant accidents. Operational transients such as reactor startup and shutdown can be simulated as well.

The thermal model was developed by dividing the MITR system into several control volumes for which energy and mass conservation laws were applied. The mass and energy equations were combined into one conservation equation that is independent of reference enthalpy. The control volumes include the entire primary system and the heat exchangers secondary side. For the core, an average and a hot channel were modeled. The hot channel model accounts for a flow disparity, nuclear peaking factors, and hot-channel engineering factors. Two types of heat exchangers were modeled: plate and shell-and-tube.

The MITR was also divided into several control volumes for which conservation of momentum was applied. The pump model consisted of an angular momentum conservation on the shaft and impeller. The dimensionless pump head capacity curve was approximated as a third degree polynomial (maximum). The MITR flow paths studied involved the "normal" loop (through heat exchangers), and the natural circulation loop. The loop pressure losses considered were friction and form. The gravity pressure

term was also included in the model. In determining the status of the natural circulation valves, a force balance on the valve (ball) was applied. With the natural circulation valve status known, the loop mass flow rates can be calculated.

The core power generation was assumed to be derived entirely from two sources: fission reactions, and post-fission radioactive decay. The fission power model consists of the point-kinetics equations using six delayed neutron groups. The decay heat model consists of seven decay-product groups.

The code has been validated by comparing simulated results with available MITR-II data for a reactor shutdown, startup, and pump coastdown. It was shown that the computational results are in acceptable agreement with the experimental data. For the MITR-II, a loss of heat sink, and two reactivity insertion transients were studied. For the MITR-III, a loss of heat sink, a pump coastdown, and two reactivity insertion transients were studied and from the results the following Limiting Safety System Settings and operational limits were proposed.

	LSSS	Operational Limit	Operational Limit Based on
Maximum Power (*MW*)	12	11.5	Overshoot from reactivity insertion not to exceed 12 MW (LSSS)
Minimum Flow Rate (*gpm*)	2500	2650	No nucleate boiling prior to scram on a loss of flow accident
Maximum Hot leg Temperature ($^{\circ}C$)	68	62	Core outlet temperature not to exceed 69 (LSSS) on a loss of heat sink accident
Maximum Control Blade Insertion time (full out to 80 % insertion, *sec.*)	N/A	0.8	No nucleate boiling prior to scram on a loss of flow accident
Maximum Shim Bank Height at Full-Power (*inches* out of core)	N/A	19	No nucleate boiling prior to scram on a loss of flow accident

6.2 RECOMMENDATIONS

The following is a list of recommendations for further refinement and application of the model developed in this thesis:

1) The model is partially applicable to two-phase condition. Additional work should be done to improve applicability in the two-phase regime.

2) Further validation of the code for slow and fast transients should be performed.

3) An extra delayed-neutron precursor group should be added to the point-kinetics model to account for the photo-neutrons created in the heavy-water tank.

4) Decay heat relation (seven group decay model) should be checked by measuring shutdown heat removal.

5) The data used in modeling the MITR-II and MITR-III should be checked for errors. Some of the dimensions (e.g., lamella heat exchangers) are not well-known. Additionally, parameters such as form-loss factors should also be replaced with updated values when new data become available.

6) Several transients not studied thus far can be analyzed using the code TAMLOC. This include a rapid cooling of the primary system and small break loss of coolant accidents. The loss of coolant accident should be studied to determine an adequate water level trip point for the MITR-III.

7) If data become available for an MITR-III pump showing the behavior of the mass flow rate as a function of time in a pump coastdown, a revision of the operational limits should be done. This revision could be done by performing the pump coastdown simulation of Section 5.4.7 with the pump's parameters (e.g., inertia, curve coefficients, etc.) adjusted to match the mass flow vs. time data.

8) For the MITR-III pump coastdown accident simulation, nucleate boiling is expected to occur several seconds after the reactor scrams. A detailed core analysis of this transient is necessary to study the consequences of nucleate boiling at very low powers (post-scram) and low mass flow rates (natural circulation). The same applies for the long range results of the loss of heat sink accident.

9) Transient analysis should be performed with the reactor set at the LSSS to demonstrate that the safety limit will not be reached. That is, in the event of a transient, the reactor will trip and enough margin exists to prevent it from reaching the safety limit (Onset of Flow Instability).

10) The MITR-III power trip setting was determined by simulating a reactivity transient from full power. The power trip setting was determined such that the power overshoot does not reach the power LSSS (12 MW). A similar transient should be analyzed with a low initial power. If this transient proves to be more limiting, the power trip setting should be changed accordingly.

APPENDIX A: NOMENCLATURE

Following is a listing of the nomenclature and the units used throughout this thesis:

A	Area [m^2]
C_i	precursor concentration of group i
C_p	Thermal Capacity [J/kg]
D_e	Equivalent diameter [m]
e	Volume-averaged mixture "enthalpy" [J/(kg-m^3)]
f	friction factor
h	Specific enthalpy [J/kg]
K	Form-loss coefficient
k	Thermal conductivity [W/(m-$^\circ$C)]
M	Mass [kg]
m	Mass flow rate [kg/s]
P	Amplitude function
p	pressure [Pa]
p*	Fluid properties reference pressure [Pa]
$\Delta p(j)$	Pressure difference across pump j [Pa]
Q	Power [W]
q''_N	Plate surface heat flux [W/m^2]
r_{ff}	Heat exchanger fouling factor [$^\circ$C/W]
S	Extraneous neutron source
T	Temperature [K]

T_b Brake-horse-power torque [N-m]

T_e Electric torque [N-m]

T_w Windage and bearing loss torque [N-m]

t time [sec]

U Total internal energy [J]

U Overall heat transfer coefficient [$W/(m^2\text{-}^\circ C)$]

V Volume [m^3]

v Specific volume [m^3/kg]

z Elevation [m]

β Effective delayed-neutron fraction

λ Decay time constant of precursors [1/sec]

Λ Prompt-neutron lifetime [sec]

ρ Mixture density [kg/m^3]

ρ reactivity

ω pump rotor angular speed [rad/s]

$\langle\ \rangle$ Spatial average

(j) Pump index

Subscripts

b break

b bulk coolant

bp Bypass

c Core

cl	Cold leg
ch	Charge-in
f	Saturated liquid
hl	Hot leg
hx(i)	Heat exchanger i
i	Control volume index
ifs	Inside flow shroud
ld	Letdown
ma	Mixing area
mx	Mixing
nc	Natural circulation
p	average plate
pi(i)	Primary inlet of heat exchanger i
po(i)	Primary outlet of heat exchanger i
si(i)	Secondary inlet of heat exchanger i
so(i)	Secondary outlet of heat exchanger i
su	Surge
th	Thermal
tm(i)	Heat exchanger i tube metal
uh	Underhead

Superscripts

n	Present time index
n+1	Advanced time index

APPENDIX B: EMPIRICAL CORRELATIONS

Onset of Nucleate Boiling

The Bergles/Roshenow onset of nucleate boiling correlation is used to determine the heat flux necessary to create the onset of nucleate boiling[37].

$$q''_{onb} = 49.2 * p^{1.156} * \left(\frac{9}{5} * \Delta T_{sat}\right)^{\frac{2.3}{p^{0.0234}}}$$

where

$(q'')_{onb}$ = Heat flux necessary for onset on nucleate boiling (flat plate approximation) (W/m^2).

p = Pressure at the nucleation site (psia). The pressure at the top of the core is used for calculations.

ΔT_{sat} = T_{wall}-T_{sat} (°C).

If the heat flux at the hot-spot exceeds $(q'')_{onb}$, then nucleate boiling is predicted to occur.

Nusselt Number

The hydraulic diameter used in determining the heat-transfer coefficient has been based on a flat cladding approximation (maintaining the same coolant channel area and clad mass). The fin effectiveness has been accounted by multiplying the heat transfer coefficient by a fin surface effectiveness provided by the user (1.9 default value). In the following correlations, the fin effectiveness multiplication factor has been omitted.

---

[37] Todreas, N. E., and Kazimi, M. S., Nuclear Systems I. Hemisphere Publishing Corporation, 1990, page 534.

- *Plate Geometry:*

  - *Laminar Flow Regime*

    The Nusselt number is obtained from data tabulated in Nuclear Systems I[38] based on a constant axial heat flux profile.

  - *Turbulent Flow Regime*[39]

    $$Nu = 0.2536 * (Re)^{0.65} * (Pr)^{0.4}$$

- *Cylindrical Geometry:*

  - *Laminar Flow Regime*

    Nu = 4.364. Note that this is not an empirical relation.

  - *Turbulent Flow Regime*

    $$Nu = 0.023 * (Re)^{0.8} * (Pr)^{0.4} \left(\frac{\mu_w}{\mu}\right)^{0.14}$$

Friction Factor

The hydraulic diameter used in calculating the friction factor is based on the entire cladding perimeter including the fins. The friction factor used in the turbulent flow regime is invariant of geometry and is given as follows:

$$f = \frac{0.3164}{(Re)^{0.25}}$$

On the other hand, in the laminar flow regime, the friction factor depends on geometry. They are as follows:

---

[38] Todreas and Kazimi, ibid., page 427, Table 10-4.

[39] Palen, J. W., Heat Exchanger Sourcebook , Hemisphere Publishing, pg. 565, 1986.

- *Plate Geometry:*

  The friction factor is obtained from Figure 9-15 in Nuclear Systems I[40].

- *Cylindrical Geometry:*

  $f = \frac{64}{Re}$. Note that this is not an empirical relation.

- *Annular Geometry:*

  $f = \frac{24}{Re}$

---

[40] Todreas and Kazimi, ibid., page 372, Figure 9-15.

APPENDIX C: USER'S MANUAL

There are two ways to run TAMLOC: with or without the data user interface (DUI). The DUI is an interface that facilitates the input preparation. However, to run the program with the DUI a mouse is required. The command to run TAMLOC with the DUI is *TAM.BAT*. The following screen should appear.

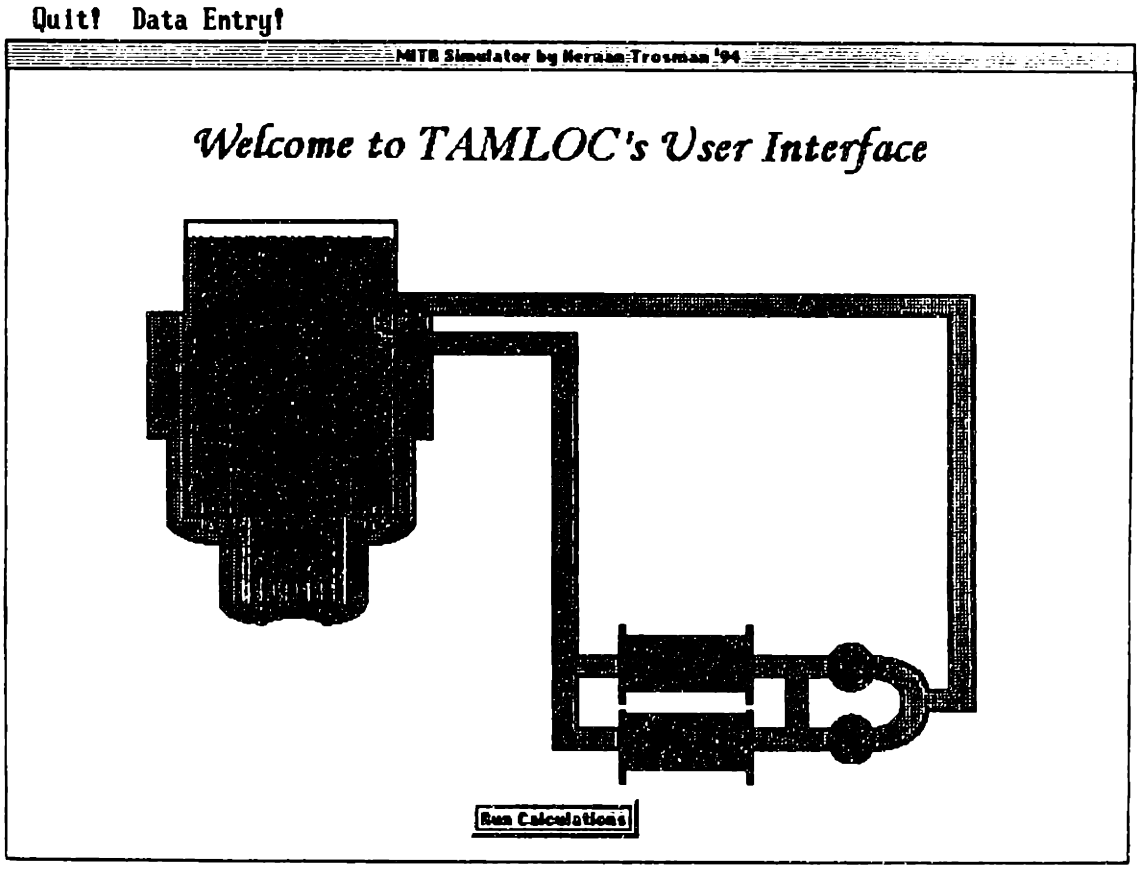

Figure C-1. Data User Interface Main Screen

From this panel you can run the code, go to the data entry panels or quit. To change any of the data or to load a file containing a set of data for a particular transient,

move the mouse to the *Data Entry* location and click on it. The following screen will appear.

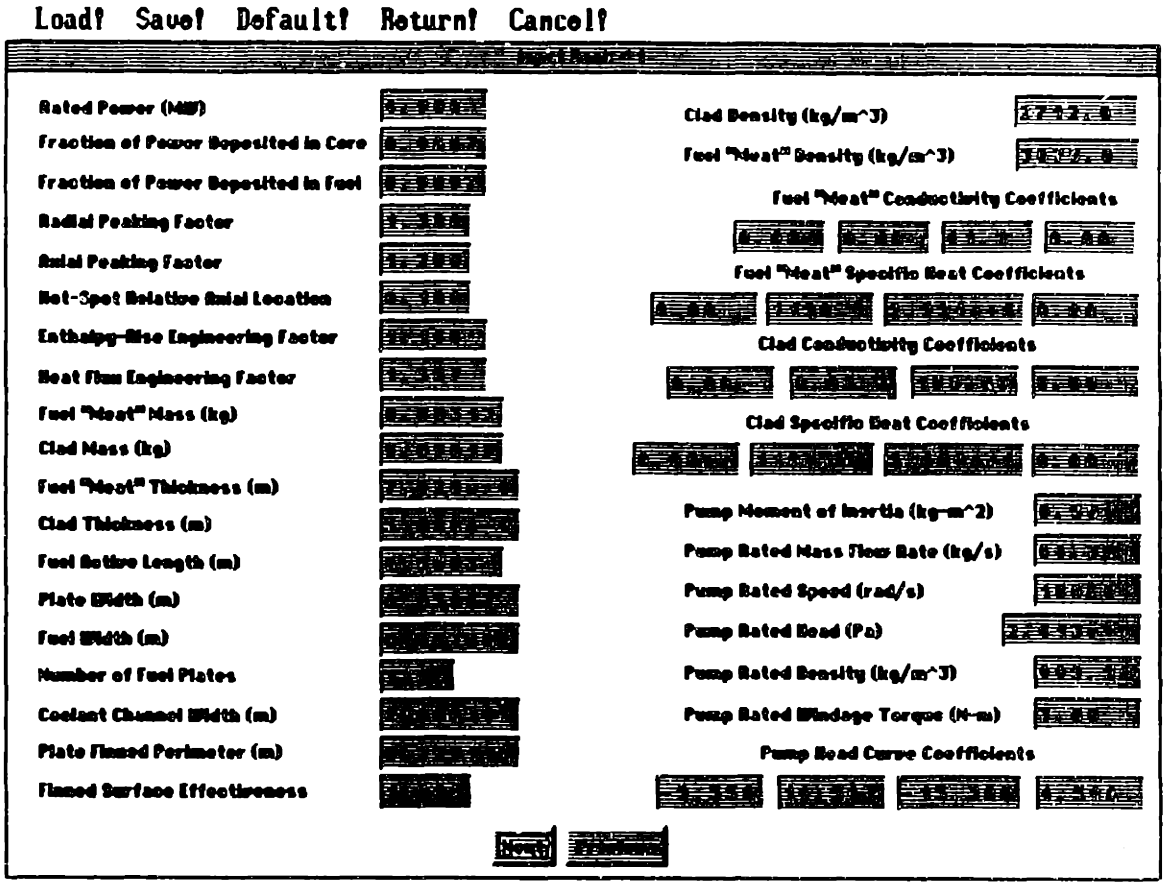

Figure C-2. Data User Interface Input Deck #1

This is the first of six data entry panels. The rest of the panels can be accessed through the *Next* and *Previous* push buttons. To change any information, click on the number you want to change and write over it. There are five menu bar commands accessible from any of the entry panels. These commands are the following:

- *Load:* It loads an existing file containing the data for all six panels. Loaded files should be binary and with an .inp extension. (i.e., coastdown.inp)

- *Save:* It saves the input created in a binary file with an .inp extension.
- *Default:* It restores the default values to all six panels.
- *Return:* It brings back the Main Panel maintaining any of the changes created in the Entry Panels.
- *Cancel:* It brings back the Main Panel discarding any changes to the Entry Panels.

Following is an explanation of the system parameters found in Input Deck #1. If an explanation is not written for a parameter it is because one is not needed.

Input Deck #1 Parameters

- *Rated Power (MW)*
- *Fraction of the Power Deposited in the Core:* This indicates how much of the power generated in the core is involved in heating up the coolant.
- *Fraction of the Power Deposited in the Fuel:* This indicates how much of the power generated in the core is involved in heating up the fuel.
- *Radial Peaking Factor:* Hot-channel power divided by the average channel power.
- *Axial Peaking Factor:* Power density in hot-spot (within hot-channel) divided by the average hot-channel power density.
- *Hot-Spot Relative Axial Location:* $0 \leq \text{value} \leq 1$
- *Fuel "Meat" Mass (kg):* The active fuel mass of a single fuel plate.
- *Clad Mass (kg):* The clad mass of a single fuel plate.
- *Fuel "Meat" Thickness (m):* Total thickness of a single fuel "meat".
- *Clad Thickness (m):* Average clad thickness.
- *Fuel Active Length (m)*

- *Plate Width (m)*

- *Fuel Width (m):* Active fuel width.

- *Number of Fuel Plates:* This is for the entire core (i.e., 330 for 22 assemblies).

- *Coolant Channel Thickness (m):* Average distance between adjacent cladding surfaces.

- *Plate Finned Perimeter (m):* Total perimeter (including the fins, both sides) for a single fuel plate.

- *Finned Surface Effectiveness:* "Finned" heat transfer coefficient divided by "Flat" heat transfer coefficient.

- *Clad Density (kg/m^3):* Clad average density for the temperature range anticipated.

- *Fuel "Meat" Density (kg/m^3):* Fuel "Meat" average density for the temperature range anticipated.

- *Fuel and Clad Properties:* This includes fuel "Meat" and clad thermal conductivity (W/m-°C) and specific heat (J/kg-°C). They are calculated assuming the following temperature dependence:

$$\text{conductivity} = C_1 * T^2 + C_2 * T + C_3 + \frac{C_4}{T}$$

$$\text{specific heat} = (C_1 * T^2 + C_2 * T + C_3 + \frac{C_4}{T})/\text{density}$$

The coefficients are in increasing order from left to right. For example, in Figure D-2, the fuel "meat" conductivity is assumed constant at 41.2 W/m-°C and the specific heat has the following temperature dependence:

$$C_p = (1120.9 * T + 2.224e6)/\rho_{meat} \quad J/kg\text{-}^\circ C$$

- *Pump Moment of Inertia ($kg\text{-}m^2$):* This should include the pump shaft, impeller and any other rotating parts.

- *Pump Rated Mass Flow Rate (kg/s)*

- *Pump Rated Speed (rad/s)*

- *Pump Rated "Head" (Pa)*

- *Pump Rated Density (kg/m³):* the liquid density at the pump suction leg for the pump's rated conditions.

- *Pump Rated Windage Torque (N-m)*

- *Pump Head Curve Coefficients:* The dimensionless head-curve is represented as follows.

$$Y = A_1 + A_2 * X + A_3 * X^2 + A_4 * X^3, \text{ where } Y = \left(\frac{H}{H_r}\right)\left(\frac{\omega_r}{\omega}\right)^2 \text{ and } X = \frac{\dot{m}\,\rho_r\,\omega_r}{\dot{m}\,\rho\,\omega}$$

H = Pump Head (m),
ρ = Liquid Density at Pump's Suction Leg (kg/m³), and
ω = Pump's Speed (rad/s).

The subscript *r* represents the value at rated conditions. The coefficients A_i should be in increasing order from left to right.

If the *Next* push button is clicked, the following screen will appear. This is Input Deck #2.

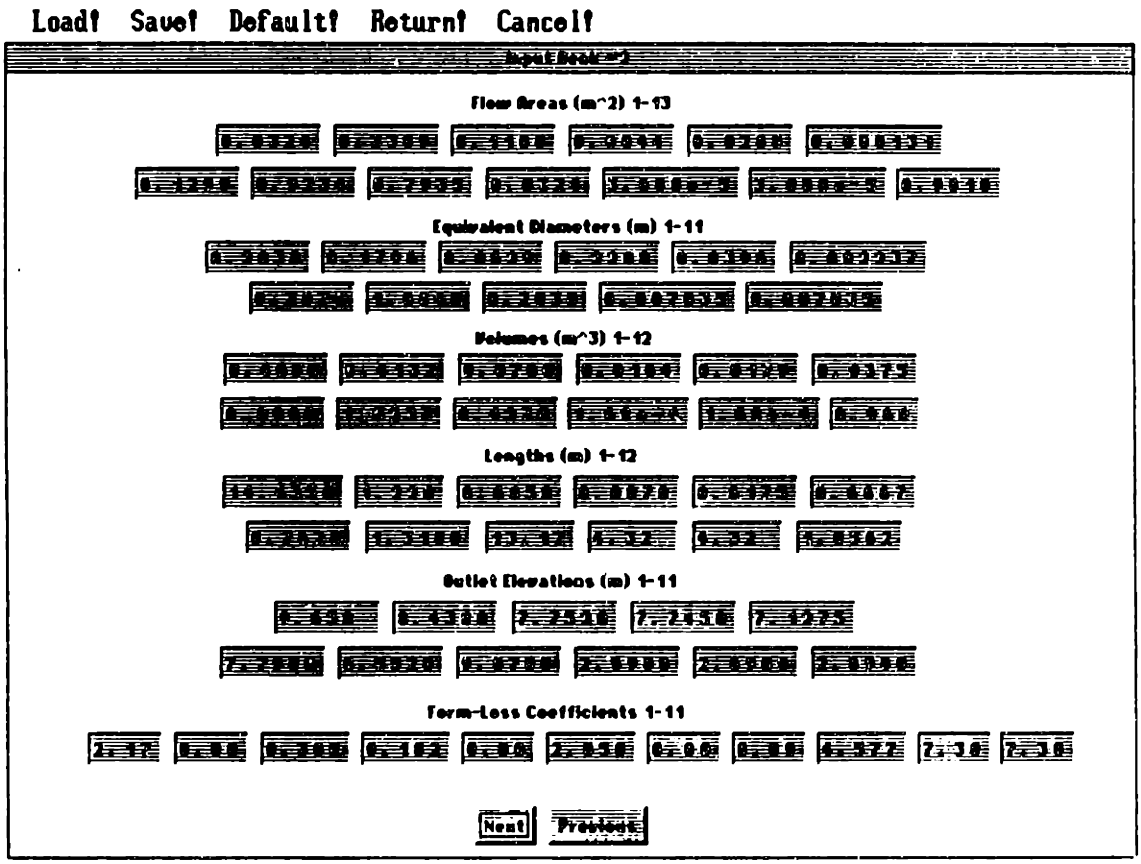

Figure C-3. Data User Interface Input Deck # 2

Input Deck # 2 Parameters

Most of the geometry of the system and the pressure loss-coefficients are included in this panel.

- *Flow Areas (m^2):* The average flow areas of the control volumes representing the MITR system. They should be placed in ascending order from left to right. The index numbers 1 through 13 are as follows:

  1. Cold Leg
  2. Region 1 of Downcomer
  3. Region 2 of Downcomer
  4. Region 3 of Downcomer
  5. Region 4 of Downcomer
  6. Core (flow area of single coolant channel)
  7. Inside Flow Shroud
  8. Mixing Area (above the flow shroud level)
  9. Mixing Area (adjacent to the flow shroud)
  10. Hot Leg
  11. Heat Exchanger # 1 (flow area of single primary coolant channel)
  12. Heat Exchanger # 2 (flow area of single primary coolant channel)
  13. Underhead

- *Equivalent Diameters (m):* The index numbers 1 through 11 are as follows:

  One through eight are the same as in the flow area input.

  9. Hot Leg
  10. Heat Exchanger # 1
  11. Heat Exchanger # 2

- *Volumes (m^3):* The index numbers 1 through 12 are as follows:

  One through eleven are identical to the equivalent diameter input.

  12. Underhead

- *Lengths (m):* The index numbers are identical to the volume input.

- *Outlet Elevations (m):* Since only relative values are meaningful, it does not matter where the zero elevation is chosen. The numbers are identical to the equivalent diameter input.

- *Form-Loss Coefficients:* The index numbers are identical to the equivalent diameter input index numbers.

Input Deck # 3 Parameters

This panel contains the necessary information about the heat exchangers, the natural circulation valve, and the primary flow rate. The panel is shown in the following figure.

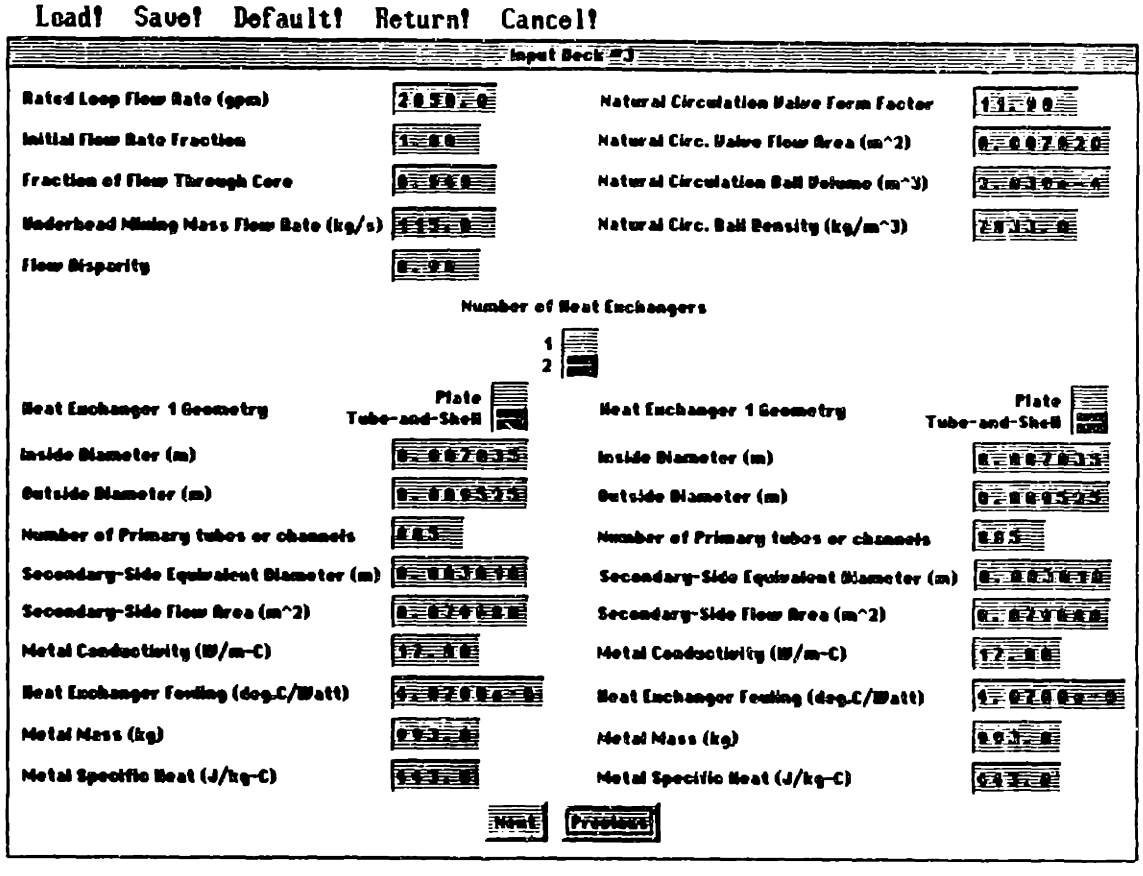

Figure C-4. Data User Interface Input Deck # 3

- *Rated Loop Flow Rate (gpm):* Volumetric flow rate at the cold leg orifice.
- *Initial Flow Rate Fraction:* Initial fraction of the rated loop flow rate.
- *Fraction of Flow Through Core*: Since core bypass flow is possible, the fraction of the total flow through the core needs to be provided.

- *Underhead Mixing Mass Flow Rate (kg/s):* In modeling the pool of water above the core, three control volumes are used: the inside flow shroud, the mixing area , and the underhead (see Figure 2.1). The model of the mixing area and the underhead includes an exchange of equal mass flow rates, leading to a possible energy transfer between these two control volumes independent of any "shrink" and "swell" that could be taking place also (a net surge flow rate).

- *Flow Disparity:* The minimum channel flow rate divided by the average channel flow rate. Used to determine the hot-channel flow rate.

- *Natural Circulation Valve Form Factor:* This is the natural circulation valve's pressure form-loss coefficient in the downward flow direction (normal). This value depends on the number of natural circulation valves opening. The dependence recommended is as follows[41]:

$$K = \frac{190.38}{N^2}$$

where N is the number of natural circulation valves opening (4).

- *Natural Circulation Valve Flow Area (m^2):* The total flow area of all four natural circulation valves.

- *Natural Circulation Ball Volume (m^3):* The volume of the ball within the natural circulation valve.

- *Natural Circulation Ball Density (kg/m^3)*

- *Number of Heat Exchangers:* This switch indicates the use of one or two heat exchangers. If one is selected, the heat exchanger # 2 information, becomes inactive.

- *Heat Exchanger Geometry:* This switch indicates whether the heat exchangers are of the plate or shell-and-tube type.

---

[41] Bamdad-Haghighi, F., "Natural Convection analysis of the MITR-II During Loss of Flow Accident," Nucl. E. and S.M. Thesis, page 72, MIT Department of Nuclear Engineering, 1977.

- *Inside Diameter (m):* Plate: The primary coolant channel thickness.
  Shell-and-Tube: The inside diameter of the tubes.

- *Outside Diameter (m):* Plate: The inside diameter plus twice the plate's thickness.
  Shell-and-Tube: The outside diameter of the tubes.

- *Number of primary tubes or channels:* Plate: Number of primary coolant channels.
  Shell-and-Tube: Number of primary tubes.

- *Secondary-Side Equivalent Diameter (m)*

- *Secondary-Side Flow Area (m^2):* This is the **total** (not single channel) flow area of the secondary side of the heat exchanger.

- *Metal Conductivity (W/m-°C):* The average value of the tube or plate metal conductivity for the anticipated temperature range.

- *Heat Exchanger Fouling (°C/W):* Note that this value is not in units of $\frac{°C\ m^2}{W}$ making the fouling independent of surface area. **The fouling is based on the total outer (secondary) surface area.** Be aware that the initial steady-state calculations are quite sensitive to this value and convergence may be a problem for some values.

- *Metal Mass (kg):* The **total** mass for the tubes or plates involved in the transfer of heat.

- *Metal Specific Heat (J/kg-°C):* The average value of the tube or plate metal specific heat for the anticipated temperature range.

If one heat exchanger is selected, the model also assumes single pump operation. Therefore, it is important to make sure that the *Rated Loop Flow Rate* is consistent with a single pump operation. That is, if one heat exchanger is selected and the Rated Loop Flow Rate remains the default value (for two pumps/heat exchangers), the pump head calculations (based on the coefficients mentioned earlier) will give a smaller value than expected or perhaps even a negative value!

Input Deck # 4 Parameters

This panel includes information about the trip settings, point-kinetics parameters, control blade information, water level, and miscellaneous piping elevations. The panel is shown in the following figure.

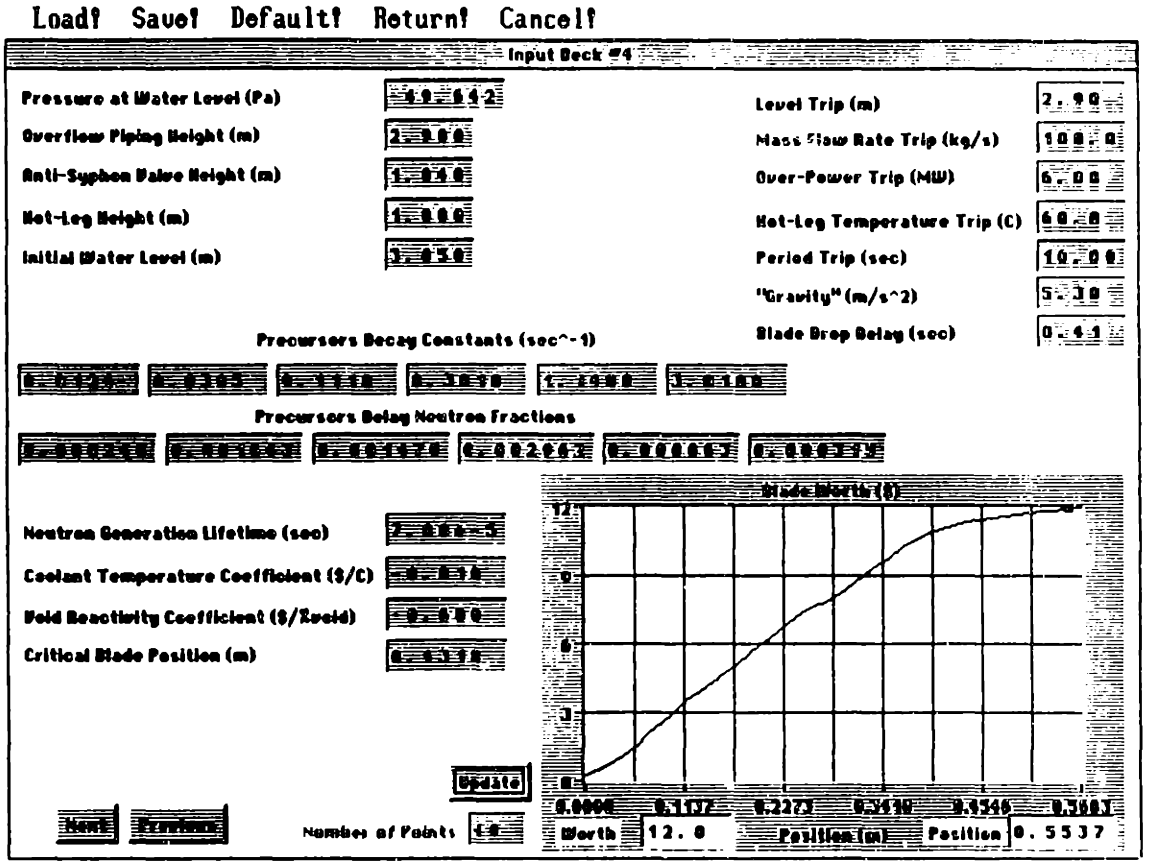

Figure C-5. Data User Interface Input Deck # 4

- ***Pressure at Water Level (Pa)***: Gauge pressure at water level.
- ***Overflow Piping Height (m):*** Distance from the upper grid plate to the point from which the cleanup flow is extracted.
- ***Anti-Siphon Valve Height (m):*** Distance from the upper grid plate to the top of the anti-siphon valve.
- ***Hot Leg Height (m):*** Distance from the upper grid plate to the hot leg pipe elevation.

- *Initial water level (m):* Distance from the upper grid plate to the water surface.

- *Level Trip (m):* Lowest allowable water level. If the water level gets below this level the reactor will scram.

- *Mass Flow Rate Trip (kg/s):* Lowest allowable Mass Flow Rate. If the mass flow rate gets below this value the reactor will scram.

- *Over-Power Trip (MW):* Power at which the reactor will scram if exceeded.

- *Hot-Leg Temperature Trip ($^{\circ}C$):* Hot Leg Inlet Temperature which if exceeded will trip the reactor.

- *Period Trip (sec):* Lowest allowable reactor period. If the reactor period gets below this value, the reactor will be tripped.

- *"Gravity" (m/s^2):* This acceleration is used in calculating the position of the control blade bank after a trip signal is received. The initial velocity is taken as zero and the position as a function of time is calculated using the common "gravity drop" equation. The acceleration used differs from the normal gravity acceleration due to buoyancy forces on the control blades, friction at the magnet coupling, water turbulence, etc.

- *Blade Drop Delay (sec):* Once a trip signal is received, the control blades will not begin dropping the control blade until this time delay has elapsed.

- *Precursors Decay Constants (sec^{-1}):* These are the six-group precursor groups decay constants. The order of the input is not important as long as the same order is used in the *Precursors Delayed Neutron Fractions*.

- *Precursors Delayed Neutron Fractions:* These are the six-group delayed neutron fractions.

- *Neutron Generation Lifetime (sec)*

- *Coolant Temperature Coefficient ($/C):* Reactivity coolant temperature coefficient. An average value for the entire core should be used. Also, since the coefficient is temperature dependent, an appropriate

average value for the anticipated temperature range should be used.

- *Void Reactivity Coefficient ($/% void):* Reactivity coolant void coefficient. The same discussion in the *Coolant Temperature Coefficient* applies here.

- *Critical Blade Position (m):* The initial position of the control blades (from the bottom of the active core). This is the initial level used in dropping the control blades in the case of a reactor trip.

- *Blade Worth Graph:* This graphical interface allows the user to draw with the mouse the control blade bank reactivity worth (in dollars) as a function of active fuel position. Although, the control blades length differ slightly (about an inch) from the active fuel length they were approximated as having the same length as the active fuel. If the active fuel length is changed (Input Deck # 1) the axis will change automatically.

  To draw a curve, place the mouse in the position you want to start and "click and drag" the mouse along the line you want to create. Then, click on the *update* push button next to the graph. The data user interface reads 40 screen pixels distributed uniformly to create the graph just drawn. Therefore, it is advised to draw the curves slowly to allow the code to read the pixels without skipping any, creating undesirable effects. Anyhow, since the resolution is finite, the graph may not be completely smooth.

  If a change in the shape of the graph is desired, simply redraw the graph and push *update*. Note that if only a portion of the graph is unwanted, redrawing the entire graph is not needed. Just redraw over the unwanted section and push *update*.

  Two indicators labeled Worth and Position are located on the bottom portion of the graph border. These are helpful in giving you more detailed information of the position of the cursor as you create a curve. In addition, you can use these indicators to review a finished curve. To do so, click on any portion of the graph border. To move the cursor, use the arrow keys. Most of this information is also relevant for the forcing functions found in panels five and six.

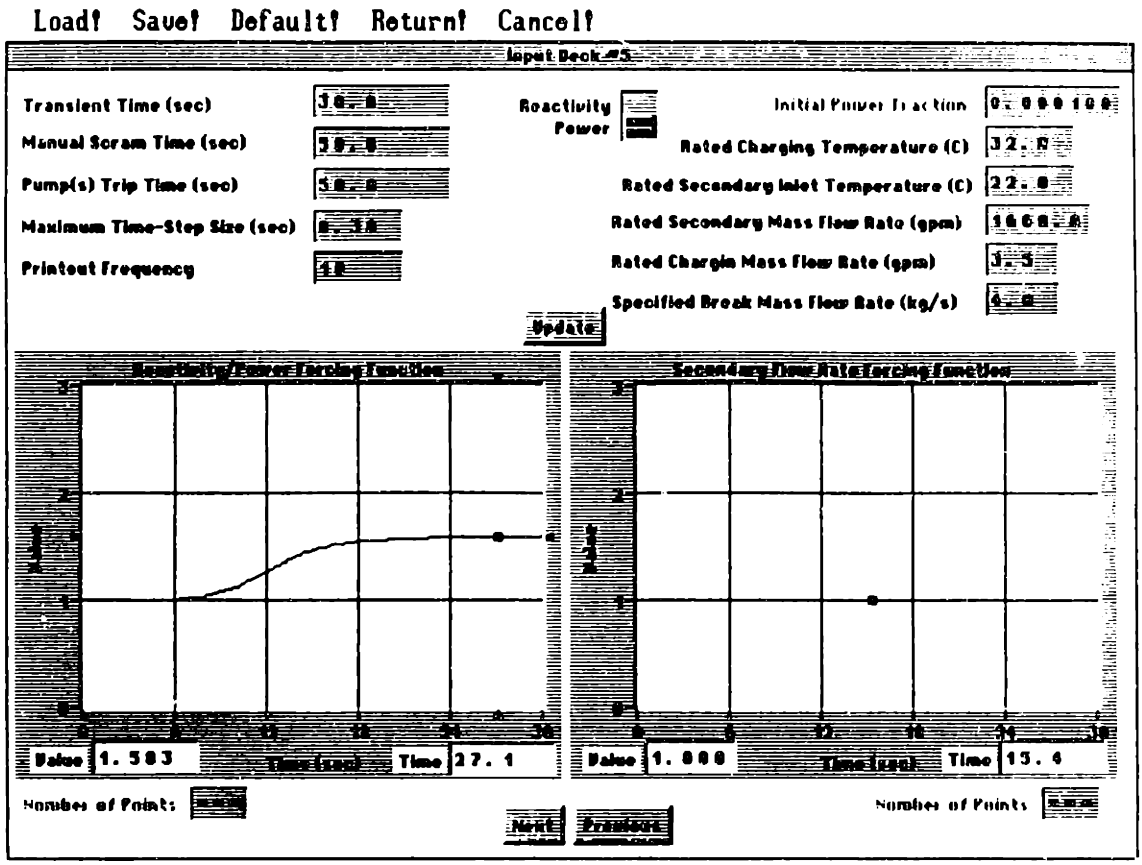

Figure C-6. Data User Interface Input Deck # 5

- *Transient Time (sec)*
- *Manual Scram Time (sec)*
- *Pump(s) Trip Time (sec):* Time at which the pump(s) loose their electric torque and begin to coastdown.
- *Maximum Time-Step Size (sec):* The time-step size is determined by the fluid transport time through the core. In the case of a pump coastdown, the time-step would increase and, as the flow goes to zero, the time-step size would approach infinity. To avoid this, the time-step size is not allow to become larger than the *Maximum Time-Step Size*.

- *Printout Frequency:* This number determines the plotting resolution. For example, if a value N is selected, every N time-steps, the temperatures, powers and other output data is read for plotting.

- *Reactivity/Power Switch:* This switch indicates whether the transient will be driven by a power or a reactivity forcing function. If power is selected, the point-kinetics subroutine is skipped. Therefore, there will be no feedback effects. In addition, if the reactor scrams, an instantaneous zero fission power is assumed. That is, the control blade insertion is not modeled. If reactivity is selected, the *initial power fraction* input becomes active since a critical reactor can be critical at any power.

- *Rated Charging Temperature (°C):* The rated cleanup return flow temperature. The forcing function for the charging temperature is normalized to this value.

- *Rated Secondary Inlet Temperature (°C):* The secondary inlet temperature forcing function is normalized to this value.

- *Rated Secondary Mass Flow Rate (gpm):* The secondary mass flow rate forcing function is normalized to this value.

- *Rated Charging Mass Flow Rate (gpm):* The cleanup return mass flow rate forcing function is normalized to this value.

- *Specified Break Mass Flow Rate (kg/s):* The break mass flow rate forcing function is normalized to this value.

- *Reactivity/Power Forcing Function:* To draw a forcing function follow the directions given for the *Blade Worth Graph*. However, the number of pixels read in this graph and the rest of the graphs are 200, so the mouse movement must be very slow.

  The y-axis of this graph changes depending on the *Reactivity/Power* switch selection since negative reactivities make sense while negative powers do not. Also, if the *Transient Time* is changed, the x-axis changes automatically.

Input Deck # 6 Parameters

This panel includes four forcing functions: secondary inlet temperature, charging mass flow rate, charging temperature, and break mass flow rate. The panel is shown in the following figure.

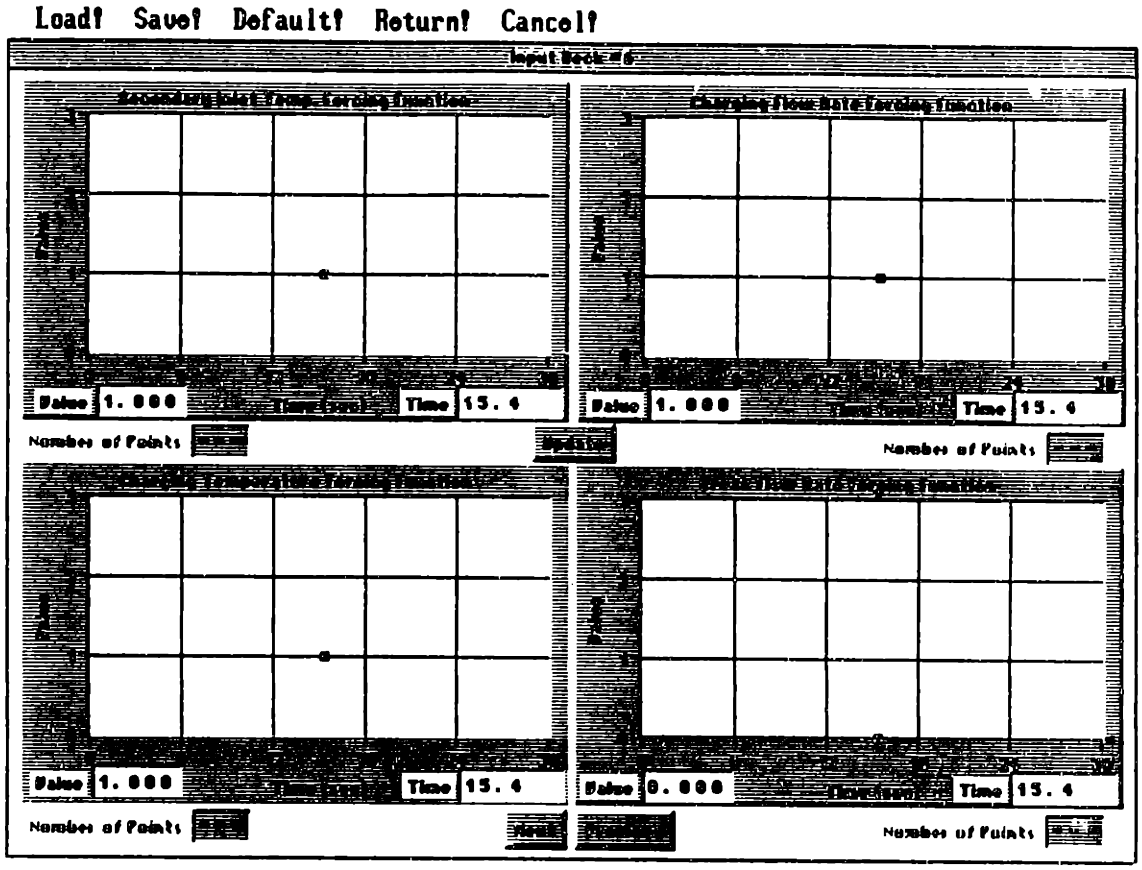

Figure C-7. Data User Interface Input Deck # 6

Once the input is completed, click on the menu bar command *Return*. From the Main Screen, press the *Run Calculations* push-button. This exits the data user interface and runs the transient calculations (TAMLOC). An indication that the program is

running is printed on the screen. Once the calculations are completed, a plotting program is run. The output program main screen is shown in the following figure.

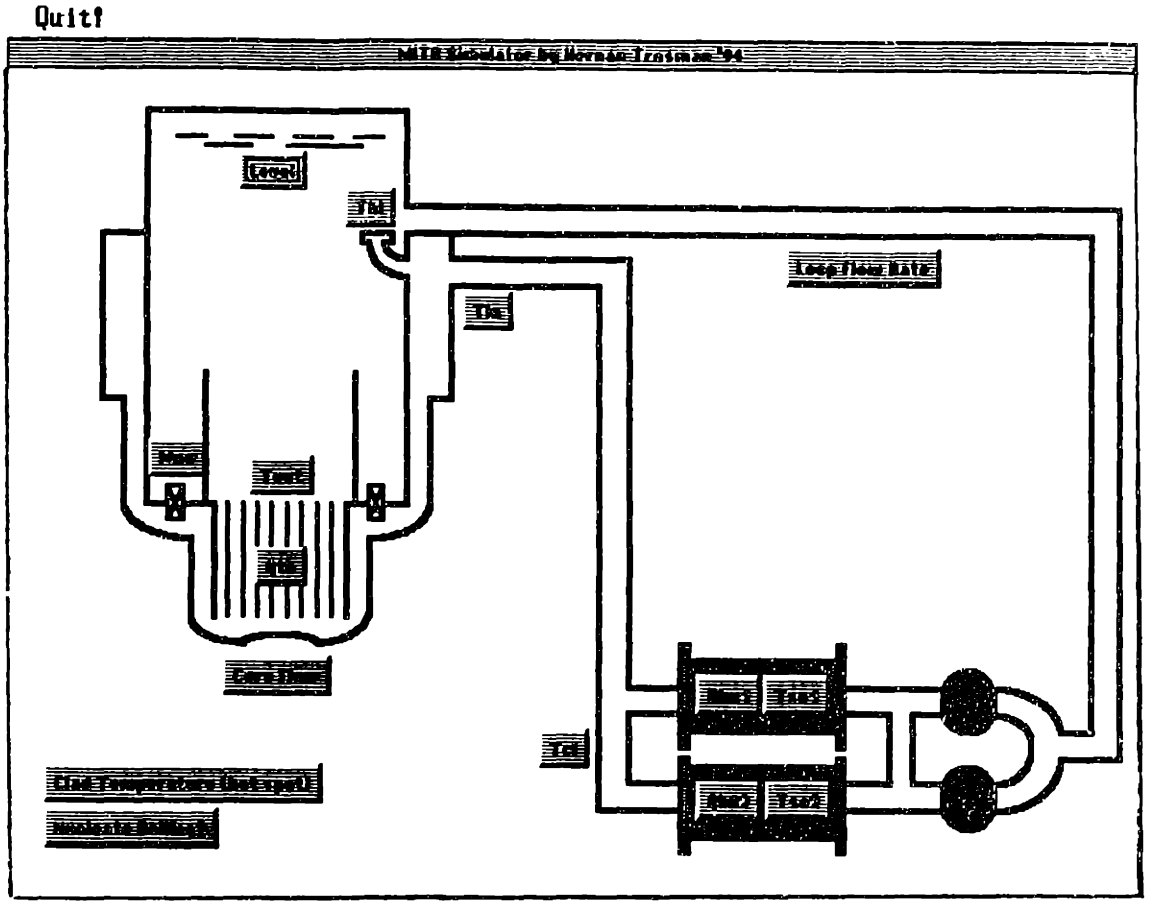

Figure C-8. Data User Interface Output Main Screen

The output temperatures include the hot leg inlet, the cold leg inlet and outlet, the core outlet, the clad (at hot-spot) and both heat exchangers secondary outlet. The output mass flow rates include the loop and the core. The core power generation and both heat exchangers power are available for plotting also. The rest include the water level, the natural circulation mass flow rate and a nucleate boiling indicator. To quit, simply click on the *Quit* menu bar command. To view a plot click on the particular

parameter you are interested on. For example, if the core outlet temperature (T_{out}) push-button is pressed the following screen will appear.

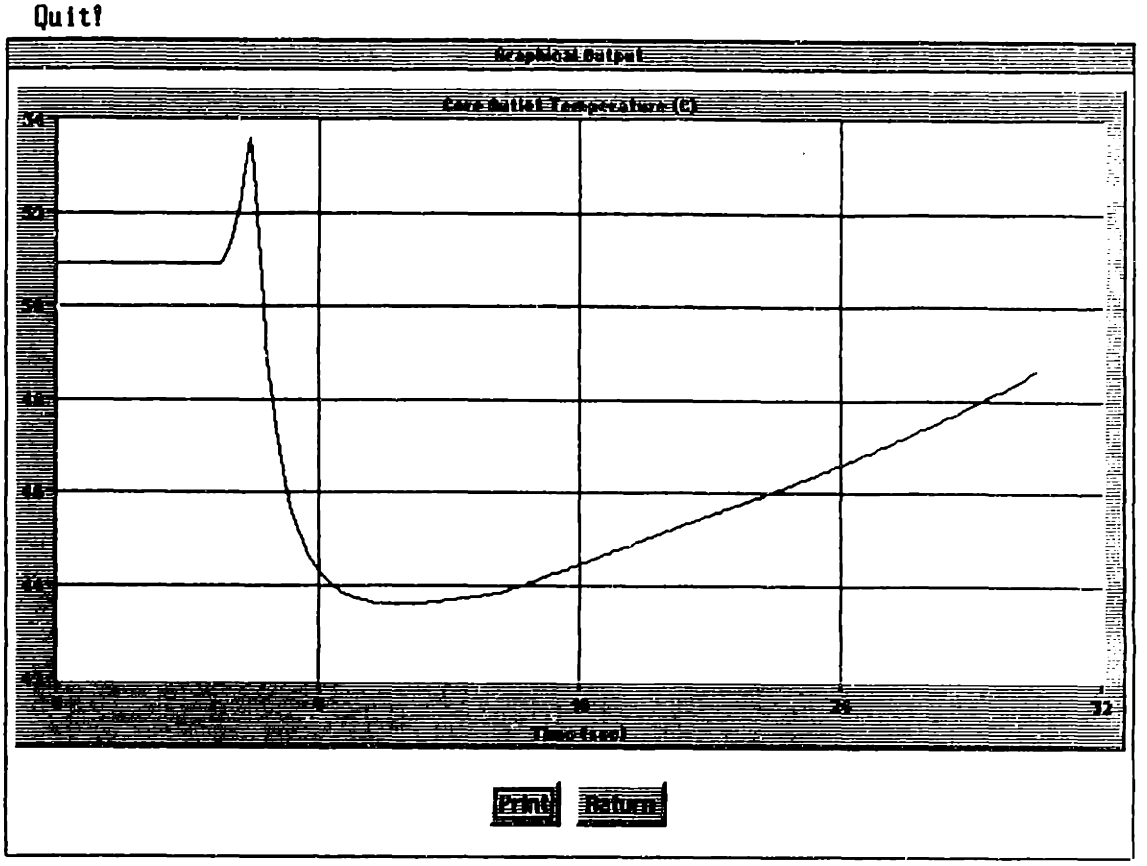

Figure C-9. Data User Interface Graphical Output Screen

Two options are available from this screen: *Print* and *Return*. The *Print* push-button, as the name implies, sends the screen to the printer for a hard copy. The *Return* push-button brings back the Main Output screen. Although the *Quit* command is shown, it is not accessible from this screen.

To run TAMLOC without the data user interface, a text file with all of the input information must be created and given the name *INPUT.DAT*. The data should be

separated by a comma (unless it is the last number of a line) and placed in the following order:

LINE # 1:

1. Rated Power
2. Fraction of Power Deposited in Core
3. Fraction of Power Deposited in Fuel

LINE # 2:

1. Radial Peaking Factor
2. Axial Peaking Factor
3. Hot-Spot Relative Axial Location
4. Enthalpy-Rise Engineering Factor
5. Heat Flux Engineering Factor

LINE # 3:

1. Rated Loop Flow Rate
2. Fraction of Flow Through Core
3. Initial Flow Rate Fraction
4. Flow Disparity

LINE # 4:

1. Rated Secondary Mass Flow Rate
2. Rated Charging Mass Flow Rate
3. Specified Break Mass Flow Rate
4. Underhead Mixing Mass Flow Rate

LINE # 5:

1. Rated Secondary Inlet Temperature
2. Rated Charging Temperature

LINE # 6:

1. Transient Time
2. Manual Scram Time
3. Pump(s) Trip Time
4. Maximum Time-Step Size
5. Printout Frequency

LINE # 7:

1. Level Trip
2. Hot Leg Temperature Trip
3. Mass Flow Rate Trip
4. Overpower Trip
5. "Gravity"

LINE # 8:

Driving Forcing Function (integer)
0 = reactivity, 1 = power

LINE # 9:

If a zero (reactivity) is selected this line should be the Initial Power Fraction. Otherwise, ignore this line.

LINE # 10:

The number of data pairs used to represent represent either the reactivity or power forcing function (integer-minimum of two).

LINE # 11:

Reactivity or Power Forcing Function in the following format:

$time_1$, $value_1$, $time_2$, $value_2$, ...

LINE # 12:

The number of data pairs used to represent the charging mass flow rate forcing function (integer-minimum of two).

LINE # 13:
Charging Mass Flow Rate Forcing Function. Same format as line # 11.

LINE # 14:
The number of data pairs used to represent the charging temperature forcing function (integer-minimum of two).

LINE # 15:

Charging Temperature Forcing Function. Same format as line # 11.

LINE # 16:

The number of data pairs used to represent the secondary mass flow rate forcing function (integer-minimum of two).

LINE # 17:

Secondary Mass Flow Rate Forcing Function. Same format as line # 11.

LINE # 18:

The number of data pairs used to represent the secondary inlet temperature forcing function (integer-minimum of two).

LINE # 19:

Secondary Inlet Temperature Forcing Function. Same format as line # 11.

LINE # 20:

The number of data pairs used to represent the break mass flow rate forcing function. (integer-minimum of two).

LINE # 21:

Break Mass Flow Rate Forcing Function Same format as line # 11.

LINE # 22:

1. Pump Moment of Inertia
2. Pump Rated Mass Flow Rate
3. Pump Rated Speed
4. Pump Rated Head
5. Pump Rated Density
6. Pump Rated Windage Torque

LINE # 23:

The pump(s) head curve coefficients A_1 through A_4 (separated by commas).

LINE # 24:

The number of heat exchangers (integer- 1 or 2).

LINE # 25:

(for heat exchanger # 1)

1. Geometry Indicator (1=plate, 2=shell)
2. Inside Diameter
3. Outside Diameter
4. Number of primary tubes or plates

LINE # 26:

(for heat exchanger # 1)

1. Secondary-Side Equivalent Diameter
2. Total Secondary-Side Flow Area
3. Metal Conductivity
4. Fouling

LINE # 27:

(for heat exchanger # 1)

1. Metal Mass
2. Metal Specific Heat

LINES # 28, 29, & 30:

If two heat exchangers selected, repeat lines 25, 26, and 27 for heat exchanger # 2

LINE # 31:

1. Fuel "Meat" Mass
2. Clad Mass

LINE # 32:

1. Fuel "Meat" Density
2. Clad Density

LINE # 33:

1. Fuel "Meat" Thickness
2. Clad Thickness
3. Active Fuel Length
4. Plate Width
5. Fuel "Meat" Width
6. Number of Plates in Core

LINE # 34:

The coefficients C_1 through C_4 (separated by commas) used to determine the fuel "meat" thermal conductivity as a function of temperature.

LINE # 35:

The coefficients C_1 through C_4 (separated by commas) used to determine the fuel "meat" specific heat as a function of temperature

LINE # 36:

The coefficients C_1 through C_4 (separated by commas) used to determine the clad thermal conductivity as a function of temperature.

LINE # 37:

The coefficients C_1 through C_4 (separated by commas) used to determine the clad specific heat as a function of temperature

LINE # 38:

1. Core Coolant Channel Width
2. Finned Plate Perimeter
3. Finned Surface Effectiveness

LINE # 39:

The components flow areas 1 through 12 (separated by commas), where the numbers

represent the following control volumes: (1) Cold Leg, (2) Region 1, (3) Region 2, (4) Region 3, (5) Region 4, (6) Core (single channel), (7), Inside Flow Shroud, (8) Mixing Area (upper), (9) Hot Leg, (10) Heat Exchanger # 1, (11) Heat Exchanger # 2, (12) Underhead.

LINE # 40:

Flow Area of the Portion of the Mixing Area Control Volume adjacent to the flow shroud (annular region).

LINE # 41:

System Equivalent Diameters.
(1 through 11; the ordering was explained in the *Input Deck # 2* section).

LINE # 42:

System Volumes
(1 through 12; the ordering was explained in the *Input Deck # 2* section).

LINE # 43:

System Lengths.
(1 through 12; the ordering was explained in the *Input Deck # 2* section).

LINE # 44:

System Outlet Elevations
(1 through 11; the ordering was explained in the *Input Deck # 2* section).

LINE # 45:

System Form-Loss Coefficients.
(1 through 11; the ordering was explained in the Input Deck # 3 section).

LINE # 46:

1. Natural Circulation Valve Form-Loss Coefficient
2. Natural Circulation Valve Flow Area
3. Natural Circulation Ball Volume
4. Natural Circulation Ball Density

LINE # 47:

1. Pressure at Water Level
2. Initial Water Level
3. Overflow Piping Height
4. Hot Leg Height

LINE # 48:

The precursors delayed neutron groups decay constants (6 separated by commas). They must be in the same order as line # 49.

LINE # 49:

The precursors delayed neutron fractions (6 separated by commas).

LINE # 50:

1. Prompt-Neutron Generation Lifetime
2. Coolant Temperature Reactivity Coefficient
3. Void Reactivity Coefficient

LINE # 51:

The number of data pairs used to represent the control blade bank worth graph. (integer-minimum of two).

LINE # 52:

The Integral Control Blade Bank Worth Curve. The format is as follows:

$height_1$, $worth_1$, $height_2$, $worth_2$, ...

LINE # 53:

Critical Blade Position (from the bottom of the core).

Once the *INPUT.DAT* file is created, the program can be run by typing *TAMLOC.EXE* at the prompt. However, before running the program make sure that there are no files with the names *OUTPUT* and *PLOT.DAT.*

To view the output, type *TAMOUT.EXE.* This starts the plotting program previously mentioned. In addition to the plotting program, there is an output text file named *OUTPUT* containing the input information, the system initial conditions and transient calculation comments. This file can be viewed by using any text editor program and it is helpful in "debugging" an input file or determining when the reactor scrammed (transient calculation comments). Also, if the program crashes, this file can sometimes help you in determining what the problem is (transient calculation comments). However, sometimes you are on your own. The user is responsible for making sure the input data makes sense!

APPENDIX D: INPUT DATA

```
4.9,0.9667,0.9097
1.38,1.2,0.1,1.0,1.0
2055.0,0.94,1.0,1.0
1660.0,3.5,4.0,120.0
22.0,32.0
5500,1E+6,44E7,1.0,195
2.9,60,0.0,6.0,10.0,5.3,0.41
1
80
0.0,0.0002,60.0,0.0003,120,0.0005,180,0.0008,240,0.0014,300,0.0022,360,0.0035,420,0.0057,480,0.0088,540,0.0140,600,0.0223,
660,0.0348,720,0.0395,780,0.0424,840,0.0466,900,0.0508,960,0.0509,1020,0.0542,1080,0.0655,1140,0.0817,1200,0.0977,1260,
0.1019,1320,0.1017,1380,0.1016,1440,0.1174,1500,0.1514,1560,0.1898,1620,0.2030,1680,0.2041,1740,0.2041,1800,0.2041,1860,
0.2052,1920,0.2052,1980,0.2183,2040,0.2743,2100,0.3094,2160,0.3072,2220,0.3039,2280,0.3083,2340,0.3478,2400,0.4060,2460,
0.4114,2520,0.4038,2580,0.4049,2640,0.4005,2700,0.4005,2760,0.4082,2820,0.4093,2880,0.4093,2940,0.4126,3000,0.4093,3060,
0.4235,3120,0.4597,3180,0.5080,3240,0.5267,3300,0.5519,3360,0.5706,3420,0.5782,3480,0.5848,3540,0.6002,3600,0.6079,3660,
0.6068,3720,0.6188,3780,0.6079,3840,0.6133,3900,0.6649,3960,0.7604,4020,0.8207,4080,0.8185,4140,0.8229,4200,0.8141,4260,
0.8185,4320,0.8514,4380,0.9831,4440,0.9996,4500,1.0029,4560,0.9930,4620,0.9930,4680,0.9930,4740,0.9985
3
0.0,1.0,1.0,1.0,3.0,1.0
2
0.0,1.0,1.0,1.0
4
0.0,1.0,1.0,1.0,3.0,1.0,4.0,1.0
40
0.0,1.0,555,1.0,646,1.02,1100,1.02,1191,1.04,1555,1.04,1646,1.06,1737,1.07,1828,1.08,1919,1.09,2010,1.1,2100,1.11,2191,1.13,
2282,1.14,2373,1.15,2464,1.18,2555,1.19,2646,1.22,2737,1.23,2828,1.25,2919,1.23,3009,1.23,3100,1.21,3191,1.22,3282,1.21,3373,
1.22,3464,1.23,3828,1.23,3918,1.16,4009,1.11,4100,1.09,4191,1.04,4282,1.02,4373,1.0,4464,0.98,4555,0.96,4646,0.94,4736,0.93,
4828,0.91,4900,0.91
2
0.0,0.0,1.0,0.0
0.5,64.3,180.64,241.3E3,992.2,20.0
-2.556,14.247,-15.306,4.596
2
2,0.007035,0.009525,885
0.00301,0.07968,17.0,4.07E-6
993,443.8
2,0.007035,0.009525,885
0.00301,0.07968,17.0,4.07E-6
993,443.8
0.08312446,0.0961893
3675,2712.6
7.62E-4,5.08E-4,0.5683,0.058674,0.0528828,330
0.0,0.0,41.2,0.0
0.0,1120.9,2.224E6,0.0
0.0,0.0,186.0,0.0
0.0,1187.0,2.409E6,0.0
0.002235,0.229108,1.9
0.0324,0.3389,0.1108,0.004375,0.0288,0.000131,0.1299,0.9234,0.0324,3.888E-5,3.888E-5,0.981
0.7935
0.203,0.1796,0.0629,0.1045,0.0396,0.002237,0.3874,1.084,0.203,0.007035,0.007035
0.468,0.4132,0.076,0.007467,0.0179,0.0375,0.099,1.8237,0.427,1.68E-4,1.68E-4,0.96
14.435,1.22,0.6858,0.072,0.6175,0.66675,0.762,1.318,13.17,4.32,4.32,1.0562
9.658,8.438,7.752,7.745,7.1275,7.790,8.552,9.870,2.690,2.690,2.690
2.17,0.0,0.30,0.18207,0.00,2.05,0.00,0.00,4.577,7.30,7.30
11.9,0.030512,0.000204,2503
-49.642,3.05,2.98,1.88,1.84
0.0124,0.0305,0.111,0.301,1.14,3.01
0.000248,0.001643,0.001470,0.002962,0.000863,0.000315
70E-6,-0.02107,-0.600
2
0.0,0.0,0.5683,10.0
0.4318
```

Figure D-1. MITR-II Startup Input Data

```
4.9,0.9667,0.9097
1.38,1.2,0.1,1.0,1.0
2055.0,0.94,1.0,1.0
1660.0,3.5,4.0,120.0
20.0,32.0
5500,1E+6,44E7,1.0,195
2.9,60,0.0,6.0,10.0,5.3,0.41
1
20
0.0,1.0,299.8,0.820816,599.76,0.820204,899.7,0.819796,1199.82,0.819388,1500.24,0.620204,
1800.82,0.619388,2101.44,0.618776,2402.09,0.616531,2702.94,0.419592,3004.05,0.418367,
3305.22,0.417755,3606.45,0.417143,3907.72,0.400408,4209.23,0.217551,4510.88,0.216735,
4812.59,0.215918,5114.33,0.21551,5416.12,0.11651,5718.03,0.115245
3
0.0,1.0,1.0,1.0,3.0,1.0
2
0.0,1.0,1.0,1.0
4
0.0,1.0,1.0,1.0,3.0,1.0,4.0,1.0
20
0.0,1.0,299.8,1.0,599.76,0.98,899.7,0.95,1199.82,0.9375,1500.24,0.96,1800.82,0.925,
2101.44,0.9125,2402.09,0.895,2702.94,0.88,3004.05,0.855,3305.22,0.835,3606.45,0.82,
3907.72,0.805,4209.23,0.79,4510.88,0.7625,4812.59,0.75,5114.33,0.7125,5416.12,0.71,
5718.03,0.71
2
0.0,0.0,1.0,0.0
0.5,64.3,180.64,241.3E3,992.2,20.0
-2.556,14.247,-15.306,4.596
2
2,0.007035,0.009525,885
0.00301,0.07968,17.0,4.07E-6
993,443.8
2,0.007035,0.009525,885
0.00301,0.07968,17.0,4.07E-6
993,443.8
0.08312446,0.0961893
3675,2712.6
7.62E-4,5.08E-4,0.5683,0.058674,0.0528828,330
0.0,0.0,41.2,0.0
0.0,1120.9,2.224E6,0.0
0.0,0.0,186.0,0.0
0.0,1187.0,2.409E6,0.0
0.002235,0.229108,1.9
0.0324,0.3389,0.1108,0.004375,0.0288,0.000131,0.1299,0.9234,0.0324,3.888E-5,3.888E-5,0.981
0.7935
0.203,0.1796,0.0629,0.1045,0.0396,0.002237,0.3874,1.084,0.203,0.007035,0.007035
0.468,0.4132,0.076,0.007467,0.0179,0.0375,0.099,1.8237,0.427,1.68E-4,1.68E-4,0.96
14.435,1.22,0.6858,0.072,0.6175,0.66675,0.762,1.318,13.17,4.32,4.32,1.0562
9.658,8.438,7.752,7.745,7.1275,7.790,8.552,9.870,2.690,2.690,2.690
2.17,0.0,0.30,0.18207,0.00,2.05,0.00,0.00,4.577,7.30,7.30
11.9,0.030512,2.039E-4,2503
-49.642,3.05,2.98,1.88,1.84
0.0124,0.0305,0.111,0.301,1.14,3.01
0.000248,0.001643,0.001470,0.002962,0.000863,0.000315
70E-6,-0.02107,-0.600
2
0.0,0.0,0.5683,10.0
0.4318
```

Figure D-2. MITR-II Shutdown Input Data

```
5.000000,0.966700,0.909700
1.38800,1.0500000,1.00000,1.527,1.146
2050.000000,0.940000,1.000000,0.9
1660.000000,3.500000,4.000000,115.000000
26.600000,32.000000
1000.000000,7500.000000,7500.000000,0.300000,1
2.900000,60.000000,100.000000,6.000000,10.000000,5.300000,0.410000
0
1.000000
2
0.0,0.0,1000.0,0.0
2
0.0,1.0,1000.0,1.0
2
0.0,1.0,1000.0,1.0
4
0.0,1.0,30.0,1.0,35.0,0.0,1000.0,0.0
2
0.0,1.0,1000.0,1.0
2
0.0,0.0,1000.0,0.0
0.500000,64.300000,180.640000,241300.000000,992.200000,20.000000
-2.556000,14.247000,-15.306000,4.596000
2
2,0.007035,0.009525,885
0.003010,0.079680,17.000000,4.070000e-06
993.000000,443.800000
2,0.007035,0.009525,885
0.003010,0.079680,17.000000.4.070000e-06
993.000000,443.800000
0.083120,0.096190
3675.000000,2712.600000
0.000762,0.000508,0.568300,0.058670,0.052880,330
0.000000,0.000000,41.200000,0.000000
0.000000,1120.90000,2.224E6,0.000000
0.000000,0.000000,186.000000,0.000000
0.000000,1187.000000,2409000.000000,0.000000
0.002240,0.229110,1.900000
0.0324,0.3389,0.1108,0.004735,0.0288,0.000131,0.1299,0.9234,0.0324,0.000039,0.000039,0.981
0.793500
0.203000,0.179600,0.062900,0.220000,0.039600,0.002237,0.387400,1.084000,0.203000,0.007035,0.007035
0.468000,0.413200,0.076000,0.016400,0.017900,0.037500,0.099000,1.823700,0.42700,0.000168,0.000168,0.960
14.435000,1.220000,0.685800,0.007000,0.617500,0.666700,0.762000,1.318000,13.1700,4.320000,4.320,1.05620
9.658000,8.438000,7.752000,7.745000,7.127500,7.790000,8.552000,9.870000,2.690000,2.690000,2.690000
2.170000,0.000000,0.300000,0.182070,0.000000,2.050000,0.000000,0.000000,4.577000,7.300000,7.300000
11.900000,0.030512,0.000204,2503.000000
-49.642000,3.050000,2.980000,1.880000,1.840000
0.012400,0.030500,0.111000,0.301000,1.140000,3.010000
0.000248,0.001643,0.001470,0.002962,0.000863,0.000315
0.000070,-0.010000,-0.600000
22
0.0,0.0,0.0508,0.55,0.0762,1.2,0.1016,1.9,0.127,2.65,0.1524.3.5,0.1778,4.3,0.2032,5.1,0.2286,5.9,0.254,6.7,
0.2794,7.4,0.3048,8.0,0.330,8.6,0.3556,9.2,0.381,9.7,0.4064,10.2,0.4318,10.6,0.4572,11.0,0.4826,11.25,0.508,
11.5,0.5334,11.6,0.5683,11.7
0.5175
```

Figure D-3. MITR-II Loss of Heat Sink Input Data

5.000000,0.966700,0.909700
1.1310000,2.104,0.0000,1.527,1.146
2050.000000,0.940000,1.000000,0.9
1660.000000,3.500000,4.000000,115.000000
26.600000,32.000000
30.000000,7500.000000,7500.000000,0.300000,1
2.900000,60.000000,112.700000,6.000000,10.000000,5.300000,0.410000
0
1.000000
3
0.0,0.0,10.0,0.0,202,2.0
2
0.0,1.0,30.0,1.0
2
0.0,1.0,30.0,1.0
2
0.0,1.0,30.0,1.0
2
0.0,1.0,30.0,1.0
2
0.0,0.0,30.0,0.0
0.500000,64.300000,180.640000,241300.000000,992.200000,20.000000
-2.556000,14.247000,-15.306000,4.596000
2
2,0.007035,0.009525,885
0.003010,0.079680,17.000000,4.070000e-06
993.000000,443.800000
2,0.007035,0.009525,885
0.003010,0.079680,17.000000,4.070000e-06
993.000000,443.800000
0.083120,0.096190
3675.000000,2712.600000
0.000762,0.000508,0.568300,0.058670,0.052880,330
0.000000,0.000000,41.200000,0.000000
0.000000,1120.90000,2.224E6,0.000000
0.000000,0.000000,186.000000,0.000000
0.000000,1187.000000,2409000.000000,0.000000
0.002240,0.229110,1.900000
0.032400,0.338900,0.110800,0.004735,0.028800,0.000131,0.129900,0.923400,0.0324,0.000039,0.000039,0.9810
0.793500
0.203000,0.179600,0.062900,0.220000,0.039600,0.002237,0.387400,1.084000,0.203000,0.007035,0.007035
0.468000,0.413200,0.076000,0.016400,0.017900,0.037500,0.099000,1.823700,0.4270,0.000168,0.000168,0.9600
14.435000,1.220000,0.685800,0.007000,0.617500,0.666700,0.762000,1.318000,13.17000,4.320000,4.320,1.0562
9.658000,8.438000,7.752000,7.745000,7.127500,7.790000,8.552000,9.870000,2.690000,2.690000,2.690000
2.170000,0.000000,0.300000,0.182070,0.000000,2.050000,0.000000,0.000000,4.577000,7.300000,7.300000
11.900000,0.030512,0.000204,2503.000000
-49.642000,3.050000,2.980000,1.880000,1.840000
0.012400,0.030500,0.111000,0.301000,1.140000,3.010000
0.000248,0.001643,0.001470,0.002962,0.000863,0.000315
0.000070,-0.010000,-0.600000
22
0.0,0.0,0.0508,0.55,0.0762,1.2,0.1016,1.9,0.127,2.65,0.1524,3.5,0.1778,4.3,0.2032,5.1,0.2286,5.9,0.254,6.7,
0.2794,7.4,0.3048,8.0,0.330,8.6,0.3556,9.2,0.381,9.7,0.4064,10.2,0.4318,10.6,0.4572,11.0,0.4826,11.25,0.508,
11.5,0.5334,11.6,0.5683,11.7
0.5175

Figure D-4. MITR-II Blade Withdrawal Input Data (4.25 in/min)

5.000000,0.966700,0.909700
1.131000,2.104,0.00000,1.527,1.146
2050.000000,0.940000,1.000000,0.9
1660.000000,3.500000,4.000000,115.000000
26.600000,32.000000
30.000000,7500.000000,7500.000000,0.300000,1
2.900000,60.000000,112.700000,6.000000,10.000000,5.300000,0.410000
0
1.000000
3
0.0,0.0,10.0,0.0,106,2.0
2
0.0,1.0,30.0,1.0
2
0.0,1.0,30.0,1.0
2
0.0,1.0,30.0,1.0
2
0.0,1.0,30.0,1.0
2
0.0,0.0,30.0,0.0
0.500000,64.300000,180.640000,241300.000000,992.200000,20.000000
-2.556000,14.247000,-15.306000,4.596000
2
2,0.007035,0.009525,885
0.003010,0.079680,17.000000,4.070000e-06
993.000000,443.800000
2,0.007035,0.009525,885
0.003010,0.079680,17.000000,4.070000e-06
993.000000,443.800000
0.083120,0.096190
3675.000000,2712.600000
0.000762,0.000508,0.568300,0.058670,0.052880,330
0.000000,0.000000,41.200000,0.000000
0.000000,1120.90000,2.224E6,0.000000
0.000000,0.000000,186.000000,0.000000
0.000000,1187.000000,2409000.000000,0.000000
0.002240,0.229110,1.900000
0.032400,0.338900,0.110800,0.004735,0.028800,0.000131,0.129900,0.923400,0.0324,0.000039,0.000039,0.9810
0.793500
0.203000,0.179600,0.062900,0.220000,0.039600,0.002237,0.387400,1.08400,0.203000,0.007035,0.007035
0.468000,0.413200,0.076000,0.016400,0.017900,0.037500,0.099000,1.8237,0.427000,0.000168,0.000168,0.9600
14.435000,1.220000,0.685800,0.007000,0.617500,0.666700,0.762000,1.3180,13.170000,4.320000,4.3200,1.0562
9.658000,8.438000,7.752000,7.745000,7.127500,7.790000,8.552000,9.870000,2.690000,2.690000,2.690000
2.170000,0.000000,0.300000,0.18207,0.000000,2.050000,0.000000,0.000000,4.577000,7.300000,7.300000
11.900000,0.030512,0.000204,2503.000000
-49.642000,3.050000,2.980000,1.880000,1.840000
0.012400,0.030500,0.111000,0.301000,1.140000,3.010000
0.000248,0.001643,0.001470,0.002962,0.000863,0.000315
0.000070,-0.010000,-0.600000
22
0.0,0.0,0.0508,0.55,0.0762,1.2,0.1016,1.9,0.127,2.65,0.1524,3.5,0.1778,4.3,0.2032,5.1,0.2286,5.9,0.254,6.7,
0.2794,7.4,0.3048,8.0,0.330,8.6,0.3556,9.2,0.381,9.7,0.4064,10.2,0.4318,10.6,0.4572,11.0,0.4826,11.25,0.508,
11.5,0.5334,11.6,0.5683,11.7
0.5175

Figure D-5. MITR-II Blade Withdrawal Input Data (8.50 in/min)

```
5.000000,0.966700,0.909700
1.388000,1.050000,1.00000,1.527,1.146
2050.000000,0.940000,1.000000,0.9
1660.000000,3.500000,4.000000,115.000000
26.600000,32.000000
400.000000,7500.000000,5.000000,0.300000,1
2.900000,60.000000,112.700000,6.000000,10.000000,5.300000,0.410000
0
1.000000
2
0.0,0.0,400,0.0
2
0.0,1.0,400,1.0
2
0.0,1.0,400,1.0
2
0.0,1.0,400,1.0
2
0.0,1.0,400,1.0
2
0.0,0.0,400,0.0
0.500000,64.300000,180.640000,241300.000000,992.200000,20.000000
-2.556000,14.247000,-15.306000,4.596000
2
2,0.007035,0.009525,885
0.003010,0.079680,17.000000,4.070000e-06
993.000000,443.800000
2,0.007035,0.009525,885
0.003010,0.079680,17.000000,4.070000e-06
993.000000,443.800000
0.083120,0.096190
3675.000000,2712.600000
0.000762,0.000508,0.568300,0.058670,0.052880,330
0.000000,0.000000,41.200000,0.000000
0.000000,1120.90000,2.224E6,0.000000
0.000000,0.000000,186.000000,0.000000
0.000000,1187.000000,2409000.000000,0.000000
0.002240,0.229110,1.900000
0.032400,0.338900,0.110800,0.004735,0.028800,0.000131,0.129900,0.923400,0.0324,0.000039,0.000039,0.9810
0.793500
0.203000,0.179600,0.062900,0.220000,0.039600,0.002237,0.387400,1.084000,0.203000,0.007035,0.007035
0.468000,0.413200,0.076000,0.016400,0.017900,0.037500,0.099000,1.8237,0.427000,0.000168,0.000168,0.9600
14.435000,1.220000,0.685800,0.007000,0.617500,0.666700,0.762000,1.3180,13.170000,4.320000,4.3200,1.0562
9.658000,8.438000,7.752000,7.745000,7.127500,7.790000,8.552000,9.870000,2.690000,2.690000,2.690000
2.170000,0.000000,0.300000,0.18207,0.000000,2.050000,0.000000,0.000000,4.577000,7.300000,7.300000
11.900000,0.030512,0.000204,2503.000000
-49.642000,3.050000,2.980000,1.880000,1.840000
0.012400,0.030500,0.111000,0.301000,1.140000,3.010000
0.000248,0.001643,0.001470,0.002962,0.000863,0.000315
0.000070,-0.010000,-0.600000
22
0.0,0.0,0.0508,0.55,0.0762,1.2,0.1016,1.9,0.127,2.65,0.1524,3.5,0.1778,4.3,0.2032,5.1,0.2286,5.9,0.254,6.7,
0.2794,7.4,0.3048,8.0,0.330,8.6,0.3556,9.2,0.381,9.7,0.4064,10.2,0.4318,10.6,0.4572,11.0,0.4826,11.25,0.508,
11.5,0.5334,11.6,0.5683,11.7
0.5175
```

Figure D-6. MITR-II Pump Coastdown Input Data

```
10.000000,0.966700,0.909700
1.1310000,2.1037500,0.00000,1.527,1.146
2500.000000,0.940000,1.000000,0.916
2290.000000,5.000000,4.000000,135.000000
25.600000,32.000000
600.000000,7000.00000,7000.000000,0.300000,10
2.900000,662.000000,112.750000,11.000000,5.000000,5.300000,0.410000
0
1.000000
3
0.0,0.0,10.0,0.0,106,0.0
2
0.0,1.0,35.0,1.0
2
0.0,1.0,35.0,1.0
3
0.0,1.0,180.0,1.0,210,0.0
2
0.0,1.0,35.0,1.0
2
0.0,0.0,35.0,0.0
0.3620000,78.600000,185.350000,425000.000000,992.200000,20.000000
1.305200,-0.25533,-0.04985,0.0
2
1,0.001375,0.004775,67
0.00275,0.056196,13.650000,9.483000e-27
480.400000,896.000000
1,0.001375,0.004775,67
0.00275,0.056196,13.650000,9.483000e-27
480.400000,896.000000
0.083120,0.096190
3675.000000,2712.600000
0.000762,0.000508,0.568300,0.058670,0.052880,330
0.000000,0.000000,35.800000,0.000000
0.000000,1069.400000,2072000.000,0.000000
0.000000,0.000000,186.000000,0.000000
0.000000,1187.000000,2409000.000000,0.000000
0.002240,0.229110,1.900000
0.032400,0.338900,0.110800,0.004375,0.028800,0.000131,0.129900,0.9234,0.0324,0.0008388,0.0008388,0.9810
0.793500
0.203000,0.179600,0.062900,0.220000,0.039600,0.002237,0.387400,1.084000,0.203000,0.00275,0.00275
0.468000,0.413200,0.076000,0.016400,0.017900,0.037500,0.099000,1.8237,0.427000,0.00108,0.00108,0.960000
14.435000,1.220000,0.685800,0.007000,0.617500,0.666700,0.762000,1.3180,13.170000,1.290000,1.2900,1.0562
9.658000,8.438000,7.752000,7.745000,7.127500,7.790000,8.552000,9.870000,2.690000,2.690000,2.690000
2.170000,0.000000,0.300000,0.182070,0.000000,2.050000,0.000000,0.000000,4.577000,19.390000,19.300000
11.900000,0.030512,0.000204,2503.000000
-49.642000,3.050000,2.980000,1.880000,1.840000
0.012400,0.030500,0.111000,0.301000,1.140000,3.010000
0.000248,0.001643,0.001470,0.002962,0.000863,0.000315
0.000070,-0.010000,-0.600000
2
0.0,0.0,0.5683,12
0.431800
```

Figure D-7. MITR-III Loss of Heat Sink Input Data (no scram)

```
10.000000,0.966700,0.909700
1.1310000,2.1037500,0.00000,1.527,1.146
2500.000000,0.940000,1.000000,0.916
2290.000000,5.000000,4.000000,135.000000
25.80000,32.000000
40.000000,7000.00000,7000.000000,0.100000,1
2.900000,662.000000,112.750000,111.000000,0.000000,5.300000,0.410000
0
1.000000
3
0.0,0.0,10.0,0.0,202,2.0
2
0.0,1.0,35.0,1.0
2
0.0,1.0,35.0,1.0
3
0.0,1.0,180.0,1.0,210,1.0
2
0.0,1.0,35.0,1.0
2
0.0,0.0,35.0.0.0
0.3620000,78.600000,185.350000,425000.000000,992.200000,20.000000
1.305200,-0.25533,-0.04985,0.0
2
1,0.001375,0.004775,67
0.00275,0.056196,13.650000,9.483000e-27
480.400000,896.000000
1,0.001375,0.004775,67
0.00275,0.056196,13.650000,9.483000e-27
480.400000,896.000000
0.083120,0.096190
3675.000000,2712.600000
0.000762,0.000508,0.568300,0.058670,0.052880,330
0.000000,0.000000,35.800000,0.000000
0.000000,1069.400000,2072000.000,0.000000
0.000000,0.000000,186.000000,0.000000
0.000000,1187.000000,2409000.000000,0.000000
0.002240,0.229110,1.900000
0.032400,0.338900,0.110800,0.004375,0.028800,0.000131,0.129900,0.9234,0.0324,0.0008388,0.0008388,0.9810
0.793500
0.203000,0.179600,0.062900,0.220000,0.039600,0.002237,0.387400,1.084000,0.203000,0.00275,0.00275
0.468000,0.413200,0.076000,0.016400,0.017900,0.037500,0.099000,1.823700,0.427000,0.00108,0.00108,0.9600
14.435000,1.220000,0.685800,0.007000,0.617500,0.666700,0.762000,1.318000,13.170000,1.2900,1.2900,1.0562
9.658000,8.438000,7.752000,7.745000,7.127500,7.790000,8.552000,9.870000,2.690000,2.690000,2.690000
2.170000,0.000000,0.300000,0.182070,0.000000,2.050000,0.000000,0.000000,4.577000,19.300000,19.300000
11.900000,0.030512,0.000204,2503.000000
-49.642000,3.050000,2.980000,1.880000,1.840000
0.012400,0.030500,0.111000,0.301000,1.140000,3.010000
0.000248,0.001643,0.001470,0.002962,0.000863,0.000315
0.000070,-0.010000,-0.600000
2
0.0,0.0,0.5683,12.0
0.431800
```

Figure D-8. MITR-III Blade Withdrawal Input Data (4.25 in/min, no scram)

```
10.000000,0.966700,0.909700
1.1310000,2.1037500,0.00000,1.527,1.146
2500.000000,0.940000,1.000000,0.916
2290.000000,5.000000,4.000000,135.000000
25.40000,32.000000
35.000000,7000.00000,7000.000000,0.300000,1
2.900000,662.000000,112.750000,111.000000,0.000000,5.300000,0.410000
0
1.000000
3
0.0,0.0,10.0,0.0,106,2.0
2
0.0,1.0,35.0,1.0
2
0.0,1.0,35.0,1.0
3
0.0,1.0,180.0,1.0,210,1.0
2
0.0,1.0,35.0,1.0
2
0.0,0.0,35.0,0.0
0.3620000,7E.600000,185.350000,425000.000000,992.200000,20.000000
1.305200,-0.25533,-0.04985,0.0
2
1,0.001375,0.004775,67
0.00275,0.056196,13.650000,9.483000e-27
480.400000,896.000000
1,0.001375,0.004775,67
0.00275,0.056196,13.650000,9.483000e-27
480.400000,896.000000
0.083120,0.096190
3675.000000,2712.600000
0.000762,0.000508,0.568300,0.058670,0.052880,330
0.000000,0.000000,35.800000,0.000000
0.000000,1069.400000,2072000.000,0.000000
0.000000,0.000000,186.000000,0.000000
0.000000,1187.000000,2409000.000000,0.000000
0.002240,0.229110,1.900000
0.032400,0.338900,0.110800,0.004375,0.028800,0.000131,0.129900,0.9234,0.0324,0.0008388,0.0008388,0.9810
0.793500
0.203000,0.179600,0.062900,0.220000,0.039600,0.002237,0.387400,1.084000,0.203000,0.00275,0.00275
0.468000,0.413200,0.076000,0.016400,0.017900,0.037500,0.099000,1.823700,0.427000,0.00108,0.00108,0.9600
14.435000,1.220000,0.685800,0.007000,0.617500,0.666700,0.762000,1.318000,13.170000,1.2900,1.2900,1.0562
9.658000,8.438000,7.752000,7.745000,7.127500,7.790000,8.552000,9.870000,2.690000,2.690000,2.690000
2.170000,0.000000,0.300000,0.182070,0.000000,2.050000,0.000000,0.000000,4.577000,19.300000,19.300000
11.900000,0.030512,0.000204,2503.000000
-49.642000,3.050000,2.980000,1.880000,1.840000
0.012400,0.030500,0.111000,0.301000,1.140000,3.010000
0.000248,0.001643,0.001470,0.002962,0.000863,0.000315
0.000070,-0.010000,-0.600000
2
0.0,0.0,0.5683,12.0
0.431800
```

Figure D-9. MITR-III Blade Withdrawal Input Data (8.50 in/min, no scram)

```
10.000000,0.966700,0.909700
1.1310000,2.1037500,0.00000,1.527,1.146
2500.000000,0.940000,1.000000,0.916
2290.000000,5.000000,4.000000,135.000000
25.40000,32.000000
20.0000,7000.00000,0.000000,0.100000,1
2.900000,662.000000,0.0000,111.000000,0.000000,5.300000,0.410000
0
1.000000
3
0.0,0.0,10.0,0.0,106,0.0
2
0.0,1.0,35.0,1.0
2
0.0,1.0,35.0,1.0
3
0.0,1.0,180.0,1.0,210,1.0
2
0.0,1.0,35.0,1.0
2
0.0,0.0,35.0,0.0
0.3620000,78.600000,185.350000,425000.000000,992.200000,20.000000
1.305200,-0.25533,-0.04985,0.0
2
1,0.001375,0.004775,67
0.00275,0.056196,13.650000,9.483000e-27
480.400000,896.000000
1,0.001375,0.004775,67
0.00275,0.056196,13.650000,9.483000e-27
480.400000,896.000000
0.083120,0.096190
3675.000000,2712.600000
0.000762,0.000508,0.568300,0.058670,0.052880,330
0.000000,0.000000,35.800000,0.000000
0.000000,1069.400000,2072000.000,0.000000
0.000000,0.000000,186.000000,0.000000
0.000000,1187.000000,2409000.000000,0.000000
0.002240,0.229110,1.900000
0.032400,0.338900,0.110800,0.004375,0.028800,0.000131,0.129900,0.9234,0.0324,0.0008388,0.0008388,0.9810
0.793500
0.203000,0.179600,0.062900,0.220000,0.039600,0.002237,0.387400,1.084000,0.203000,0.00275,0.00275
0.468000,0.413200,0.076000,0.016400,0.017900,0.037500,0.099000,1.823700,0.427000,0.00108,0.00108,0.9600
14.435000,1.220000,0.685800,0.007000,0.617500,0.666700,0.762000,1.318000,13.170000,1.2900,1.2900,1.0562
9.658000,8.438000,7.752000,7.745000,7.127500,7.790000,8.552000,9.870000,2.690000,2.690000,2.690000
2.170000,0.000000,0.300000,0.182070,0.000000,2.050000,0.000000,0.000000,4.577000,19.300000,19.300000
11.900000,0.030512,0.000204,2503.000000
-49.642000,3.050000,2.980000,1.880000,1.840000
0.012400,0.030500,0.111000,0.301000,1.140000,3.010000
0.000248,0.001643,0.001470,0.002962,0.000863,0.000315
0.000070,-0.010000,-0.600000
2
0.0,0.0,0.568?,12.0
0.431800
```

Figure D-10. MITR-III Pump Coastdown Input Data (no scram)

```
10.000000,0.966700,0.909700
1.1310000,2.10375,0.00000,1.527,1.146
2800.000000,0.940000,1.000000,0.916
2290.000000,5.000000,4.000000,135.000000
26.60000,32.000000
400.000000,7000.00000,500.000000,0.30000,1
2.900000,62.000000,165.46,11.5000000,10.000000,5.300000,0.3860000
0
1.000000
3
0.0,0.0,2.0,0.0,209,0.0
2
0.0,1.0,35.0,1.0
2
0.0,1.0,35.0,1.0
3
0.0,1.0,10.0,1.0,40,0.0
3
0.0,1.0,5.0,1.0,50,1.0
2
0.0,0.0,35.0,0.0
0.55,87.400000,185.350000,405000.000000,992.200000,5.000000
1.305200,-0.25533,-0.04985,0.0
2
1,0.001375,0.004775,67
0.00275,0.056196,13.650000,9.483000e-27
480.400000,896.000000
1,0.001375,0.004775,67
0.00275,0.056196,13.650000,9.483000e-27
480.400000,896.000000
0.083120,0.096190
3675.000000,2712.600000
0.000762,0.000508,0.568300,0.058670,0.052880,330
0.000000,0.000000,35.800000,0.000000
0.000000,1069.400000,2072000.000,0.000000
0.000000,0.000000,186.000000,0.000000
0.000000,1187.000000,2409000.000000,0.000000
0.002240,0.229110,1.900000
0.032400,0.338900,0.110800,0.004375,0.028800,0.000131,0.129900,0.9234,0.0324,0.0008388,0.0008388,0.9810
0.793500
0.203000,0.179600,0.062900,0.220000,0.039600,0.002237,0.387400,1.084000,0.203000,0.00275,0.00275
0.468000,0.413200,0.076000,0.016400,0.017900,0.037500,0.099000,1.823700,0.427000,0.00108,0.00108,0.9600
14.435000,1.220000,0.685800,0.007000,0.617500,0.666700,0.762000,1.318000,13.170000,1.290000,1.29,1.0562
9.658000,8.438000,7.752000,7.745000,7.127500,7.790000,8.552000,9.870000,2.690000,2.690000,2.690000
2.170000,0.000000,0.300000,0.182070,0.000000,2.050000,0.000000,0.000000,4.577000,19.300000,19.300000
11.900000,0.030512,0.000204,2503.000000
-49.642000,3.050000,2.980000,1.880000,1.840000
0.012400,0.030500,0.111000,0.301000,1.140000,3.010000
0.000248,0.001643,0.001470,0.002962,0.000863,0.000315
0.000070,-0.010000,-0.600000
22
0.0,0.0,0.0508,0.55,0.0762,1.2,0.1016,1.9,0.127,2.65,0.1524,3.5,0.1778,4.3,0.2032,5.1,0.2286,5.9,0.254,6.7,
0.2794,7.4,0.3048,8.0,0.330,8.6,0.3556,9.2,0.381,9.7,0.4064,10.2,0.4318,10.6,0.4572,11.0,0.4826,11.25,0.508,
11.5,0.5334,11.6,0.5683,11.7
0.5175
```

Figure D-11. MITR-III Loss of Heat Sink Input Data (with scram)

```
10.000000,0.966700,0.909700
1.1310000,2.10375,0.00000,1.527,1.146
2800.000000,0.940000,1.000000,0.916
2290.000000,5.000000,4.000000,135.000000
26.60000,32.000000
40.000000,7000.00000,500.000000,0.10000,1
2.900000,62.000000,165.46,11.5000000,10.000000,5.300000,0.3860000
0
1.000000
3
0.0,0.0,10.0,0.0,202,2.0
2
0.0,1.0,35.0,1.0
2
0.0,1.0,35.0,1.0
3
0.0,1.0,10.0,1.0,40,1.0
3
0.0,1.0,5.0,1.0,50,1.0
2
0.0,0.0,35.0,0.0
0.55,87.400000,185.350000,405000.000000,992.200000,5.000000
1.305200,-0.25533,-0.04985,0.0
2
1,0.001375,0.004775,67
0.00275,0.056196,13.650000,9.483000e-27
480.400000,896.000000
1,0.001375,0.004775,67
0.00275,0.056196,13.650000,9.483000e-27
480.400000,896.000000
0.083120,0.096190
3675.000000,2712.600000
0.000762,0.000508,0.568300,0.058670,0.052880,330
0.000000,0.000000,35.800000,0.000000
0.000000,1069.400000,2072000.000,0.000000
0.000000,0.000000,186.000000,0.000000
0.000000,1187.000000,2409000.000000,0.000000
0.002240,0.229110,1.900000
0.032400,0.338900,0.110800,0.004375,0.028800,0.000131,0.129900,0.9234,0.0324,0.0008388,0.0008388,0.9810
0.793500
0.203000,0.179600,0.062900,0.220000,0.039600,0.002237,0.387400,1.084000,0.203000,0.00275,0.00275
0.468000,0.413200,0.076000,0.016400,0.017900,0.037500,0.099000,1.823700,0.427000,0.00108,0.00108,0.9600
14.435000,1.220000,0.685800,0.007000,0.617500,0.666700,0.762000,1.318000,13.170000,1.290000,1.29,1.0562
9.658000,8.438000,7.752000,7.745000,7.127500,7.790000,8.552000,9.870000,2.690000,2.690000,2.690000
2.170000,0.000000,0.300000,0.182070,0.000000,2.050000,0.000000,0.000000,4.577000,19.300000,19.300000
11.900000,0.030512,0.000204,2503.000000
-49.642000,3.050000,2.980000,1.880000,1.840000
0.012400,0.030500,0.111000,0.301000,1.140000,3.010000
0.000248,0.001643,0.001470,0.002962,0.000863,0.000315
0.000070,-0.010000,-0.600000
22
0.0,0.0,0.0508,0.55,0.0762,1.2,0.1016,1.9,0.127,2.65,0.1524,3.5,0.1778,4.3,0.2032,5.1,0.2286,5.9,0.254,6.7,
0.2794,7.4,0.3048,8.0,0.330,8.6,0.3556,9.2,0.381,9.7,0.4064,10.2,0.4318,10.6,0.4572,11.0,0.4826,11.25,0.508,
11.5,0.5334,11.6,0.5683,11.7
0.5175
```

Figure D-12. MITR-III Blade Withdrawal Input Data (4.25 in/min, with scram)

```
10.000000,0.966700,0.909700
1.1310000,2.10375,0.00000,1.527,1.146
2800.000000,0.940000,1.000000,0.916
2290.000000,5.000000,4.000000,135.000000
26.60000,32.000000
40.000000,7000.00000,500.000000,0.10000,1
2.900000,62.000000,165.46,11.5000000,10.000000,5.300000,0.3860000
0
1.000000
3
0.0,0.0,10.0,0.0,196,2.0
2
0.0,1.0,35.0,1.0
2
0.0,1.0,35.0,1.0
3
0.0,1.0,10.0,1.0,40,1.0
3
0.0,1.0,5.0,1.0,50,1.0
2
0.0,0.0,35.0,0.0
0.55,87.400000,185.350000,405000.000000,992.200000,5.000000
1.305200,-0.25533,-0.04985,0.0
2
1,0.001375,0.004775,67
0.00275,0.056196,13.650000,9.483000e-27
480.400000,896.000000
1,0.001375,0.004775,67
0.00275,0.056196,13.650000,9.483000e-27
480.400000,896.000000
0.083120,0.096190
3675.000000,2712.600000
0.000762,0.000508,0.568300,0.058670,0.052880,330
0.000000,0.000000,35.800000,0.000000
0.000000,1069.400000,2072000.000,0.000000
0.000000,0.000000,186.000000,0.000000
0.000000,1187.000000,2409000.000000,0.000000
0.002240,0.229110,1.900000
0.032400,0.338900,0.110800,0.004375,0.028800,0.000131,0.129900,0.9234,0.0324,0.0008388,0.0008388,0.9810
0.793500
0.203000,0.179600,0.062900,0.220000,0.039600,0.002237,0.387400,1.084000,0.203000,0.00275,0.00275
0.468000,0.413200,0.076000,0.016400,0.017900,0.037500,0.099000,1.823700,0.427000,0.00108,0.00108,0.9600
14.435000,1.220000,0.685800,0.007000,0.617500,0.666700,0.752000,1.318000,13.170000,1.290000,1.29,1.0562
9.658000,8.438000,7.752000,7.745000,7.127500,7.790000,8.552000,9.870000,2.690000,2.690000,2.690000
2.170000,0.000000,0.300000,0.182070,0.000000,2.050000,0.000000,0.000000,4.577000,19.300000,19.300000
11.900000,0.030512,0.000204,2503.000000
-49.642000,3.050000,2.980000,1.880000,1.840000
0.012400,0.030500,0.111000,0.301000,1.140000,3.010000
0.000248,0.001643,0.001470,0.002962,0.000863,0.000315
0.000070,-0.010000,-0.600000
22
0.0,0.0,0.0508,0.55,0.0762,1.2,0.1016,1.9,0.127,2.65,0.1524,3.5,0.1778,4.3,0.2032,5.1,0.2286,5.9,0.254,6.7,
0.2794,7.4,0.3048,8.0,0.330,8.6,0.3556,9.2,0.381,9.7,0.4064,10.2,0.4318,10.6,0.4572,11.0,0.4826,11.25,0.508,
11.5,0.5334,11.6,0.5683,11.7
0.5175
```

Figure D-13. MITR-III Blade Withdrawal Input Data (8.50 in/min, with scram)

```
10.000000,0.966700,0.909700
1.1310000,1.05,1.00000,1.527,1.146
2800.000000,0.940000,1.000000,0.934
2290.000000,5.000000,4.000000,135.000000
26.60000,32.000000
30.000000,7000.00000,1.000000,0.010000,1
2.900000,62.000000,165.46,11.5000000,10.000000,5.300000,0.3863000
0
1.000000
3
0.0,0.0,10.0,0.0,106,0.0
2
0.0,1.0,35.0,1.0
2
0.0,1.0,35.0,1.0
3
0.0,1.0,10.0,1.0,40,1.0
3
0.0,1.0,5.0,1.0,50,1.0
2
0.0,0.0,35.0,0.0
0.55,87.400000,185.350000,405000.000000,992.200000,5.000000
1.305200,-0.25533,-0.04985,0.0
2
1,0.001375,0.004775,67
0.00275,0.056196,13.650000,9.483000e-27
480.400000,896.000000
1,0.001375,0.004775,67
0.00275,0.056196,13.650000,9.483000e-27
480.400000,896.000000
0.083120,0.096190
3675.000000,2712.600000
0.000762,0.000508,0.568300,0.058670,0.052880,330
0.000000,0.000000,35.800000,0.000000
0.000000,1069.400000,2072000.000,0.000000
0.000000,0.000000,186.000000,0.000000
0.000000,1187.000000,2409000.000000,0.000000
0.002240,0.229110,1.900000
0.032400,0.338900,0.110800,0.004375,0.028800,0.000131,0.129900,0.9234,0.0324,0.0008388,0.0008388,0.9810
0.793500
0.203000,0.179600,0.062900,0.220000,0.039600,0.002237,0.387400,1.084000,0.203000,0.00275,0.00275
0.468000,0.413200,0.076000,0.016400,0.017900,0.037500,0.099000,1.823700,0.427000,0.00108,0.00108,0.9600
14.435000,1.220000,0.685800,0.007000,0.617500,0.666700,0.762000,1.318000,13.170000,1.2900,1.2900,1.0562
9.658000,8.438000,7.752000,7.745000,7.127500,7.790000,8.552000,9.870000,2.690000,2.690000,2.690000
2.170000,0.000000,0.300000,0.182070,0.000000,2.050000,0.000000,0.000000,4.577000,19.300000,19.300000
11.900000,0.030512,0.000204,2503.000000
-49.642000,3.050000,2.980000,1.880000,1.840000
0.012400,0.030500,0.111000,0.301000,1.140000,3.010000
0.000248,0.001643,0.001470,0.002962,0.000863,0.000315
0.000070,-0.010000,-0.600000
22
0.0,0.0,0.0508,0.55,0.0762,1.2,0.1016,1.9,0.127,2.65,0.1524,3.5,0.1778,4.3,0.2032,5.1,0.2286,5.9,0.254,6.7,
0.2794,7.4,0.3048,8.0,0.330,8.6,0.3556,9.2,0.381,9.7,0.4064,10.2,0.4318,10.6,0.4572,11.0,0.4826,11.25,0.508,
11.5,0.5334,11.6,0.5683,11.7
0.5175
```

Figure D-14. MITR-III Pump Coastdown Input Data

APPENDIX E: INITIAL CONDITION CALCULATION

In order to determine the initial primary and secondary temperature profiles, and the division of flow and power between the heat exchangers, a bisection method was used. The only temperature fixed is the secondary inlet to the heat exchanger given by the user. The assumption made is that both heat exchangers have equal total pressure drops.

The bisection method consists of choosing two extreme flow division cases (e.g., case 1= 30 % of flow through heat exchanger 1 and 70 % through heat exchanger 2; case 2= 70 % of flow through heat exchanger 1 and 30 % through heat exchanger 2) and checking to see if the condition of equal pressure drop along both heat exchangers lies somewhere in between. If the solution exists, the flow split is sequentially narrowed until the equal pressure drop condition is obtained. The governing energy equations for the system are as follows:

- Core energy equation

$$Q_{th} = m_c(h_{in} - h_{out}) \tag{E-1}$$

- Mixing area energy equation

$$mh_{ma} = m_c h_{out} + m_{bp} h_{in} \tag{E-2}$$

- Hot leg energy equation

$$mh_{hl} = \sum_{i} \frac{m(i)\Delta P(i)}{\rho_{hl}} + m_{ch} h_{ch} + mh_{ma} \tag{E-3}$$

- Heat exchanger (j) primary and secondary energy equations

$$Q_{hx(j)} = m(j)(h_{hl} - h_{hx(j)}) \qquad \text{(primary side)} \tag{E-4}$$

$$Q_{hx(j)} = m_s(j)(h_{hxs}(j) - h_{si}) \qquad \text{(secondary side)} \qquad \text{(E-5)}$$

- Cold leg energy equation

$$mh_{in} = \sum_j m(j)h_{hx(j)} \qquad \text{(E-6)}$$

where,

Q_{th}	=	thermal energy deposited in the primary coolant
$Q_{hx(j)}$	=	energy removal rate of heat exchanger j
m	=	loop mass flow rate
m_c	=	core mass flow rate
m_{bp}	=	core bypass mass flow rate
m_{ch}	=	charging mass flow rate
$m(i)$	=	mass flow rate through pump i
$m(j)$	=	mass flow rate through heat exchanger j
$m_s(j)$	=	mass flow rate through heat exchanger j (secondary)
h_{in}	=	core inlet enthalpy
h_{out}	=	core outlet enthalpy
h_{ma}	=	mixing area average enthalpy
h_{hl}	=	hot leg outlet enthalpy
h_{ch}	=	charging enthalpy
$h_{hx(j)}$	=	heat exchanger j primary outlet enthalpy
$h_{hxs(j)}$	=	heat exchanger j secondary outlet enthalpy
h_{si}	=	heat exchangers secondary inlet enthalpy
$\Delta P(i)$	=	pressure head delivered by pump i
ρ_{hl}	=	fluid density at the exit of the hot leg

The bisection method is performed in the following sequential order:

1. The flow split between the heat exchangers is guessed; for example, 30 % to heat exchanger 1 and 70 % to heat exchanger 2.

2. A core inlet and hot leg outlet temperature are guessed.

3. A power split between heat exchangers is guessed.

4. The core outlet and mixing area average temperatures are calculated using Equations E-1 and E-2.

5. The hot leg outlet temperature is calculated using Equation E-3. An iteration is necessary since the hot leg outlet density depends on the hot leg outlet enthalpy.

6. The heat exchanger primary and secondary outlet temperatures as well as the heat exchanger power are calculated using Equations E-4 and E-5. This involves an iterative process since the heat exchanger power must also obey Equation 2.34.

7. The core inlet temperature is calculated using Equation E-6. If the result differs from the initial guess value, the calculations of steps 4 through 7 are repeated. This iteration is repeated until the convergence criteria is met.

8. Once the temperature profile is obtained, the pressure drop of each heat exchanger is calculated. The difference between the pressure drop along each heat exchanger is calculated.

9. Steps 1 through 8 are repeated using the opposite flow split. That is, 70 % of total flow to heat exchanger 1 and 30 % to heat exchanger 2.

10. If the difference between the pressure drops of steps 8 and 9 have opposite signs then there is a flow division somewhere along those two extreme cases that satisfies the equal pressure drop condition. If this condition was not met, the flow split is narrowed and steps 2 through 8 are repeated until the difference between the pressure drop along both heat exchangers are within a specified error.

REFERENCES

Parra, S. A, "The Physics and Engineering Upgrade of the Massachusetts Institute of Technology," Ph.D. Thesis, MIT Department of Nuclear Engineering, 1993.

Kao, S. P., "A Multiple-Loop Primary System Model for Pressurized Water Reactor Plant Sensor Validation," Ph.D. Thesis, MIT Department of Nuclear Engineering, 1984.

Obenchain, C.F., "PARET- A Program for the Analysis of Reactor Transients," IDO-17282, AEC Research and Development Report, January 1969.

"MIT Research Reactor Systems Manual," Report No. MITNRL-004, Massachusetts Institute of Technology, 1980.

Meyer, J. E., "Some Physical and Numerical Considerations for the SSC-S Code," BNL-NUREG-50913, 1978.

Bamdad-Haghighi, F., "Natural Convection analysis of the MITR-II During Loss of Flow Accident," Nucl. E. and S.M. Thesis, MIT Department of Nuclear Engineering, 1977.

Meyer, J. E. and Reinhard, E. A., "Numerical Techniques for Boiling Flow Stability Analyses," Trans. ASME Series C, 87, 311-312, 1965.

Strohmayer, W. H., "Dynamic Modeling of a vertical U-Tube Steam Generators for Operational Safety Systems," Ph.D. Thesis, MIT Department of Nuclear Engineering, 1982.

Kao, C., "Simulation of MITR-II Primary System in Steady State," MIT Department of Nuclear Engineering, 1992.

DuBord, R., "Pump Coast-Down Simulation for the MITR-II," MIT Department of Nuclear Engineering, 1992.

Rust, J. H., Nuclear Power Plant Engineering, Haralson Publishing Co., Buchanon, GA, 1979.

Bjerke, M. A., et al., "A Review of Short-Term Fission-Product-Decay Power," Nuclear Safety, Vol. 18, No. 5, 1977.

Hu, L. W., "MITR-II Simulator," 22.39 Term Project, MIT Nuclear Engineering Department, 1993.

"MITR-II Integral and Differential Reactivity Worth Curves," MIT Reactor Laboratory Staff, July 1993.
Terry, K. B., "Flow Coastdown and Time to Scram for MITR-II," 22.39 Term Project, MIT Department of Nuclear Engineering, 1993.

Turek, M., "Summary of MITR-III Upgrade Studies," 22.902 Special Project, MIT Department of Nuclear Engineering, 1994.

Todreas, N. E., and Kazimi, M. S., Nuclear Systems I. Hemisphere Publishing Corporation, 1990.

Palen, J. W., Heat Exchanger Sourcebook , Hemisphere Publishing, pg. 565, 1986.